NASA Contractor Report 167959

NASA-CR-167959
19830010400

USER'S MANUAL FOR THREE-DIMENSIONAL ANALYSIS OF PROPELLER FLOW FIELDS

Denny S. Chaussee and Paul Kutler

Flow Simulations, Inc.
Sunnyvale, California

January 1983

Prepared for

NATIONAL AERONAUTICS AND SPACE ADMINISTRATION
Lewis Research Center
Under Contract NAS 3-22375

TABLE OF CONTENTS

USER'S MANUAL FOR THREE-DIMENSIONAL ANALYSIS OF PROPELLER FLOW FIELDS

by

Denny S. Chaussee
Paul Kutler
Flow Simulations, Inc.

1. SUMMARY

A detailed operating manual is presented for the prop-fan computer code (in addition to supporting programs) recently developed by Kutler, Chaussee, Sorenson, and Pulliam while at the NASA's Ames Research Center. This code solves the inviscid Euler equations using an implicit numerical procedure developed by Beam and Warming of Ames. A description of the underlying theory, numerical techniques, and boundary conditions with equations, formulas, and methods for the mesh generation program (MGP), three-dimensional prop-fan flow field program (3DPFP), and data reduction program (DRP) is provided, together with complete operating instructions. In addition, a programmer's manual is also provided to assist the user interested in modifying the codes. Included in the programmer's manual for each program is a description of the input and output variables, flow charts, program listings, sample input and output data, and operating hints.

2. INTRODUCTION

A variety of advanced propellers is being designed for high-speed aircraft of the future. It has been shown from experimental tests that the new propeller termed the prop-fan is less noisy and more efficient than other models tested, and could result in saving a large amount of airplane fuel.

The prop-fan is a small-diameter, highly loaded, multibladed, variable pitch propulsor (see Fig. 1). The blades, which are twisted and tapered, utilize thin airfoil sections with tip sweep. They are integrated with a spinner and nacelle shaped to reduce the axial Mach number through the blading. Interest in the prop-fan propulsion system concept arose as a result of its potential for significant fuel savings over conventional high bypass turbofans. Interest from a computational point of view was stimulated by the need for understanding the flow phenomena around propellers and the potential for a more efficient computer generated design.

Over the years, computational procedures for solving fluid flow problems provided an inexpensive but accurate means of determining the aerodynamic characteristics of complex configurations. In addition, they have provided the designer with an effective tool for maximizing aerodynamic efficiency without the expense of actually building and testing numerous designs. Finally, computational methods have often been capable of providing information not readily obtainable from experiments.

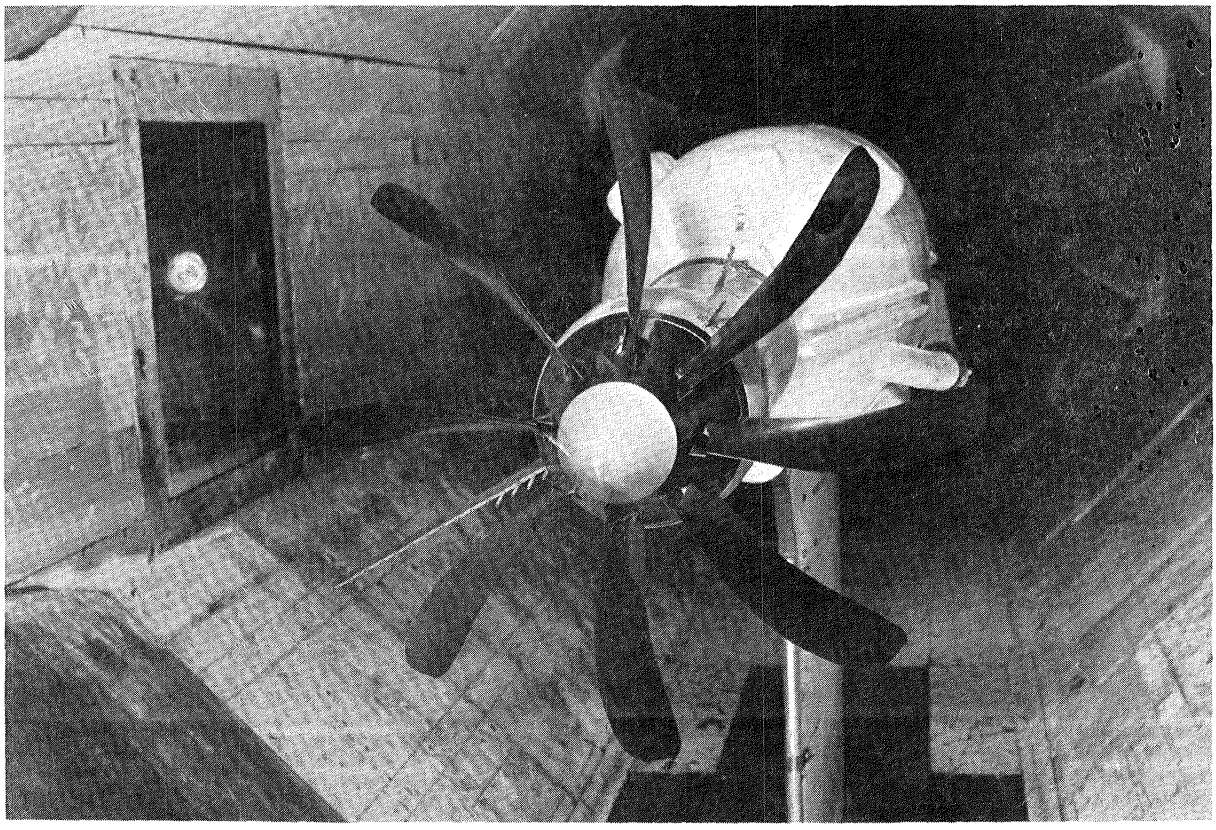

Figure 1. - Prop-fan mounted in wind tunnel.

The prop-fan is a good example of the type of configuration for which it is difficult to experimentally obtain aerodynamic information needed for performance analyses and design. The blades are virtually impossible to adequately instrument because of the high rotational velocities, and their relatively small thickness. Also, details of the surrounding flow field can only be obtained by performing costly and time consuming flow field surveys. Computationally, however, the entire flow field can be determined from a single solution of the governing equations including near- and far-field effects which can be used in acoustic analysis programs and blade surface pressure distributions which can be used in structural and aerodynamic design analysis programs.

The theoretical development and subsequent numerical solutions were concerned with simulating the inviscid flow about the prop-fan model used in the early experiments, i.e., the standard eight-bladed prop and spinner mated with an axisymmetric nacelle or afterbody (instead of the conventional three-dimensional nacelle with inlet). Such a configuration thus requires that only the flow about a single blade be computed because of periodicity. The new and unique feature of the present work over conventional efforts is that the blades are unshrouded, i.e., the flow is permitted to spill over the blade tip. In effect, the entire flow field about

a lifting wing-body combination with the added complexity of rotation was computed.

This report is broken down into two basic categories. The first is the Analysis section in which the theory used to develop the prop-fan flow field program is explained. This includes the derivation of the governing equations, a description of the numerical algorithm, body definition and mesh generation, boundary and initial conditions, and data reduction theory. The second part of this report describes the three computer programs that were developed to analyse the prop-fan flow field. These include the mesh generation program (MGP), three-dimensional prop-fan flow field program (3DPFP), and data reduction program (DRP). The description of each program includes its organization and interaction with the other programs, a flow chart, sample input and output data, operating procedures and trouble shooting hints, and a basic description of each main program and subroutine. These computer programs were written in FORTRAN IV source language and developed for use on a CDC 7600 computer using the OPT = 2 compiler.

3. LIST OF SYMBOLS

$\tilde{a}$	defined in Eq. (25)
A	axial force or Jacobian matrix, $\partial E/\partial Q$
A_b	reference area, πr_b^2
b	blade width or chord
$\tilde{b}$	defined in Eq. (25)
B	Jacobian matrix $\partial F/\partial Q$
c	speed of sound, $= (\gamma p/\rho)^{\frac{1}{2}}$
$\tilde{c}$	defined in Eq. (25)
C	Jacobian matrix $\partial G/\partial Q$
C_A	axial force coefficient
C_F	force coefficient
C_M	moment coefficient
C_N	normal force coefficient
C_P	pitching moment coefficient
C_p	pressure coefficient also (Section 7.1)
C_Q	torque coefficient
C_R	rolling moment coefficient
C_S	side force coefficient
C_T	thrust coefficient
C_p	power coefficient
C_y	yawing moment coefficient
CN	Courant number (see Eq. (7))
D	diameter of propeller
D	drag, Eq. (95)

LIST OF SYMBOLS (Continued)

$d\vec{F}$	incremental force vector, Eq. (72)
dM_p	incremental pitching moment
dN	incremental normal force, Eq. (76)
dS	incremental side force, Eq. (76)
e	total energy per unit volume
E	vector of flux quantities in ξ-direction
F	vector of flux quantities in η-direction
g	integrand of Eq. (57)
G	vector of flux quantities in ζ-direction
H	vector of source terms created by cylindrical generalized coordinate transformation
H_r	rothalpy
H_t	total enthalpy
(i_z, i_r, i_ϕ)	unit normal vector of cylindrical coordinate system
(i,j,k)	unit vectors of cartesian coordinate system
J	Jacobian or Advance ratio (u_∞/nD)
L	lift
LEA	leading edge alignment
ℓ_b	reference length
M	Mach number
M_p	pitching moment
M_R	rolling moment
M_y	yawing moment

LIST OF SYMBOLS (Continued)

n	rotational speed
$\hat{n}$	unit normal, Eqs. (32) and (54)
$\hat{n}_c$	Eq. (33)
$\hat{n}_f$	Eq. (34)
$\hat{n}_{1/2}$	Eq. (38)
N	normal force
p	static pressure
$k_i, i=0,3$	generalized metrics
q_∞	dynamic pressure = $0.5\rho_\infty v_\infty^2$
$q_i, i=1,5$	components of Q
Q	torque or vector dependent variable of integration
$\vec{r}$	distance from coordinate system origin to incremental area $d\vec{A}$, Eq. (80)
R_1	right-hand side of Eq. (54)
R_2	right-hand side of Eq. (55)
R_3	right-hand side of Eq. (56)
R_4	right-hand side of Eq. (57)
S	constant surface, Figure 9
S	side force
S	entropy Eq. (22)
S_T	cubic function used in initial startup Eq. (71a)
(t,z,r,ϕ)	independent variables, cylindrical coordinates
T	thrust
T	used in initial startup Eq. (71a)

LIST OF SYMBOLS (Concluded)

u	physical velocity in z-direction
U, $\bar{u}$	contravariant velocity defined in Eq. (2)
γ	see Eq. (5)
v	physical velocity in y- or r-direction
V, $\bar{v}$	contravariant velocity defined in Eq. (2)
$\vec{V}$	velocity vector $u\hat{i} + v\hat{j} + w\hat{k}$
$\bar{\gamma}$	See Eq. (5)
w	physical velocity in x- or ϕ-direction
W, $\bar{w}$	contravariant velocity defined in Eq. (2)
(x,y,z)	cartesian coordinate system
γ	ratio of specific heats
$\gamma_i, i=1,5$	eigenvalues of gas-dynamic equations (see Eq. (6))
x_{cp}	center of pressure
$\Delta\beta$	blade twist
Δp	incremental pressure
$\Delta\xi, \Delta\eta, \Delta\zeta$	computational mesh spacing
ρ	density
(τ,ξ,η,ζ)	transformed independent variables (Eq. (1))
ε_e	explicit smoothing coefficient in implicit algorithm
ε_i	implicit smoothing coefficient in implicit algorithm
ω	angular velocity
Subscripts	
b	body
i	integer mesh point location in ξ-direction
j	integer mesh point location in η-direction
k	integer mesh point location in ζ-direction
∞	free stream conditions

4. ANALYSIS

4.1. Derivation of Governing Equations

To enhance numerical accuracy and efficiency, non-orthogonal coordinate transformations of the governing equations in a particular base coordinate system are employed. This maps the surface of the nacelle and both sides of the blade onto constant coordinate surfaces which facilitates the application of boundary conditions and permits grid point clustering at the body when the dependent variables are expected to undergo rapid changes. Use of such transformations in addition permits utilization of uniform discretization formulas and well-ordered interior grid point solution algorithms. Under this transformation the equations can still be written in conservation law form to take advantage of the shock capturing properties.

The basic orthogonal coordinate system utilized is cylindrical with z oriented along the rotational axis, r extending radially outward from the z-axis, and ϕ the meridional angle measured from a vertical plane (see Fig. 2). It should be reiterated that for this study, only the flow between two of the blades is computed, i.e. between the face side of one blade and the camber side of the other blade because of periodicity. The cylindrical coordinates are

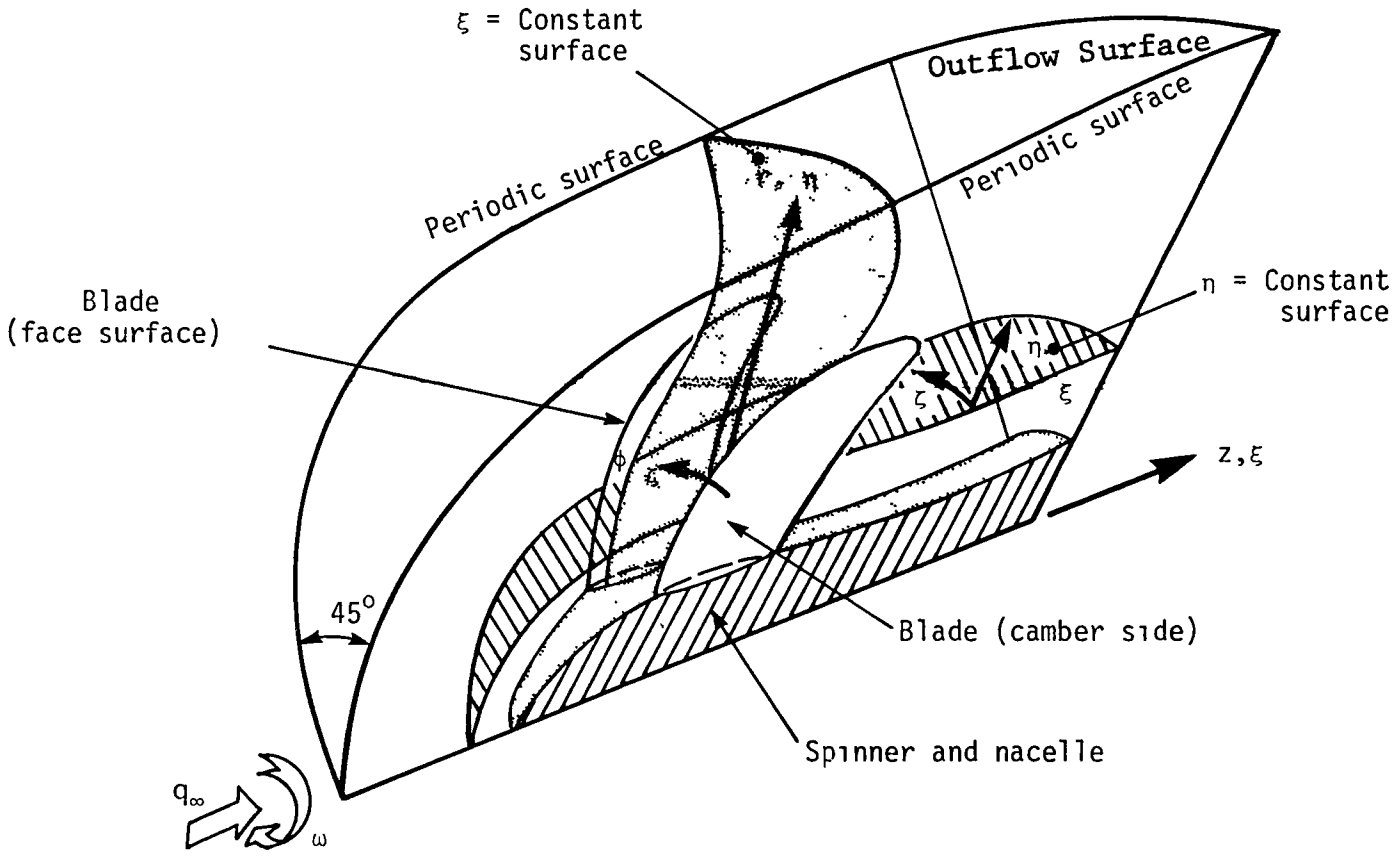

Figure 2. Coordinate System

transformed to align the blade and nacelle surfaces with various computational planes according to the following:

$$\begin{aligned} \tau &= t \\ \xi &= \xi(t,z,r,\phi) \\ \eta &= \eta(t,z,r,\phi) \\ \zeta &= \zeta(t,z,r,\phi) \end{aligned} \tag{1}$$

This generalized nonorthogonal coordinate transformation maps the spinner and nacelle onto a constant η-plane and each side of the blade, i.e., the camber and face sides, onto parts of a constant ζ-plane. The remaining parts of the constant ζ-planes are periodic surfaces. The radial far-stream and outflow boundaries are situated far enough from the prop-fan to minimize the reflection of waves.

The governing partial differential equations in weak conservation law form for cylindrical coordinates under the assumptions of inviscid compressible flow and a perfect, non-heat conducting gas for the transformation given in Eq. (1) are:

$$Q_\tau + E_\xi + F_\eta + G_\zeta + H = 0 \tag{2}$$

where

$$Q = \frac{1}{J}\begin{bmatrix} \rho \\ \rho u \\ \rho v \\ \rho w \\ e \end{bmatrix}, \quad E = \frac{1}{J}\begin{bmatrix} \rho U \\ \rho uU + p\xi_z \\ \rho vU + p\xi_r \\ \rho wU + p\xi_\phi / r \\ (e+p)U - p\xi_t \end{bmatrix}$$

$$F = \frac{1}{J}\begin{bmatrix} \rho V \\ \rho uV+p\eta_z \\ \rho uV+p\eta_r \\ \rho wV+p\eta_\phi/r \\ (e+p)V-p\eta_t \end{bmatrix}, \quad G = \frac{1}{J}\begin{bmatrix} \rho W \\ \rho uW+p\zeta_z \\ \rho vW+p\zeta_r \\ \rho wW+p\zeta_\phi/r \\ (e+p)W-p\zeta_t \end{bmatrix}, \quad H = \frac{1}{Jr}\begin{bmatrix} \rho v \\ \rho uv \\ \rho(v^2-w^2) \\ 2\rho vw \\ (e+p)v \end{bmatrix},$$

and

$$U = \xi_t + u\xi_z + v\,\xi_r + w\xi_\phi/r$$

$$V = \eta_t + u\eta_z + v\,\eta_r + w\eta_\phi/r$$

$$W = \zeta_t + u\zeta_z + v\,\zeta_r + w\zeta_\phi/r$$

U, V, and W are the contravariant velocities written without metric normalization. J is the transformation Jacobian and is defined below. Use of the Euler equations in conservation law form guarantees the accurate calculation of the shock waves occurring near the blade tips.

In the conservative variables of Eq. (2), the pressure p is nondimensionalized by p_∞, the density ρ by ρ_∞, and the cylindrical velocity components u, v, and w by $a_\infty/\sqrt{\gamma}$ where a_∞ is the free-stream speed of sound ($a_\infty^2 = \gamma p_\infty/\rho_\infty$) and γ is the ratio of specific heats. Other quantities made dimensionless are the time t by $ta_\infty/(D\sqrt{\gamma})$ and the angular velocity ω by $\omega D\sqrt{\gamma}/a_\infty$. The pressure, density, and velocity components

are related to the total energy per unit volume e by the following equation for an ideal gas:

$$e = p/(\gamma-1) + \rho(u^2 + v^2 + w^2)/2 \tag{3}$$

The metrics of Eq. (2) are obtained by the chain rule expansion of z_ξ, r_ξ, etc. and solved for ξ_z, ξ_r, etc. to yield the following expressions:

$$\begin{aligned}
\xi_t &= - z_\tau \xi_z - r_\tau \xi_r - \phi_\tau \xi_\phi & \xi_z &= (r_\eta \phi_\zeta - \phi_\eta r_\zeta)/I \\
\eta_t &= - z_\tau \eta_z - r_\tau \eta_r - \phi_\tau \eta_\phi & \xi_r &= (\phi_\eta z_\zeta - z_\eta \phi_\zeta)/I \\
\zeta_t &= - z_\tau \zeta_z - r_\tau \zeta_r - \phi_\tau \zeta_\phi & \xi_\phi &= (z_\eta r_\zeta - z_\zeta r_\eta)/I \\
\eta_z &= (\phi_\xi r_\zeta - r_\xi \phi_\zeta)/I & \zeta_z &= (r_\xi \phi_\eta - \phi_\xi r_\eta)/I \\
\eta_r &= (z_\xi \phi_\zeta - \phi_\xi z_\zeta)/I & \zeta_r &= (z_\eta \phi_\xi - \phi_\eta z_\xi)/I \\
\eta_\phi &= (r_\xi z_\zeta - z_\xi r_\zeta)/I & \zeta_\phi &= (z_\xi r_\eta - r_\xi z_\eta)/I
\end{aligned} \tag{4}$$

where

$$I = 1/J = z_\xi r_\eta \phi_\zeta + r_\xi \phi_\eta z_\zeta + \phi_\xi z_\eta r_\zeta - z_\xi \phi_\eta r_\zeta - r_\xi z_\eta \phi_\zeta - \phi_\xi r_\eta z_\zeta$$

The quantity ϕ_τ is the rotational or angular velocity of the propeller.

In general, the metrics of Eq. (4) are not known analytically and must be determined numerically at each step of the intergration procedure. To accomplish this, second-order central-difference formulas are used at interior points and three-point one-sided formulas are used at the boundaries.

The implicit algorithm to be discussed below requires the analytic determination of the Jacobians $A = \partial E/\partial Q$, $B = \partial F/\partial Q$, and $C = \partial G/\partial Q$. These Jacobian matrices resulted from the time linearization of E, F, and G in deriving the numerical algorithm. The Jacobian matrices can be written in general as follows:

$$
\text{A, B, or C} = \begin{bmatrix}
K_0 & K_1 & K_2 & \frac{K_3}{r} & 0 \\
K_1\frac{\gamma-1}{2}\bar{v}^2 - \frac{q_2}{q_1}\bar{v} & K_0 + \bar{v} + K_1(2-\gamma)\frac{q_2}{q_1} & -K_1(\gamma-1)\frac{q_3}{q_1} + K_2\frac{q_2}{q_1} & -K_1(\gamma-1)\frac{q_4}{q_1} + \frac{K_3}{r}\frac{q_2}{q_1} & K_1(\gamma-1) \\
K_2\frac{\gamma-1}{2}\bar{v}^2 - \frac{q_3}{q_1}\bar{v} & K_1\frac{q_3}{q_1} - K_2(\gamma-1)\frac{q_2}{q_1} & K_0 + \bar{v} + K_2(2-\gamma)\frac{q_3}{q_1} & K_2(\gamma-1)\frac{q_4}{q_1} + \frac{K_3}{r}\frac{q_3}{q_1} & K_2(\gamma-1) \\
K_3\frac{\gamma-1}{2}\bar{v}^2 - \frac{q_4}{q_1}\bar{v} & K_1\frac{q_4}{q_1} - \frac{K_3}{r}(\gamma-1)\frac{q_2}{q_1} & K_2\frac{q_4}{q_1} - \frac{K_3}{r}(\gamma-1)\frac{q_3}{q_1} & K_0 + \bar{v} + \frac{K_3}{r}(2-\gamma)\frac{q_4}{q_1} & \frac{K_3}{r}(\gamma-1) \\
-\gamma\frac{q_5}{q_1}\bar{v} + (\gamma-1)\bar{v}^2 & -(\gamma-1)\frac{q_2}{q_1}\bar{v} + K_1\gamma\frac{q_5}{q_1} - K_1\frac{\gamma-1}{2}\bar{v}^2 & -(\gamma-1)\frac{q_3}{q_1}\bar{v} + K_2\gamma\frac{q_5}{q_1} - K_2\frac{\gamma-1}{2}\bar{v}^2 & -(\gamma-1)\frac{q_4}{q_1}\bar{v} + \frac{K_3}{r}\gamma\frac{q_5}{q_1} - \frac{K_3}{r}\left(\frac{\gamma-1}{2}\right)\bar{v}^2 & K_0 + \gamma\bar{v}
\end{bmatrix} \tag{5}
$$

where $\bar{V} = (k_1 q_2 + k_2 q_3 + \frac{k_3}{r} q_4)/q_1$ and $\bar{V}^2 + (q_2^2 + q_3^2 + q_4^2)/q_1^2$. The terms q_i, $i = 1, 5$ are the components of the dependent variable of integration Q in Eq. (2). To obtain, for example, A, let $k_o = \xi_t$, $k_1 = \xi_z$, $k_2 = \xi_r$ and $k_3 = \xi_\phi$ in Eq. (5).

As a measure of the productivity of the implicit algorithm to be described below compared to that of conventional explicit procedures, the value of the Courant number can be computed. It requires the eigenvalues of the matrices A, B, and C. They are as follows:

$$\sigma_{1,2,3} = k_0 + uk_1 + vk_2 + \frac{w}{r} k_3$$

and

$$\sigma_{4,5} = k_0 + uk_1 + vk_2 + \frac{w}{r} k_3 \pm C\left|k_1^2 + k_2^2 + \left(\frac{k_3}{r}\right)^2\right|^{1/2}$$

where for A, $k_o = \xi_t$, etc.; for B, $k_o = \eta_t$, etc.; for C, $k_o = \zeta_t$, etc.; and c equals the local speed of sound ($c^2 = \gamma p/p$). The Courant number is defined as follows:

$$CN = \Delta\tau/|\sigma_{max}| \qquad (7)$$

where it is assumed that $\Delta\xi = \Delta\eta = \Delta\zeta = 1$, and σ_{max} is the maximum value of the eigenvalues of all the nodal points.

For the prop-fan problem described here, Eq. (2) is solved in a time-asymptotic fashion with interest only in

the steady-state solution. This is a result of the mesh rotating with the blade and the fact that a cylindrical coordinate system is used. The Q_τ term of Eq. (2) approaches zero as τ becomes large, thus establishing a convergence criterion.

4.2. Numerical Method

The numerical algorithm used to solve the conservation-law form of the Euler equations is based on a class of completely implicit, noniterative, ADI (alternating direction implicit) schemes developed by Lindemuth and Killeen[1], Briley and McDonald[2,3], and Beam and Warming[4,5]. The particular method is a generalization of a conservative, approximate factorization scheme in the "delta" form[4]. The procedure has been successfully applied by Steger and Kutler[6] and Kutler[7] for inviscid flows and by Steger[8], Pulliam and Steger[9], and numerous others, Refs. 10 and 13, for viscous flows. Use of the implicit procedure helps remove the stiffness of the problem introduced by a fine mesh. Thus, for this problem the implicit procedure permits an integration stepsize large enough to obtain steady-state solutions in considerably fewer iterations than conventional explicit procedures.

As applied to Eq. (2) the implicit, spatially factored algorithm using Euler implicit time differencing takes the form

$$|I + \Delta t\delta_\xi A^n - \varepsilon_i(J^{-1}\nabla_\xi\Delta_\xi J)^n||I + \Delta t\delta_\eta B^n - \varepsilon_i(J^{-1}\nabla_\eta\Delta_\eta J)^n|$$
$$|I + \Delta t\delta_\zeta C^n - \varepsilon_i(J^{-1}\nabla_\zeta\Delta_\zeta J)^n|\ (Q^{n+1} - Q^n) =$$
$$-\Delta t|\delta_\xi E^n + \delta_\eta F^n + H^n + \delta_\zeta G^n| - \frac{\varepsilon_e}{8}(J^n)^{-1}|(\nabla_\xi\Delta_\xi)^2$$
$$+ (\nabla_\zeta\Delta_\zeta)^2 + (\nabla_\eta\Delta_\eta)^2|\ (JQ)^n \qquad (8)$$

where A, B, and C are the Jacobian matrices $\partial E/\partial U$, $\partial F/\partial U$, and $\partial G/\partial U$, respectively, and I is the identity matrix. δ_ξ and δ_η are second-order central-difference operators, and ∇ and Δ represent the conventional forward and backward difference operators. The quantities multiplied by ε_i on the left-hand side of the equation represent implicit second-order smoothing terms (which were added later to the basic algorithm[8,9]) while the quantity multiplied by ε_e on the right-hand side represents an explicit fourth-order smoothing term.

The solution of Eq. (8) consists of first forming the right-hand term (also called the steady-state or explicit part) at each grid point. Each of the implicit operators, (for instance $\{I + \Delta t\ \delta_\xi\ A^n - \varepsilon_i(J^{-1}\nabla_\xi\Delta_\xi J)^n\}$) represent block-tridiagonal matrices which must be inverted sequentially

to obtain $\Delta Q^n = Q^{n+1} - Q^n$. A block lower-upper-decomposition algorithm, see Isaacson and Keller[12], is used for the inversion process.

For steady-state calculations $\Delta Q^n = Q^{n+1} - Q^n \to 0$ and the solution then satisfies the steady-state finite-difference (right-hand side of Eq. (8)) equations. Linear stability analysis shows unconditional stability for the "delta" form of the implicit approximate factorization algorithm. In actual practice, though, time step limitations are encountered, although they are usually much less stringent than explicit stability bounds. The smoothing terms have been added to control nonlinear instabilities. Choices of the time step Δt and the smoothing coefficients $(\varepsilon_e, \varepsilon_i)$ are usually dictated by experience. Linear analysis for the smoothing terms does show that for $\varepsilon_i = 0$, ε_e is bounded ($\varepsilon_e < 1/4$) for stability, but for $\varepsilon_i >> \varepsilon_e$, ε_e is not constrained to any limit for stability.

The metric terms are obtained using second-order finite-differences for terms such as, z_ξ, in Eqs. (4). Fourth-order accuracy in the steady-state can be obtained in an efficient manner by introducing fourth-order finite differences for the convective terms on the right-hand side of Eq. (8), while retaining second-order differences on the left-hand side. For Euler implicit time differencing this is a stable and accurate process. For more details on the above, see Pulliam and Steger[9].

The major portion of the computational work in an implicit finite-difference algorithm is contained in the solution of the set of simultaneous equations, (i.e., the block tridiagonal equations). When even an implicit algorithm is applied to a system of partial differential equations, one obtains block matrix-vector equations that are complicated and time-consuming to solve. A method for uncoupling the solution process through a diagonalization of the block-matrix structure has been presented by Pulliam and Chaussee[13]. The method was applied to an implicit approximate-factorization algorithm for the two- and three-dimensional inviscid Euler equations in general curvilinear coordinates.

The Jacobian matrices, A, B, and C, have a set of eigenvalues and a complete distinct set of eigenvectors. Similarity transformations (see Warming, Beam, and Hyett[14]) can be used to diagonalize A, B, and C where

$$A = T_\xi \hat{\Lambda}_\xi T_\xi^{-1} , \qquad B = T_\eta \hat{\Lambda}_\eta T_\eta^{-1} , \qquad C = T_\zeta \hat{\Lambda}_\zeta T_\zeta^{-1} \tag{9a}$$

$$\hat{\Lambda}_\xi = D\left[U,U,U,U + c(\xi_z^2 + \xi_r^2 + \xi_{\phi/r^2}^2)^{\frac{1}{2}},\ U - c(\xi_z^2 + \xi_r^2 + \xi_{\phi/r^2}^2)^{\frac{1}{2}}\right]$$

$$\hat{\Lambda}_\eta = D\left[V,V,V,V + c(\eta_z^2 + \eta_r^2 + \eta_{\phi/r^2}^2)^{\frac{1}{2}},\ V - c(\eta_z^2 + \eta_r^2 + \eta_{\phi/r}^2)^{\frac{1}{2}}\right]$$

$$\hat{\Lambda}_\zeta = D\left[W,W,W,W + c(\zeta_z^2 + \zeta_r^2 + \zeta_{\phi/r^2}^2)^{\frac{1}{2}},\ W - c(\zeta_z^2 + \zeta_r^2 + \zeta_{\phi/r}^2)^{\frac{1}{2}}\right] \tag{9b}$$

with

$$
T_k = \left[\begin{array}{c|c|c|c|c}
\tilde{k}_z & \tilde{k}_r & \tilde{k}_{\phi/r} & \alpha & \alpha \\
\hline
\tilde{k}_z u & \tilde{k}_r u - \tilde{k}_z \rho & \tilde{k}_{\phi/r} u + \tilde{k}_r \rho & \alpha(u + \tilde{k}_z c) & \alpha(u - \tilde{k}_z c) \\
\hline
\tilde{k}_z v + \tilde{k}_{\phi/r} \rho & \tilde{k}_r v & \tilde{k}_{\phi/r} v - \tilde{k}_z \rho & \alpha(v + \tilde{k}_r c) & \alpha(v - \tilde{k}_r c) \\
\hline
\tilde{k}_z w - \tilde{k}_r \rho & \tilde{k}_r w + \tilde{k}_z \rho & \tilde{k}_{\phi/r} w & \alpha(w + \tilde{k}_{\phi/r} c) & \alpha(w - \tilde{k}_{\phi/r} c) \\
\hline
\tilde{k}_z \frac{\phi^2}{(\gamma-1)} & \tilde{k}_r \frac{\phi^2}{(\gamma-1)} & \tilde{k}_{\phi/r} \frac{\phi^2}{(\gamma-1)} & \alpha \left\{ \frac{\phi^2 + c^2}{(\gamma-1)} \right. & \alpha \left\{ \frac{\phi^2 + c^2}{(\gamma-1)} \right. \\
+ \rho(\tilde{k}_{\phi/r} v - \tilde{k}_r w) & + \rho(\tilde{k}_z w - \tilde{k}_{\phi/r} u) & + \rho(\tilde{k}_r u - \tilde{k}_z v) & + c\tilde{\theta} \Big\} & - c\tilde{\theta} \Big\}
\end{array}\right] \qquad (9c)
$$

where $\tilde{\theta} = \tilde{k}_z u + \tilde{k}_r v + \tilde{k}_{\phi/r} w$ and, for example, $\tilde{k}_z = k_z/(k_z^2 + k_r^2 + k_{\phi/r^2}^2)^{\frac{1}{2}}$, etc. and $k = \xi$ for $\hat{A}$, $k = \eta$ for $\hat{B}$, and $k = \zeta$ for $\hat{C}$. Also $\phi^2 = 0.5(\gamma-1)(u^2+v^2+w^2)$, $\alpha = \rho c/2$ and $\beta = 1/\alpha$.

The similarity transformations are applied to Eq. (8) and then a modified form is obtained by moving T_ξ, T_η, and T_ζ outside of the difference operators δ_ξ, δ_η, and δ_ζ, respectively. This results in the diagonal form

$$T_\xi^n|I + h\delta_\xi \hat{\Lambda}_\xi^n|N|I + h\delta_\eta \hat{\Lambda}_\eta^n|\hat{P}|I + h\delta_\zeta \hat{\Lambda}_\zeta^n|(T_\zeta^{-1})^n \Delta Q^n = \hat{R}^n \qquad (10a)$$

with $\hat{N} = T_\xi^{-1} T_\eta$, $\hat{N}^{-1} = T_\eta^{-1} T_\xi$, $\hat{P} = T_\eta^{-1} T_\zeta$, $\hat{P}^{-1} = T_\zeta^{-1} T_\eta$,

where

$$T_k^{-1} T_z = \begin{bmatrix} m_1 & m_2 & m_3 & -\mu m_4 & \mu m_4 \\ -m_2 & m_1 & m_4 & \mu m_3 & -\mu m_3 \\ -m_3 & -m_4 & m_1 & -\mu m_2 & \mu m_2 \\ \mu m_4 & -\mu m_3 & \mu m_2 & \mu^2(1+m_1) & \mu^2(1-m_1) \\ -\mu m_4 & \mu m_3 & -\mu m_2 & \mu^2(1-m_1) & \mu^2(1+m_1) \end{bmatrix} \qquad (10b)$$

$$m_1 = \tilde{k}_x \tilde{l}_x + \tilde{k}_y \tilde{l}_y + \tilde{k}_z \tilde{l}_z, \quad m_3 = \tilde{k}_x \tilde{l}_z - \tilde{k}_z \tilde{l}_x,$$
$$m_2 = \tilde{k}_x \tilde{l}_y - \tilde{k}_y \tilde{l}_x, \quad m_4 = \tilde{k}_y \tilde{l}_z - \tilde{k}_z \tilde{l}_y,$$
$$\text{and} \quad \mu = 1/\sqrt{2}$$

The source term and smoothing terms are dropped for simplicity.

The right-hand side, $\hat{R}^n$, is exactly the same as in Eq. (8) and is formed in the same way. The implicit part of the algorithm now consists of 5x5 matrices, (i.e., T_ξ^n) and scalar tridiagonal operators, since, for example, $|I + h\delta_\xi \hat{\Lambda}_\xi|$ is made up of diagonal blocks. Therefore, the implicit part of the solution process consists of 3 matrix-vector multiplies (i.e., $T_\xi^{-1}\hat{R}$) and 5 scalar tridiagonal inversions per direction (i.e., $|I + h\delta_\xi \hat{\Lambda}_\xi|^{-1} T^{-1}\hat{R}$). This produces a substantial reduction in the total number of operators required for the implicit algorithm over the standard form.

Pulliam and Chaussee[13] show that the diagonal algorithm retains the stability and convergence properties of the standard algorithm. Also, since the right-hand side is identical for the two algorithms, the steady-state solution is not affected by the diagonalization. Reductions in CPU time of up to 30% can be realized by using the diagonal form.

4.3. Geometry and Mesh Generation Descriptions

The generation of a computational mesh for calculating the flow through and around a Prop-Fan configuration consists of three steps. Step one is composed of generating an x-y-z system of points given the coordinates of the nacelle and blades. Step two consists of reading the x-y-z locations of step one and forming a system of parametric cubic patches.

Step three takes the patches of step two and based on the specified clustering and/or stretching of points, creates a mesh which is used by the computational code.

The geometry for the blade, spinner, and nacelle are provided by the user. These characteristics, shown in Figures 3 and 4, consist of the blade twist in degrees, $\Delta\beta$, based on the blade angle at 75% blade radius, the local blade chord ratio, b/D, and the leading edge alignment ratio, LEA/D, where D is the tip diameter. The thickness ratio distribution for each section is also needed in tabular form. The ultimate goal of this part of the mesh generation scheme was to smoothly transition from the twisting and tapering of the blade to a set of surfaces which have zero twist or taper above an $r/D = 1$ and with slope $d\phi/dz = 0$ at the stagnation point of the nacelle and a zero slope at some specified distance downstream from the blade trailing edge. The two transition curves which are employed in this part of the analysis are parabolic and cubic curve fits. These curves allow for end points and/or slopes at the end points to be specified in the transitioning process. For the case of a parabola the following equations and conditions are used.

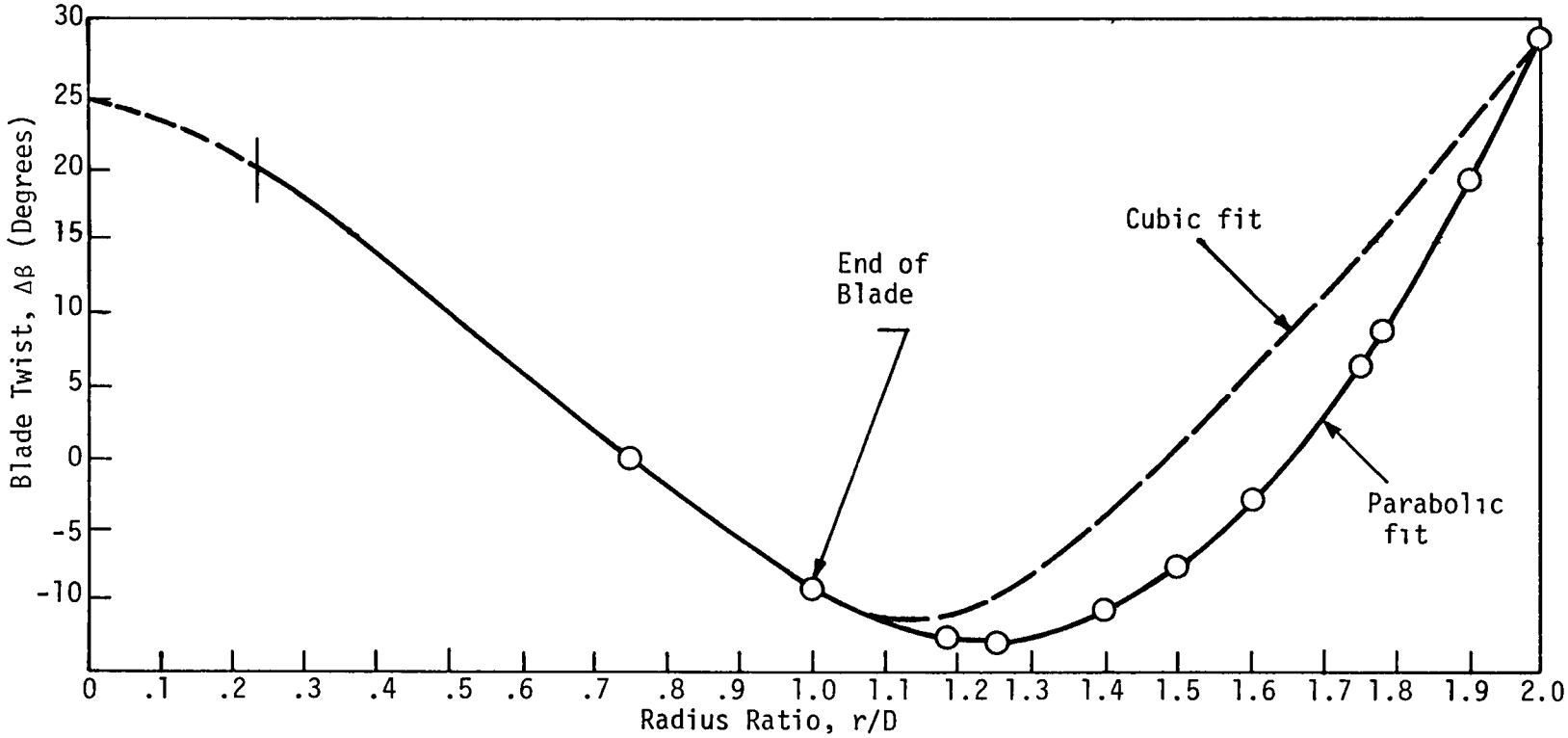

Figure 3. Prop-Fan Blade Characteristics--Blade Twist

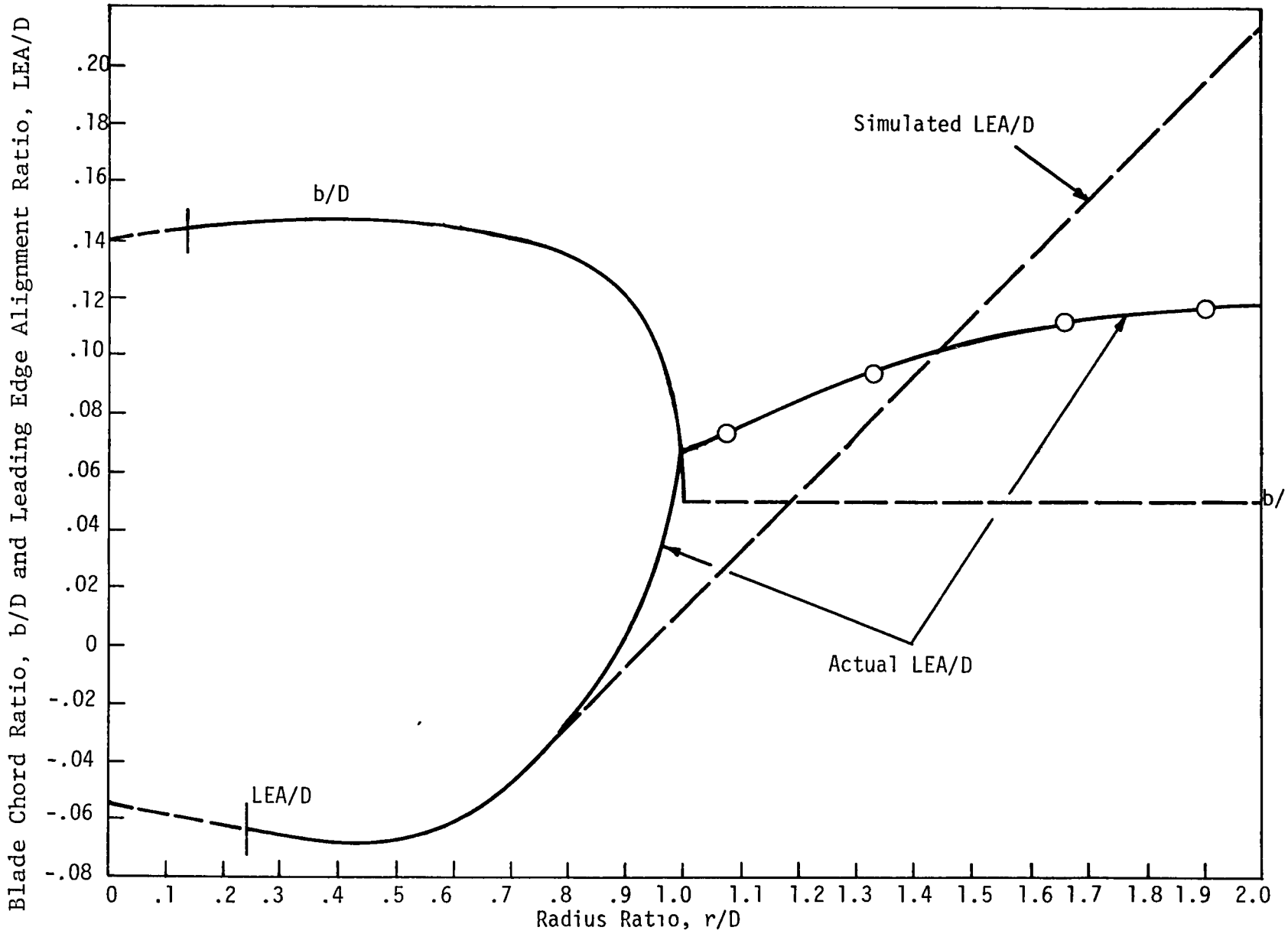

Figure 4. Prop-Fan Blade Characteristics--Blade Chord Ratio and Leading Edge Alignment Ratio

General Equation: $Y = aX^2 + bX + c$

Given: $X_{initial}$ X_{final} $Y_{initial}$, Y_{final}, and $\frac{dY}{dX}_{initial}$

Final form of the coefficients:

$$a = \frac{Y_i'}{X_i - X_f} + \frac{(Y_f - Y_i)}{(X_f - X_i)^2}$$

$$b = -Y_i' \frac{(X_i + X_f)}{(X_i - X_f)} - 2X_i \frac{(Y_f - Y_i)}{(X_f - X_i)^2} \qquad (11)$$

$$c = Y_f - X_f \; Y_i' \frac{X_i}{(X_f - X_i)} + (X_f - 2X_i) \frac{(Y_f - Y_i)}{(X_f - X_i)^2}$$

where subscripts i and f stand for initial and final conditions, respectively.

If a cubic is used, the following equations and conditions are used.

General Equation: $X = aY^3 + bY^2 + cY + d$

Given: $X_{initial}$ X_{final} $X'_{initial}$ $Y_{initial}$, Y_{final}, X'_{final}

Final form of the coefficients:

$$a = \frac{2(X_f - X_i) - (Y_f - Y_i)(X_f' + X_i')}{-(Y_f - Y_i)^3}$$

$$b = \frac{(X_f - X_i) - X_i'(Y_f - Y_i)}{(Y_f - Y_i)^2} - a \cdot (Y_f + 2Y_i)$$

$$c = X_i' - b \cdot (2Y_i) - a \cdot (3Y_i^2) \qquad (12)$$

$$d = X_f - a \cdot (Y^3) - b \cdot (Y^2) - c \cdot (Y)$$

where the subscripts i and f are the same as before. A user has to be careful when using cubics or parabolas.

Once these surfaces shown in Figure 5 have been specified, it is an easy matter to extend the surfaces at constant values of any specified outer boundary. Usually this boundary is chosen to be far enough removed from the configuration such that there are no outer interactions effecting the computation. If a tunnel wall is to be specified, this would become the outer boundary.

This whole procedure is automated with only outer boundary points and/or slopes specified in addition to the coordinates of the blade and nacelle surfaces. These parameters are presented in Figure 5.

Step 2 is a self sufficient part of the grid generation program. An x-y-z set of points from step one is all that is necessary to create a series of parametric cubic patches which describes the entire mesh system in terms of cubic equations.

In this section, an attempt will be made to briefly familiarize the user with terminology and definitions associated with the creation of a parametric cubic patch interpolation surface. This section is not intended to be a comprehensive narrative on parametric cubic interpolation. A far better approach to understanding the subject would begin with a thorough study of curves. Since this would be beyond the scope of this report, only three-dimensional

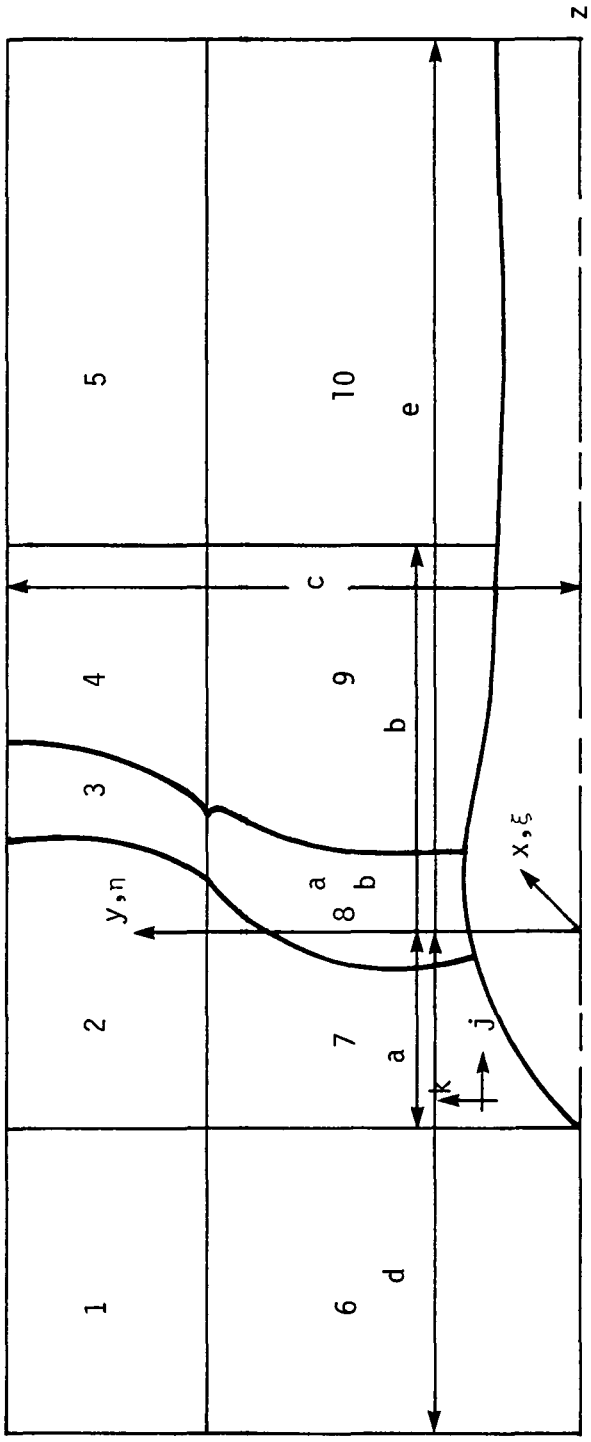

Figure 5. Patch Numbering System

surfaces will be treated. The main purpose is to orient the user prior to presenting the user instructions in a following section.

The basic element of the mesh generation code is the parametric bicubic patch. The patch represents a continuous mapping of a portion of the three-dimensional surface into a unit square by means of the equation

$$r(u,w) = \sum_{i=1}^{4} \sum_{j=1}^{4} A_{ij}\, u^{i-1}\, w^{j-1} \quad (0 \le u,\ w \le 1) \qquad (13)$$

This rather simple equation lends itself to fast, efficient computation. From a practical standpoint, the most important aspect of this equation is the determination of the coefficients $\vec{A}_{ij}$. The coefficients $\vec{A}_{ij}$ are referred to as the algebraic form of the patch coefficients. Although this form permits efficient evaluation, it reveals very little information about the patch or how a user might determine the $\vec{A}_{ij}$. Using matrix notation, Equation (13) can also be written in the form

$$\vec{r}(u,w) = U\vec{M}\vec{B}\vec{M}^{T}W^{T} \qquad (14)$$

where U and W are the vectors $(u^3, u^2, u, 1)$ and $(w^3, w^2, w, 1)$, and the matrix, M, is given by

$$M = \begin{bmatrix} 2 & -2 & 1 & 1 \\ -3 & 3 & -2 & -1 \\ 0 & 0 & 1 & 0 \\ 1 & 0 & 0 & 0 \end{bmatrix} \qquad (15)$$

The vector matrix $\vec{B}$ is referred to as the geometric form of the patch coefficients and consists of the following elements:

$$\vec{B} = \begin{bmatrix} \vec{r}(0,0) & \vec{r}(0,1) & \frac{\partial \vec{r}}{\partial w}(0,0) & \frac{\partial \vec{r}}{\partial w}(0,1) \\ \vec{r}(1,0) & \vec{r}(1,1) & \frac{\partial \vec{r}}{\partial w}(1,0) & \frac{\partial \vec{r}}{\partial w}(1,1) \\ \frac{\partial \vec{r}}{\partial u}(0,0) & \frac{\partial \vec{r}}{\partial u}(0,1) & \frac{\partial^2 \vec{r}}{\partial u \partial w}(0,0) & \frac{\partial^2 \vec{r}}{\partial u \partial w}(0,1) \\ \frac{\partial \vec{r}}{\partial u}(1,0) & \frac{\partial \vec{r}}{\partial u}(1,1) & \frac{\partial^2 \vec{r}}{\partial u \partial w}(1,0) & \frac{\partial^2 \vec{r}}{\partial u \partial w}(1,1) \end{bmatrix} \qquad (16)$$

Most notable about the geometric form of the patch coefficients is that it contains information evaluated only at the patch corner points. In this form, all elements but the lower right-hand quadrant in Equation (16) become geometrically identifiable as corner point locations and tangent vectors. In fact, using the boundary curve numbering convention shown in Figure 6 the first two rows of B completely specify boundary curves 1 and 3 while the first two columns specify curves 2 and 4.

Thus, 12 of the 16 elements of $\vec{B}$ may be determined from knowledge of the patch boundary curves. It should be mentioned that while Figure 6 shows the patch having four distinct boundary curves, degenerate cases often occur in practice

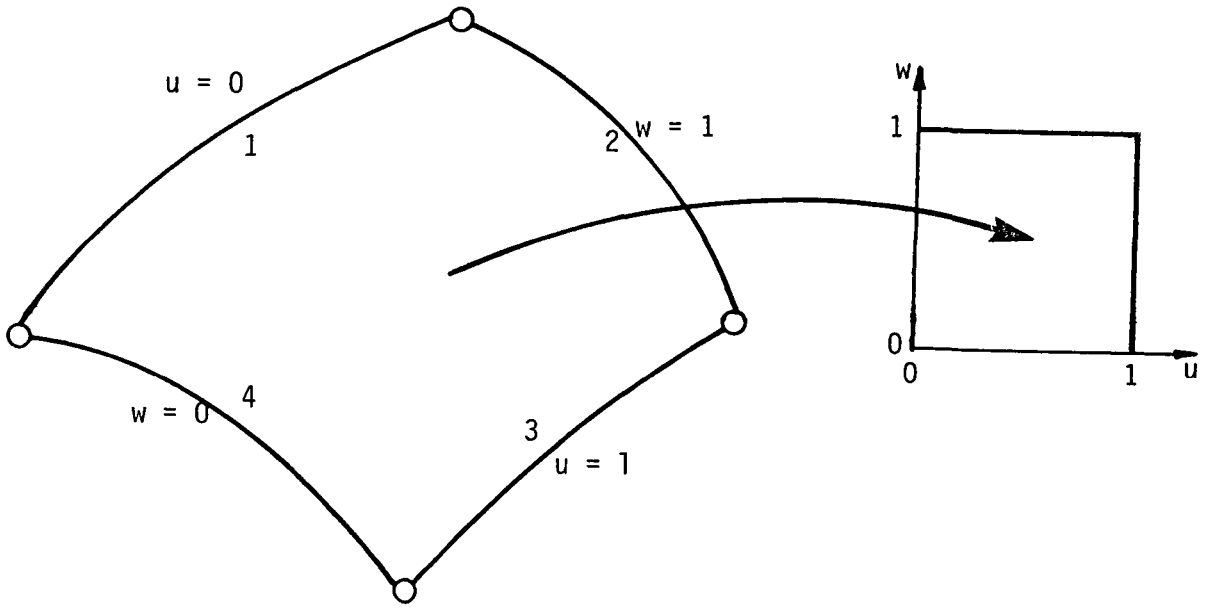

Figure 6. Mapping of the Patch from Physical Space to Parametric Space

where one or more of the curves reduce to a point. The mixed derivatives control the behavior of the interpolation surface in the interior of the patch. When Coons originally formulated the patch concept, the mixed derivatives, or twist vectors as they are referred to in the literature, were identically zero. Thus, the entire patch depended only on the nature of the boundary curves. Although the simplicity of this concept is attractive, the attendant loss of capability is considered unacceptable.

One of the more subtle features of parametric interpolation concerns the parameters themselves. The unspecified relationship between the parameter and physical arc length creates an additional degree of freedom. To illustrate this point, consider a single curve segment to be represented by a parametric cubic of the form

$$r(\vec{u}) = \sum_{i=1}^{4} \vec{A}_i u^{i-1} \tag{17}$$

The coefficients $\vec{A}_i$ may be determined by specifying $\vec{r}$ and $\frac{d\vec{r}}{du}$ at the curve end points. At first glance, this appears to be equivalent to specifying the end-point locations and slopes. However, the end-point slopes or direction cosines are represented by unit vectors $\frac{d\vec{r}}{ds}$ where s is the arc length along the curve. Thus,

$$\frac{d\vec{r}}{du} = \frac{d\vec{r}}{ds} \cdot \frac{ds}{du} \tag{18}$$

An entire family of parametric cubic curves can be created which satisfies the same end-point conditions by varying the assumed value of $\frac{ds}{du}$ at either end-point. Specifying end-point locations and slopes for an ordinary cubic (e.g., y(x)) determines a single unique curve.

The determination of the twist vectors at the patch corner points is much more difficult since they are not as geometrically identifiable as are the slopes or point locations.

For this reason, the methods used in the present program remove this burden from the user.

Finally, this allows for full geometric derivative information available for any part of the mesh since the cubic functions are analytical in nature. The coefficients of the cubics are stored off line during the computational cycle to be available whenever needed in step 3.

In the third and final step, the computational mesh used in the flow field code is created from the series of patches in step 2.

Capsulizing, the overall procedure, steps one through three, has been automated (overlayed on the computer) to the extent that a user need only furnish the x-y-z points of: the blades, the location of the upstream, outer and downstream boundaries, and the spacing of the points in such critical regions as the leading and trailing edge of the blades, the tip region of the blade, and the region in close proximity to the nacelle surface. The final mesh is then created and stored on disc or tape for future use by the flow field code. It should be noted that the mesh should be displayed via computer generated plots. This allows for an evaluation of the grid system before it is actually used in conjunction with the flow field code.

4.4. Boundary and Initial Conditions

The interior of the computational domain is solved implicitly by integrating the Euler equations. To complete the problem, boundary conditions must be specified on all surfaces of the computational volume. On the impermeable surfaces (blade, spinner, nacelle), a surface tangency conditions is imposed. This consists of employing schemes, with as much accuracy as possible, such as Kentzer's method, a normal momentum approach as is done in the present code, or the method of characteristics. At the upstream and downstream boundaries, anechoic like boundary conditions will be imposed. Free-stream values are used at radial far-stream boundaries with the exception being tunnel walls. These would require the tangency condition to be applied. In the region of the blade leading and trailing edges and at the blade tip a Kutta condition is used as in the usual airfoil analysis to allow for the flow to leave the surface of the blade smoothly.

The following sections discuss ways of making the tangency condition at the blade and nacelle surfaces more exact, applying a three-dimensional Kutta-like condition and applying a subsonic outflow condition.

4.4.1. Tangency Condition

Presently a straightforward approach is used at both the blade and nacelle surfaces to satisfy tangency. This consists in the case of the blade surface, of specifying the appropriate contravarient velocity to be zero (no flow through the surface) $\bar{w} = 0$ and solving, along the $\xi(x,y,z,t)$ = constant surface, the system of equations

$$\begin{bmatrix} u \\ v \\ w \end{bmatrix} = J^{-1} \begin{bmatrix} (\eta_r\zeta_\phi - \eta_\phi\zeta_r)/r & -(\xi_r\zeta_\phi - \xi_\phi\zeta_r)/r & (\xi_r\eta_\phi - \eta_r\xi_\phi)/r \\ -(\eta_z\zeta_\phi - \eta_\phi\zeta_z)/r & (\xi_z\zeta_\phi - \xi_\phi\zeta_z)/r & -(\xi_z\eta_\phi - \xi_\phi\eta_z)/r \\ (\eta_z\zeta_r - \eta_r\zeta_z) & -(\xi_z\zeta_r - \xi_r\zeta_z) & (\xi_z\eta_r - \xi_r\eta_z) \end{bmatrix} \begin{bmatrix} \bar{u} - \xi_t \\ \bar{v} - \eta_t \\ \bar{w} - \zeta_t \end{bmatrix} \tag{19}$$

to obtain the cylindrical components of velocity u, v, and w. To solve this system, a complete set of contravariant velocities must be known and thus the $\bar{u}$ and $\bar{v}$ contravariant velocities are linearly extrapolated from known data on the interior. The pressure is obtained by zeroth-order extrapolation from the interior field and the density is calculated either by assuming constant entropy on the surface or by zeroth-order extrapolation. This completes the set of equations for the boundary conditions at the nacelle and blade surfaces.

Unfortunately due to the extrapolation of the variables, the condition of total rothalpy equals a constant throughout the flow field is not satisfied. The total rothalpy is defined in a rotating system as

$$H_R = H_t - 2r\omega w \tag{20}$$

where $H_t = \frac{\gamma}{\gamma-1}\frac{p}{\rho} + \frac{1}{2}(u^2 + v^2 + w^2)$ is the definition of total enthalpy in a non-rotating system. It can be seen that rothalpy and enthalpy equal each other if the system is not rotating. In a uniform free stream, the total rothalpy is defined as

$$H_R = \frac{\gamma}{\gamma-1}\frac{p_\infty}{\rho_\infty} + \frac{1}{2}(u_\infty^2 + v_\infty^2 + w_\infty^2) \tag{21}$$

and it is held fixed at this value throughout the computational domain. In the following development, it is assumed the pressure was obtained by extrapolation, the density from the constant entropy relation

$$\rho = \left(\frac{p}{S}\right)^{\frac{1}{\gamma}} \tag{22}$$

where $S = \frac{p_\infty}{\rho_\infty^{\gamma}}$

and the cylindrical velocities by solving the system of Eq. (19). There are three surfaces along which tangency has to be satisfied:

I. Blade surface

II. Nacelle surface

III. Blade-nacelle intersection.

At the blade surface, the contravariant velocity

$$\bar{w} = \zeta_t + u\zeta_z + v\zeta_r + \frac{w}{r}\zeta_\phi = 0 \tag{23}$$

and the total rothalpy, H_R

$$u^2 + v^2 + w^2 - 2r\omega w = 2(H_R - \frac{\gamma}{\gamma-1}\frac{p}{\rho}) \tag{24}$$

are known. Since there are two equations in the three unknowns u, v, and w, one of the velocity components, u, is accepted as being correct. The remaining components, v and w are found by solving Eqs. (23) and (24), simultaneously. Doing this gives the v-velocity and w-velocity in terms of the accepted u-velocity and they are written as

$$\left.\begin{aligned} w &= r\omega + \left[\frac{-\tilde{b} \pm \sqrt{\tilde{b}^2 - 4\tilde{a}\tilde{c}}}{2\tilde{a}}\right] \\ v &= -\frac{1}{\zeta_r}\left[u\zeta_z + (w - r\omega)\frac{\zeta_\phi}{r}\right] \end{aligned}\right\} \tag{25}$$

where $\tilde{a} = 1$

$$\tilde{b} = \frac{2ur\zeta_z}{\zeta_\phi}$$

$$\tilde{c} = \frac{r^2}{\zeta_\phi^2}\left[u^2\zeta_z^2 - \zeta_r^2\{2(H_R - \frac{\gamma}{\gamma-1}\frac{p}{\rho}) - u^2 + r^2\omega^2\}\right]$$

By using Eq. (25), the variables at the blade surface satisfy both surface tangency and the fact that total rothalpy equals a constant.

At the nacelle surface, the contravariant velocity

$$\bar{v} = \eta_t + u\eta_z + v\eta_r + \frac{w}{r}\eta_\phi = 0 \tag{26}$$

and the total rothalpy, Eq. (21), are known. In this case, the w velocity is accepted and Eqs. (24) and (26) are solved simultaneously to yield

$$u = \left[\frac{2r\omega w - w^2 + 2\left(H_R - \frac{\gamma}{\gamma-1}\frac{p}{\rho}\right)}{1 + \frac{\eta_z^2}{\eta_r^2}} \right]^{\frac{1}{2}} \tag{27}$$

and

$$v = -\frac{\eta_z}{\eta_r} u \tag{28}$$

Once again, the conditions of surface tangency and total rothalpy equals a constant are satisfied when Eqs. (27) and (28) are used in conjunction with the fact that w, p, and ρ are known.

The final case occurs when the blade and nacelle intersect. At this junction both Eqs. (23) and (26) are satisfied due to a simultaneous condition of surface tangency on the blade and nacelle surfaces. Accepting the pressure, p, and the density, ρ, the cylindrical velocity components are calculated from

$$v = \left[\frac{\eta_z^2 \zeta^2 \left(2\left\{H_R - \frac{\gamma}{\gamma-1}\frac{p}{\rho}\right\} + r^2\omega^2\right)}{\zeta_\phi^2\{\eta_r^2 + \eta_z^2\} + r^2\{\eta_r\zeta_z - \zeta_r\eta_z\}^2} \right]^{\frac{1}{2}} \tag{29}$$

and

$$u = -v\frac{\eta_r}{\eta_z} \tag{30}$$

and

$$w = r\omega + \frac{vr}{\eta_z \zeta_\phi} (\eta_r \zeta_z - \zeta_r \eta_z) \tag{31}$$

These velocity components satisfy both surface tangency and the condition of total rothalpy equals constant at the blade nacelle intersection.

4.4.2. Kutta Condition

This is a hypothesis put forth by Kutta and Joukowsky to allow the inviscid flow past an airfoil to have a form approximating an ideal one and yet be physically possible. This hypothesis is necessary since no fluid can flow around a sharp trailing edge--because any velocity around an arc of zero radius would mean an infinite acceleration. The flow no sooner starts than it finds itself sliding tangentially past the trailing edge which approximates the physical situation.

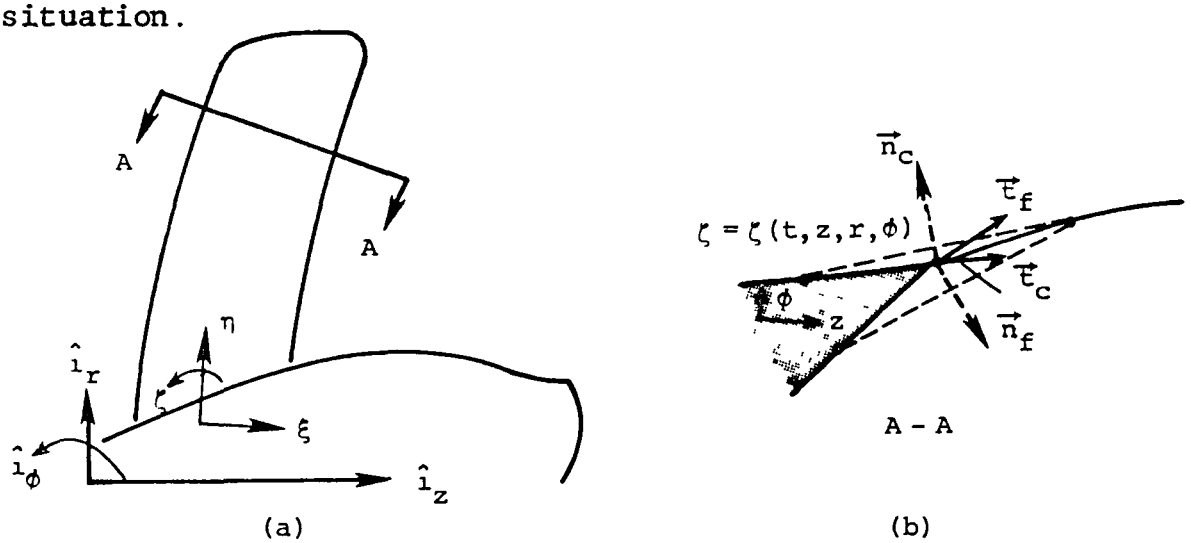

Figure 7. Kutta Condition Geometry

In general, the unit normal to a ζ = constant surface, Figure 7, is written

$$\hat{n} = \frac{\zeta_z \hat{i}_z + \zeta_r \hat{i}_r + \frac{\zeta_\phi}{r} \hat{i}_\phi}{(\zeta_z^2 + \zeta_r^2 + \{\frac{\zeta_\phi}{r}\}^2)^{\frac{1}{2}}} \tag{32}$$

To implement the Kutta-Joukowsky condition, the unit normals of the face side and of the camber side are calculated and then these vectors are used to form a plane which is normal to the trailing edge of the blade and any given radial location. The resulting procedure is as follows. First form the unit normals

$$\hat{n}_c = \left. \frac{\zeta_z \hat{i}_z + \frac{\zeta_\phi}{r} \hat{i}_\phi}{(\zeta_z^2 + \{\frac{\zeta_\phi}{r}\}^2)^{\frac{1}{2}}} \right|_{\text{camber}} \tag{33}$$

and

$$\hat{n}_f = \left. \frac{\zeta_z \hat{i}_z + \frac{\zeta_\phi}{r} \hat{i}_\phi}{(\zeta_z^2 + \{\frac{\zeta_\phi}{r}\}^2)^{\frac{1}{2}}} \right|_{\text{face}} \tag{34}$$

Since two vectors from a plane, the scalar product of Eqs. (33) and (34) is performed to give

$$\hat{n}_c \cdot \hat{n}_f = |\hat{n}_c| |\hat{n}_f| \cos\theta \tag{35}$$

which defines the angle θ between these vectors in the plane.

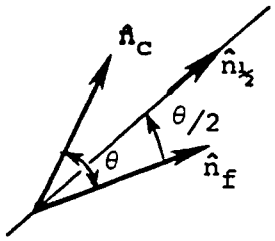

Figure 8. Vector Representation

The desired result is finding a vector which bisects the unit normals $\hat{n}_c$ and $\hat{n}_f$. This is written

$$\hat{n}_c \cdot \hat{n}_{\frac{1}{2}} = |\hat{n}_c|^{1} |\hat{n}_{\frac{1}{2}}| \cos \theta/2 \tag{36}$$

$$\hat{n}_f \cdot \hat{n}_{\frac{1}{2}} = |\hat{n}_f|^{1} |\hat{n}_{\frac{1}{2}}| \cos \theta/2 \tag{37}$$

$$\hat{n}_{\frac{1}{2}} = 1 \tag{38}$$

Equations (36), (37), and (38) form a set of three equations in three unknowns and are cast in the following form

$$\begin{aligned} \hat{n}_{\frac{1}{2}} &= a\hat{i}_z + b\hat{i}_r + c\hat{i}_\phi \\ \hat{n}_c &= d\hat{i}_z + e\hat{i}_r + f\hat{i}_\phi \\ \hat{n}_f &= r\hat{i}_z + s\hat{i}_r + t\hat{i}_\phi \end{aligned} \tag{39}$$

where the coefficients d, e, f, r, s, and t are known from the metrics and a, b, and c are the unknown quantities. From Figure 8 the angle θ is determined from

$$\hat{n}_c \cdot \hat{n}_f = \cos\,\theta = d\cdot r + e\cdot s + f\cdot t \tag{40}$$

the system of Eqs. (39) and (40) are solved for

$$\begin{aligned} a &= \frac{1}{d}\cos\theta/2 - e\cdot b - f\cdot c \\ b &= A - c\cdot B \\ c &= \frac{-B_c \pm \sqrt{B_c^2 - 4A_c\,C_c}}{2A_c} \end{aligned} \tag{41}$$

where

$$A = \left(\frac{r - d}{er - S\cdot d}\right)\cos\,\theta/2$$

$$B = \frac{f\cdot r - t\cdot d}{e\cdot r - S\cdot d}$$

$$A_c = d^2(B^2 + 1) + f^2 + e^2\cdot B^2 - 2f\cdot e\cdot B$$

$$B_c = 2\{(eB - f)\cos\,\theta/2 + e\cdot f\cdot A - e^2\cdot AB - A\cdot B\cdot d^2\}$$

$$C_c = d^2(A^2 - 1) + e^2A^2 + \cos^2\,\theta/2 - 2e\cdot A\cdot\cos\,\theta/2$$

The velocity vector at the trailing edge is required to lie in the direction of the unit normal $\hat{n}_{\frac{1}{2}}$. The pressure is obtained by averaging the values from the camber and face side of the blade and the density is obtained from the

definition of total rothalpy after the velocity components have been adjusted such that they vectorially lie in the direction of the unit normal $\hat{n}_{\frac{1}{2}}$ which bisects the unit normals of the camber and face side of the blade.

This same procedure with slight modifications could be used at the tip of the blade to assure the flow leaves the tip smoothly rather than attempting an infinite acceleration around the tip.

4.4.3. Subsonic Outflow

The relationships enforcing boundary conditions at the subsonic outflow are determined from the governing partial differential equations using the theory of the method of characteristics (MOC). The flow for this study is considered to be nonviscous and non-heat conducting. The equations cast in cylindrical coordinates for nonviscous, non-heat conducting, adiabatic, compressible flow are given below.

Continuity

$$\frac{\partial \rho}{\partial t} + \rho\frac{\partial u}{\partial z} + u\frac{\partial \rho}{\partial z} + \frac{\rho}{r}\frac{\partial v}{\partial r} + \frac{v}{r}\frac{\partial \rho}{\partial r} + \frac{\rho}{r}\frac{\partial w}{\partial \phi} + \frac{w}{r}\frac{\partial \rho}{\partial \phi} = -\frac{\rho v}{r} \qquad (42)$$

z-Momentum

$$\frac{\partial u}{\partial t} + u\frac{\partial u}{\partial z} + v\frac{\partial u}{\partial r} + \frac{w}{r}\frac{\partial u}{\partial \phi} + \frac{1}{\rho}\frac{\partial p}{\partial z} = 0 \qquad (43)$$

r-Momentum

$$\frac{\partial v}{\partial t} + u\frac{\partial v}{\partial z} + v\frac{\partial v}{\partial r} + \frac{w}{r}\frac{\partial v}{\partial \phi} + \frac{1}{\rho}\frac{\partial p}{\partial r} = \frac{w^2}{r} \tag{44}$$

ϕ-Momentum

$$\frac{\partial w}{\partial t} + u\frac{\partial w}{\partial z} + v\frac{\partial w}{\partial r} + \frac{w}{r}\frac{\partial w}{\partial \phi} + \frac{1}{\rho}\frac{\partial p}{\partial \phi} = -\frac{vw}{r} \tag{45}$$

Energy

$$\frac{\partial \rho}{\partial t} + u\frac{\partial \rho}{\partial z} + v\frac{\partial \rho}{\partial r} + \frac{w}{r}\frac{\partial \rho}{\partial \phi} + \frac{\rho}{r}\left\{\frac{\partial u}{\partial z} + \frac{\partial v}{\partial r} + \frac{\partial w}{\partial \phi}\right\}$$
$$= c^2\left[\frac{\partial \rho}{\partial t} + u\frac{\partial \rho}{\partial z} + v\frac{\partial \rho}{\partial r} + \frac{w}{r}\frac{\partial \rho}{\partial \phi} + \frac{\rho}{r}\left\{\frac{\partial u}{\partial z} + \frac{\partial v}{\partial r} + \frac{\partial w}{\partial \phi}\right\}\right] \tag{46}$$

where c is the isentropic speed of sound for a perfect gas.

Equations (42) - (46) are in cylindrical coordinates, thus in order to obtain these equations in a generalized coordinate frame of reference, the following transformation must be applied.

$$\begin{aligned} \tau &= t \\ \xi &= \xi(t, r, \phi, z) \\ \eta &= \eta(t, r, \phi, z) \\ \zeta &= \zeta(t, r, \phi, z) \end{aligned} \tag{47}$$

By applying transformation (47), the partial derivatives in Eqs. (42) - (46) may be written generally as

$$\frac{\partial}{\partial t} = \frac{\partial}{\partial \tau} + \frac{\partial}{\partial \xi}\frac{\partial \xi}{\partial t} + \frac{\partial}{\partial \eta}\frac{\partial \eta}{\partial t} + \frac{\partial}{\partial \zeta}\frac{\partial \zeta}{\partial t}$$

$$\frac{\partial}{\partial z} = \frac{\partial}{\partial \tau}\frac{\partial \tau}{\partial z} + \frac{\partial}{\partial \xi}\frac{\partial \xi}{\partial z} + \frac{\partial}{\partial \eta}\frac{\partial \eta}{\partial z} + \frac{\partial}{\partial \zeta}\frac{\partial \zeta}{\partial z}$$

$$\frac{\partial}{\partial r} = \frac{\partial}{\partial \tau}\frac{\partial \tau}{\partial r} + \frac{\partial}{\partial \xi}\frac{\partial \xi}{\partial r} + \frac{\partial}{\partial \eta}\frac{\partial \eta}{\partial r} + \frac{\partial}{\partial \zeta}\frac{\partial \zeta}{\partial r} \qquad (48)$$

$$\frac{\partial}{\partial \phi} = \frac{\partial}{\partial \tau}\frac{\partial \tau}{\partial \phi} + \frac{\partial}{\partial \xi}\frac{\partial \xi}{\partial \phi} + \frac{\partial}{\partial \eta}\frac{\partial \eta}{\partial \phi} + \frac{\partial}{\partial \zeta}\frac{\partial \zeta}{\partial \phi}$$

Combining Eq. (46) and Eq. (42), Eqs. (42) - (45) are written in generalized coordinates utilizing the derivative definitions of Eq. (48).

Continuity

$$\frac{\partial p}{\partial \tau} + \bar{u}\frac{\partial p}{\partial \xi} + \bar{v}\frac{\partial p}{\partial \eta} + \bar{w}\frac{\partial p}{\partial \zeta} + \rho c^2\left[\frac{\partial u}{\partial \xi}\frac{\partial \xi}{\partial z} + \frac{\partial v}{\partial \xi}\frac{\partial \xi}{\partial r} + \frac{1}{r}\frac{\partial w}{\partial \xi}\frac{\partial \xi}{\partial \phi} + \frac{\partial u}{\partial \eta}\frac{\partial \eta}{\partial z}\right.$$
$$\left. + \frac{\partial v}{\partial \eta}\frac{\partial \eta}{\partial r} + \frac{1}{r}\frac{\partial w}{\partial \eta}\frac{\partial \eta}{\partial \phi} + \frac{\partial u}{\partial \zeta}\frac{\partial \zeta}{\partial z} + \frac{\partial v}{\partial \zeta}\frac{\partial \zeta}{\partial r} + \frac{1}{r}\frac{\partial w}{\partial \zeta}\frac{\partial \zeta}{\partial \phi}\right] = 0 \qquad (49)$$

ξ-Momentum

$$\frac{\partial u}{\partial \tau} + \bar{u}\frac{\partial u}{\partial \xi} + \bar{v}\frac{\partial u}{\partial \eta} + \bar{w}\frac{\partial u}{\partial \zeta} + \frac{1}{\rho}\left[\frac{\partial p}{\partial \xi}\frac{\partial \xi}{\partial z} + \frac{\partial p}{\partial \eta}\frac{\partial \eta}{\partial z} + \frac{\partial p}{\partial \zeta}\frac{\partial \zeta}{\partial z}\right] = 0 \qquad (50)$$

η-Momentum

$$\frac{\partial v}{\partial \tau} + \bar{u}\frac{\partial v}{\partial \xi} + \bar{v}\frac{\partial v}{\partial \eta} + \bar{w}\frac{\partial v}{\partial \zeta} + \frac{1}{\rho}\left[\frac{\partial p}{\partial \xi}\frac{\partial \xi}{\partial r} + \frac{\partial p}{\partial \eta}\frac{\partial \eta}{\partial r} + \frac{\partial p}{\partial \zeta}\frac{\partial \zeta}{\partial r}\right] = 0 \qquad (51)$$

ζ-Momentum

$$\frac{\partial w}{\partial \tau} + \bar{u}\frac{\partial w}{\partial \xi} + \bar{v}\frac{\partial w}{\partial \eta} + \bar{w}\frac{\partial w}{\partial \zeta} + \frac{1}{\rho}\frac{1}{r}\left[\frac{\partial p}{\partial \xi}\frac{\partial \xi}{\partial \phi} + \frac{\partial p}{\partial \eta}\frac{\partial \eta}{\partial \phi} + \frac{\partial p}{\partial \zeta}\frac{\partial \zeta}{\partial \phi}\right] = 0 \qquad (52)$$

where the contravariant velocities are defined as

$$\bar{u} = \frac{\partial \xi}{\partial t} + u\frac{\partial \xi}{\partial z} + v\frac{\partial \xi}{\partial r} + \frac{w}{r}\frac{\partial \xi}{\partial \phi}$$

$$\bar{v} = \frac{\partial \eta}{\partial t} + u\frac{\partial \eta}{\partial z} + v\frac{\partial \eta}{\partial r} + \frac{w}{r}\frac{\partial \eta}{\partial \phi} \qquad (53)$$

$$\bar{w} = \frac{\partial \zeta}{\partial t} + u\frac{\partial \zeta}{\partial z} + v\frac{\partial \zeta}{\partial r} + \frac{w}{r}\frac{\partial \zeta}{\partial \phi}$$

The method of characteristics will now be formulated by using the set of Eqs. (49), (50), (51), and (52). A linear combination of the continuity Eq. (49), the ξ-momentum Eq. (50), and η-momentum Eq. (51) and the ζ-momentum equation from (52) is obtained by multiplying them by scalars μ_1, μ_2, μ_3, μ_4, respectively. The new vector coefficients of these equations now contain the scalar quantity μ_i. The plane containing the new vector coefficients of the equation is called the characteristic plane. A normal to this plane is $\bar{\lambda}$ and is called a characteristic normal. The dot product of the new coefficient vector and the normal vector $\bar{\lambda}$ must be zero. This procedure will be followed to determine in the characteristic compatibility equation in the ξ-direction for the exit boundary condition.

Rewriting Eqs. (49), (50), (51), and (52)

$$p_\tau + \bar{u}p_\xi + \rho c^2\left(u_\xi \xi_z + v_\xi \xi_r + \frac{w_\xi}{r}\xi_\phi\right) = R_1 \qquad (54)$$

$$= -\bar{v}p_\eta - \bar{w}p_\xi - \rho c^2\left(u_\eta \eta_z + v_\eta \eta_r + \frac{w_\eta}{r}\eta_\phi + u_\zeta \zeta_z + v_\zeta \zeta_r + \frac{w_\zeta}{r}\zeta_\phi\right)$$

$$u_\tau + \bar{u}u_\xi + \frac{1}{\rho} p_\xi \xi_z = R_2 = -\bar{v}u_\eta - \bar{w}u_\zeta - \frac{1}{\rho}(p_\eta \eta_z + p_\zeta \zeta_z) \quad (55)$$

$$v_\tau + \bar{u}v_\xi + \frac{1}{\rho} p_\xi \xi_r = R_3 = -\bar{v}v_\eta - \bar{w}v_\zeta - \frac{1}{\rho}(p_\eta \eta_r + p_\zeta \zeta_r) \quad (56)$$

$$w_\tau + \bar{u}w_\xi + \frac{1}{\rho} p_\xi \frac{\xi_\phi}{r} = R_4 = -\bar{v}w_\eta - \bar{w}w_\zeta - \frac{1}{\rho}\left(p_\eta \frac{\eta_\phi}{r} + p_\zeta \frac{\zeta_\phi}{r}\right) \quad (57)$$

A characteristic like compatibility equation in physical space can be derived by making a linear combination of the above equations.

$$\mu_1 \left[p_\tau + \left(\frac{\mu_1 \bar{u} + \mu_2 \frac{\xi_z}{\rho} + \mu_3 \frac{\xi_r}{\rho} + \mu_4 \frac{\xi_\phi}{r\rho}}{\mu_1} \right) p_\xi \right]$$

$$+ \mu_2 \left[u_\tau + \left(\frac{\mu_2 \bar{u} + \mu_1 \rho c^2 \xi_z}{\mu_2} \right) u_\xi \right]$$

$$+ \mu_3 \left[v_\tau + \left(\frac{\mu_3 \bar{u} + \rho c^2 \xi_r \mu_1}{\mu_3} \right) v_\xi \right]$$

$$+ \mu_4 \left[w_\tau + \left(\frac{\mu_4 \bar{u} + \mu_1 \rho c^2 \frac{\xi_\phi}{r}}{\mu_4} \right) w_\xi \right]$$

$$= \mu_1 R_1 + \mu_2 R_2 + \mu_3 R_3 + \mu_4 R_4 \quad (58)$$

For a characteristic-like equation, the following relations must hold

$$\begin{aligned}
\mu_1\bar{u} + \mu_2 \frac{\xi_z}{\rho} + \mu_3 \frac{\xi_r}{\rho} + \mu_4 \frac{\xi_\phi}{r\rho} &= \lambda\mu_1 \\
\mu_1\rho c^2 \xi_z + \mu_2\bar{u} &= \lambda\mu_2 \\
\mu_1\rho c^2 \xi_r + \mu_3\bar{u} &= \lambda\mu_3 \\
\mu_1\rho c^2 \frac{\xi_\phi}{r} + \mu_4\bar{u} &= \lambda\mu_4
\end{aligned} \tag{59}$$

or rewriting Eq. (59)

$$\begin{aligned}
(\bar{u}-\lambda)\mu_1 + \frac{\xi_z}{\rho}\mu_2 + \frac{\xi_r}{\rho}\mu_3 + \frac{\xi_\phi}{\rho r}\mu_4 &= 0 \\
\rho c^2 \xi_z \mu_1 + (\bar{u}-\lambda)\mu_2 &= 0 \\
\rho c^2 \xi_r \mu_1 + (\bar{u}-\lambda)\mu_3 &= 0 \\
\rho c^2 \frac{\xi_\phi}{r}\mu_1 + (\bar{u}-\lambda)\mu_4 &= 0
\end{aligned} \tag{60}$$

$$\begin{bmatrix}
\bar{u}-\lambda & \frac{\xi_z}{\rho} & \frac{\xi_r}{\rho} & \frac{\xi_\phi}{\rho r} \\
\rho c^2 \xi_z & \bar{u}-\lambda & 0 & 0 \\
\rho c^2 \xi_r & 0 & \bar{u}-\lambda & 0 \\
\rho c^2 \frac{\xi_\phi}{r} & 0 & 0 & \bar{u}-\lambda
\end{bmatrix}
\begin{bmatrix} \mu_1 \\ \mu_2 \\ \mu_3 \\ \mu_4 \end{bmatrix} = 0 \tag{61}$$

A nontrivial solution exists if the determinant of the coefficient matrix vanishes. The expansion of the coefficient matrix determinant gives the characteristic equation

$$(\bar{u}-\lambda)^2 \left[(\bar{u}-\lambda)^2 - c^2 \left(\xi_z^2 + \xi_r^2 + \frac{\xi_\phi^2}{r} \right) \right] = 0 \tag{62}$$

The roots of this characteristic equation are

$$\begin{aligned} \lambda_{1,2} &= \pm \bar{u} \\ \lambda_{3,4} &= \bar{u} \pm c \sqrt{\xi_z^2 + \xi_r^2 + \frac{\xi_\phi^2}{r^2}} \end{aligned} \tag{63}$$

if

$$\begin{aligned} \mu_1 &= \bar{u}-\lambda \\ \mu_2 &= -\rho c^2 \xi_z \\ \mu_3 &= -\rho c^2 \xi_r \\ \mu_4 &= -\rho c^2 \frac{\xi_\phi}{r} \end{aligned}$$

The compatibility equation in the ξ-direction is written as

$$\mu_1 \{p_\tau + \lambda p_\xi\} + \mu_2 \{u_\tau + \lambda u_\xi\} + \mu_3 \{v_\tau + \lambda v_\xi\} + \mu_4 \{w_\tau + \lambda w_\xi\} - \sum_{i=1}^{4} \mu_i R_i = 0 \tag{64}$$

where λ and μ_i are defined in Eq. (63).

For the outflow (exit) boundary condition, which is a finite distance downstream of the blade trailing edge, a constant pressure is specified. This specification is c consistent with the physical aspects of the problem and the theory of characteristics. The $\bar{u}$-c characteristic brings information into the central volume from outside when $\bar{u} < c$. Thus one dependent variable such as the back pressure must be specified. The remaining dependent variables are determined by using the up running characteristic (+) in the compatibility relationship, Eq. (64), to solve for the axial velocity, u. The term R_i is evaluated using data from the previous time step. The momentum equations are used to solve for the remaining velocity components, v and w, and using the energy equation to solve for the density.

The uprunning characteristic form of the compatibility equation, Eq. (64), with the appropriate λ and μ_i's is written as

$$
\begin{aligned}
&p_\tau + \left[\bar{u} + c\sqrt{\xi_z^2 + \xi_r^2 + \left(\frac{\xi_\phi}{r}\right)^2}\right] p_\xi \\
&+ \frac{\rho c \xi_z}{\sqrt{\xi_z^2 + \xi_r^2 + \left(\frac{\xi_\phi}{r}\right)^2}} \left\{u_\tau + \left[\bar{u} + c\sqrt{\xi_z^2 + \xi_r^2 + \left(\frac{\xi_\phi}{r}\right)^2}\right] u_\xi\right\} \\
&+ \frac{\rho c \xi_r}{\sqrt{\xi_z^2 + \xi_r^2 + \left(\frac{\xi_\phi}{r}\right)^2}} \left\{v_\tau + \left[\bar{u} + c\sqrt{\xi_z^2 + \xi_r^2 + \left(\frac{\xi_\phi}{r}\right)^2}\right] v_\xi\right\} \qquad (65) \\
&+ \frac{\rho c \xi_\phi}{r\sqrt{\xi_z^2 + \xi_r^2 + \left(\frac{\xi_\phi}{r}\right)^2}} \left\{w_\tau + \left[\bar{u} + c\sqrt{\xi_z^2 + \xi_r^2 + \left(\frac{\xi_\phi}{r}\right)^2}\right] w_\xi\right\} \\
&= \frac{\rho c}{\sqrt{\xi_z^2 + \xi_r^2 + \left(\frac{\xi_\phi}{r}\right)^2}} \left[\xi_z R_2 + \xi_r R_3 + \frac{\xi_\phi R_4}{r}\right] + R_1
\end{aligned}
$$

With p specified as a constant in time, $p_\tau = 0$, Eq. (65) is solved for u_τ

$$u_\tau = -\left[\bar{u} + c\sqrt{\xi_z^2 + \xi_r^2 + \left(\frac{\xi_\phi}{r}\right)^2}\right]u_\xi + R_2 + \frac{\xi_r}{\xi_z} R_3 + \frac{\xi_\phi}{\xi_z}\frac{R_4}{r} + \frac{R_1}{\xi_z}$$

$$- \frac{\xi_r}{\xi_z}\left\{ v_\tau + \left[\bar{u} + c\sqrt{\xi_z^2 + \xi_r^2 + \left(\frac{\xi_\phi}{r}\right)^2}\right] v_\xi \right\}$$

$$- \frac{\xi_\phi}{r\xi_z}\left\{ w_\tau + \left[\bar{u} + c\sqrt{\xi_z^2 + \xi_r^2 + \left(\frac{\xi_\phi}{r}\right)^2}\right] w_\xi \right\}$$

$$- \frac{\sqrt{\xi_z^2 + \xi_r^2 + \left(\frac{\xi_\phi}{r}\right)^2}}{\rho c \xi_z}\left\{ \cancel{p_\tau}^{\,0} + \left[\bar{u} + c\sqrt{\xi_z^2 + \xi_r^2 + \left(\frac{\xi_\phi}{r}\right)^2}\right] p_\xi \right\} \qquad (66)$$

For the grid being considered in this report, it is known that $\xi_r = \xi_\phi = 0$ at the downstream boundary, causing a simplification of Eq. (66). If this was not the case, Eq. (66) would have to be solved simultaneously with the v- and w-momentum equation.

Writing equations with the simplification, $\xi_r = \xi_\phi = 0$ the equation for the u-velocity is obtained.

$$u_\tau = -(\bar{u} + c\xi_z)u_\xi + R_2 + \frac{R_1}{\xi_z} - \frac{1}{\rho c}\left(\cancel{p_\tau}^{\,0} + c\xi_z\, p_\xi\right) \qquad (67)$$

The v and w velocities are obtained from the momentum equations (51) and (52),

$$v_\tau = -(\bar{u}v_\xi + \bar{v}v_\eta + \bar{w}v_\zeta) - \frac{1}{\rho}(p_\xi \xi_r + p_\eta \eta_r + p_\zeta \zeta_r) \qquad (68)$$

and

$$w_\tau = -(\bar{u}w_\xi + \bar{v}w_\eta + \bar{w}w_\zeta) - \frac{1}{\rho}(p_\xi \xi_\phi + p_\eta \eta_\phi + p_\zeta \zeta_\phi)/r \qquad (69)$$

The density is then determined from the following form of the energy equation

$$\frac{Dp}{Dt} = c^2 \frac{D\rho}{Dt} \qquad (70a)$$

where $\frac{D}{Dt}$ is the substantial derivative. Expanding Eq. (70a) and making the appropriate substitutions a characteristic-like equation for density is obtained,

$$\rho_\tau = \frac{(p_\tau + \bar{u}p_\xi + \bar{v}p_\eta + \bar{w}p_\zeta)}{c^2} - \bar{u}\rho_\xi - \bar{v}\rho_\eta - \bar{w}\rho_\zeta \qquad (70b)$$

Since pressure, p, is specified, Eqs. (67), (68), (69), and (70b) are used to solve for the remaining independent variables u, v, w, and ρ at the subsonic exit plane.

4.4.4. Initial Conditions

There are two possibilities to be considered:

1) Startup from a specified free stream,

2) Startup from a previously calculated solution.

When starting from a specified free stream, the free stream variables are specified at every nodal point at time T = 0. As marching proceeds in time from T = 0, the tangency condition is imposed according to the cubic formula

$$S_T = 10 - 15T + 6T^2 + T^3 \tag{71a}$$

as applied to the velocity components

$$\begin{aligned} u_{T+1} &= u_T S_T + u_\infty (1.-S_T) \\ v_{T+1} &= v_T S_T + v_\infty (1.-S_T) \\ w_{T+1} &= w_T S_T + w_\infty (1.-S_T) \end{aligned} \tag{71b}$$

with the following restriction imposed, T = 1.0 then S_T = 1.0 where

$$T = (\text{Iteration step})/(\text{number of steps to slow start tangency B.C.}) \tag{71c}$$

The remaining variables are accepted as predicted by the numerical algorithm in conjunction with the total rotholpy and entrapy requirement.

This procedure is used over a finite number of time steps to allow for a smooth adjustment from a constant field to one with a large perturbation caused by the body imposed upon it.

When starting from a previously calculated solution using new specified flow conditions, the procedure is the same as before with the exception being the u_∞, v_∞, and w_∞ velocity components being replaced by the initial velocity components from the previous solution.

If a solution is being continued in time with the same flow conditions, it is just a simple matter of reading all of the necessary information at the previous time level from the stored calculated solution.

4.5. Output Data Manipulation

Possibly the most important part of any design computer code is its output. To enable the designer to best evaluate a given configuration, the detailed surface pressures and the overall forces and moments on the blades and nacelle are necessary. The blade section aerodynamic coefficients and the overall performance coefficients of the blading are also of great importance in making the right choice of the most efficient airfoil section. In addition, computer generated plots of the various aspects of the flow field surrounding the Prop-Fan configuration would be beneficial in the design process.

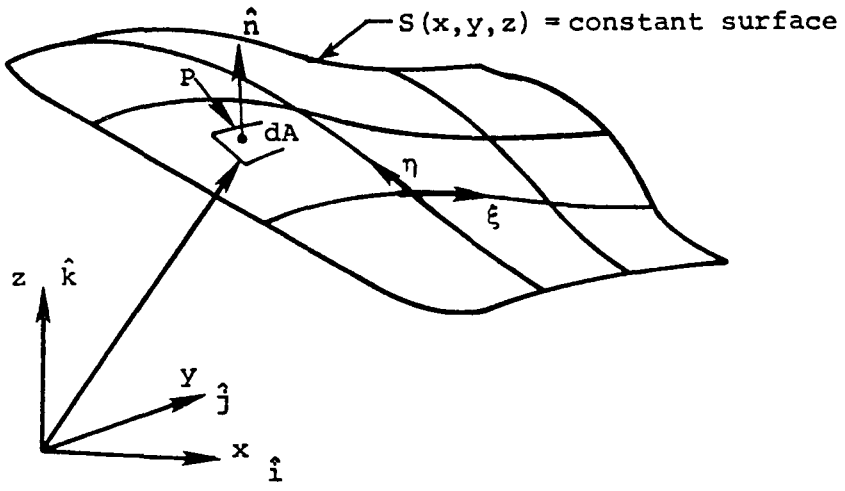

Figure 9. Surface Definition

Since force and moment coefficients are required for both the blades and the nacelle, a generalized derivation is included in this section. The surface definition in generalized coordinates for the calculation of forces and moments is shown in the Figure above. The incremental force acting on the area segment of the surface, dA can be written

$$\vec{dF} = -\Delta p \, \hat{n} \, dA \tag{72}$$

where the unit normal to the area segment is defined as

$$\hat{n} = \frac{\nabla S}{|\nabla S|} = \frac{S_x \hat{i} + S_y \hat{j} + S_z \hat{k}}{(S_x^2 + S_y^2 + S_z^2)^{\frac{1}{2}}} \tag{73}$$

The incremental area in generalized coordinates is

$$dA = \left[\left(\frac{\partial(y,z)}{\partial(\xi,\eta)}\right)^2 + \left(\frac{\partial(z,x)}{\partial(\xi,\eta)}\right)^2 + \left(\frac{\partial(x,y)}{\partial(\xi,\eta)}\right)^2\right]^{\frac{1}{2}} d\xi d\eta$$

$$= \frac{\left[S_x^2 + S_y^2 + S_z^2\right]^{\frac{1}{2}}}{J} d\xi d\eta \tag{74}$$

where J is the Jacobian.

Thus the incremental force, $\vec{dF}$, can be written in generalized coordinates as

$$\vec{dF} = -\frac{\Delta p}{J}(S_x \hat{i} + S_y \hat{j} + S_z \hat{k})\, d\xi d\eta \tag{75}$$

In order to determine the various components of the force, the scalar product incremental force $\vec{dF}$ with the unit vector components, $\hat{i}$, $\hat{j}$, $\hat{k}$, has to be formed. The usual convention for assigning forces is shown in the following Figure.

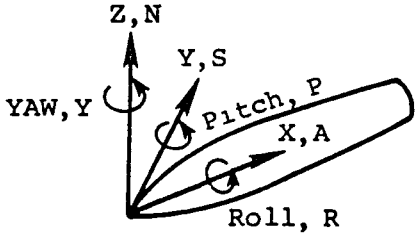

Figure 10. Force Assignment Conventions

The various components, N, S, A, of the total force F are defined as the normal force, side force, and axial force, respectively. To arrive at a mathematical definition of the various components, the scalar product of the generalized incremental force $\vec{dF}$ with the unit vectors $\hat{i}$, $\hat{j}$, $\hat{k}$ is formed to give

$$\begin{aligned} dN &= \vec{dF}\cdot\hat{k} = -\frac{\Delta p}{J} S_z \, d\xi d\eta \\ dA &= \vec{dF}\cdot\hat{i} = -\frac{\Delta p}{J} S_x \, d\xi d\eta \\ dS &= \vec{dF}\cdot\hat{j} = -\frac{\Delta p}{J} S_y \, d\xi d\eta \end{aligned} \tag{76}$$

and integrating these incremental forces, the total force in each direction is obtained as follows

Normal Force

$$N = -\int_{\eta}\int_{\xi} \frac{\Delta p}{J} S_z \, d\xi d\eta \tag{77}$$

Axial Force

$$A = -\int_{\eta}\int_{\xi} \frac{\Delta p}{J} S_x \, d\xi d\eta \tag{78}$$

Side Force

$$S = -\int_{\eta}\int_{\xi} \frac{\Delta p}{J} S_y \, d\xi d\eta \tag{79}$$

The incremental moments $\vec{dM}$ are obtained by forming the vector product of the radius $\vec{r}$ with the incremental force $\vec{dF}$ to give

$$\vec{dM} = \vec{r} \times \vec{dF} \tag{80}$$

where

$$\vec{r} = x\hat{i} + y\hat{j} + r\hat{k}$$

Thus, the following equation is obtained for the total incremental moment, dM,

$$\vec{dM} = -\frac{\Delta p}{J}\left[(yS_z - zS_y)\hat{i} + (zS_x - xS_z)\hat{j} + (xS_y - yS_x)\hat{k} \right] d\xi d\eta \tag{81}$$

and as in the forces, the various components of the total moment can be written as

$$\begin{aligned} dM_R &= \vec{dM}\cdot\hat{i} \\ dM_p &= \vec{dM}\cdot\hat{j} \\ dM_y &= \vec{dM}\cdot\hat{k} \end{aligned} \tag{82}$$

where the sign convention for these moments is defined in Figure 4. Integrating these incremental moments yields the following total moments measured with respect to the nose of the body

Rolling Moment

$$M_R = -\int_{\xi}\int_{\eta} \frac{\Delta p}{J} (yS_z - zS_y)\, d\xi d\eta \tag{83}$$

Pitching Moment

$$M_p = -\int_{\xi}\int_{\eta} \frac{\Delta p}{J} (zS_x - xS_z)\, d\xi d\eta \tag{84}$$

Yawing Moment

$$M_y = - \int_{\xi}\int_{\eta} \frac{\Delta P}{J} (xS_y - yS_x) d\xi d\eta \tag{85}$$

Typically, the center of pressure may also be of interest and it is defined as

$$X_{cp} = - \frac{\text{PITCHING MOMENT}}{\text{NORMAL FORCE}} = - \frac{M_p}{N} \tag{86}$$

Also, the forces and moments are converted to nondimensional coefficients as follows

$$C_F = \frac{\text{Force}}{(\text{Dynamic Pressure})(\text{Reference Area})}$$

$$C_M = \frac{\text{Moment}}{(\text{Dynamic Pressure})(\text{Reference Area})(\text{Reference Length})} \tag{87}$$

where

$$q = \frac{1}{2} \rho_\infty v_\infty^2 = \text{dynamic pressure}$$

$$A = \pi r_b^2 = \text{reference area}$$

$$\ell_b = \text{reference length}$$

The various forces and moments are then written in coefficient form as

$$C_A = \frac{A}{q_\infty A_b}$$
$$C_N = \frac{N}{q_\infty A_b} \tag{88}$$
$$C_s = \frac{S}{q_\infty A_b}$$

$$c_p = \frac{M_p}{q_\infty A_b \ell_b}$$
$$C_R = \frac{M_R}{q_\infty A_b \ell_b} \tag{89}$$
$$C_y = \frac{M_y}{q_\infty A_b \ell_b}$$

and

$$X_{cp} = - \frac{C_p}{C_N}$$

This generalized derivation of the force and moment coefficients will be applied in the sections to give values for the blades and nacelle.

4.5.1. Blade Properties

The blade properties are broken up into three distinct categories, each giving valuable information to the designer. In the first category, the aerodynamic coefficients of the blading are calculated. These coefficients consist of the

axial force, normal force, and side force along with the pitching moment, rolling moment, and the yawing moment. The second category defines the performance coefficient, torque coefficient, and the power coefficient. The independent variables compose the three category. These are generally the pressure, density, velocity, and energy variations on the blade surface. This category would be considered as a standard output with categories one and two being more specifically aimed at the Prop-Fan problem. With this in mind, a description of both category one and category two follows. The geometric relationships are shown in Figure 11 below.

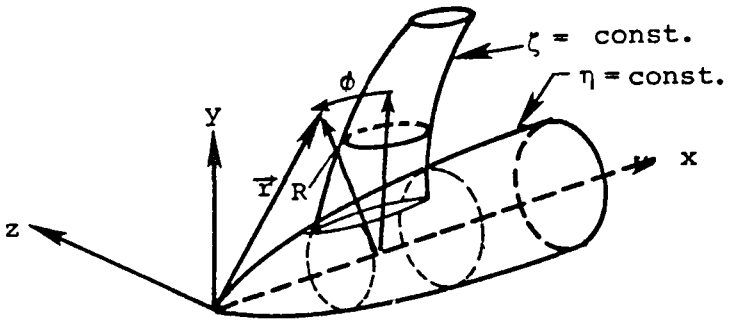

Figure 11. Geometric Relationships for Conversion to Cylindrical Coordinates

The generalized cartesian coordinate development of forces and moments is now converted to cylindrical coordinates using the relations

$$\begin{aligned} x &= z \\ y &= R\cos\phi \\ z' &= R\sin\phi \end{aligned} \tag{90}$$

and the fact that the cylindrical Jacobian is equal to R times the cartesian Jacobian,

$$J_{cyl} = R \cdot J \tag{91}$$

Using the coordinate transformation Eq. (72) the cylindrical Jacobian Eq. (91) and the generalized forces and moments Eq. (76) and (82), the incremental forces and moments in cylindrical coordinates are

$$dF_{AXIAL} = -\frac{pR\xi_z}{J_{cyl}}\, d\xi d\eta$$

$$dF_{NORMAL} = -\frac{pR}{J_{cyl}}\left(\cos\phi\,\xi_R - \frac{\sin\phi}{R}\,\xi_\phi\right) d\xi d\eta$$

$$dF_{SIDE} = -\frac{pR}{J_{cyl}}\left(\sin\phi\,\xi_R + \frac{\cos\phi}{R}\,\xi_\phi\right) d\xi d\eta$$

$$dM_{ROLL} = -\frac{pR}{J_{cyl}}\,\xi_\phi\, d\xi d\eta$$

$$dM_{PITCH} = - \frac{pR}{J_{cyl}} \left(z\{\cos\phi\xi_R - \frac{\sin\phi}{R}\ \xi_\phi\} - R\cos\phi\xi_z\right) d\xi d\eta$$

and

$$dM_{YAW} = - \frac{pR}{J_{cyl}} \left(-z\{\sin\phi\xi_R + \frac{\cos\phi}{R}\ \xi_\phi\} + R\sin\phi\xi_z\right) d\xi d\eta \quad (92)$$

The equation set (92) is integrated in space by using the trapezoidal rule to obtain the total force and moment coefficients contributed by the blades.

Propeller characteristics are normally defined in terms of efficiency, η, thrust coefficient, C_T, torque coefficient, C_Q, power coefficient, C_p, and advance ratio $V/(nD)$. The determination of these characteristics is presented below. The notation is given in the following Figure.

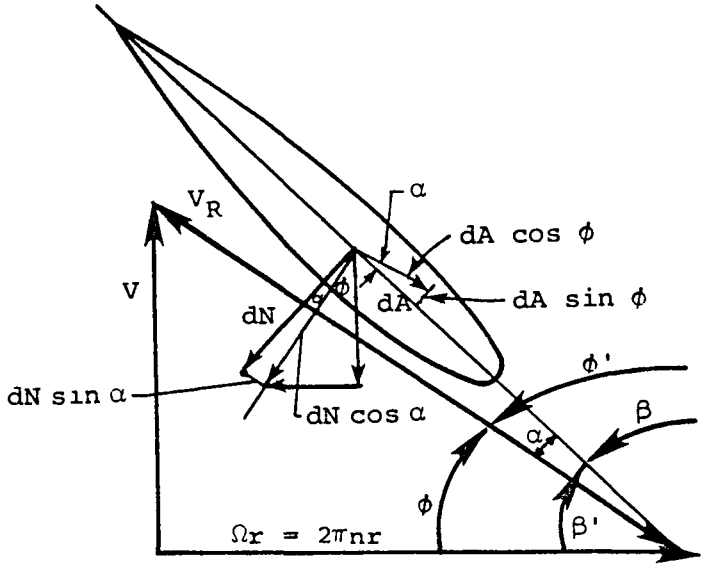

Figure 12. Notation for Propeller Characteristics

In the Figure

β = geometric blade angle, based on chord, at station r

ϕ = effective pitch angle

α = effective angle of attack = $(90^\circ - \beta) - \phi$

V = free-stream velocity

Ωr = linear velocity due to rotation at station r

dL = elemental lift

dN = elemental normal force

dD = elemental drag

dA = elemental axial force

From an examination of the Figure, it will be noted that the elemental lift and drag forces are taken respectively perpendicular and parallel to the velocity vector V_R. Because the velocity V_R is the resultant of V and Ωr, it represents the net flow past the element.

The elemental thrust is the force produced by the blade element along the line of flight, or

$$dT = dL\cos\phi - dD\sin\phi \tag{93}$$

The elemental lift and drag can be written in terms of the normal force and axial force as

$$dL = dN\cos\alpha - dA\sin\alpha \tag{94}$$

and

$$dD = dN\sin\alpha + dA\cos\alpha \tag{95}$$

This form of the coefficients is chosen since the forces and moments in this report are derived to be consistent with a body axis system rather than a wind axis system. Therefore, the elemental thrust is

$$dT = dN\cos(\alpha+\phi) - dA\sin(\alpha+\phi). \tag{96}$$

The elemental torque is the force produced by the blade element resisting rotation multiplied by the radial distance r to the center of rotation, or

$$dQ = r\ dL\sin\phi + r\ dD\cos\phi \tag{97}$$

Using Eqs. (94) and (95) in Eq. (97), the elemental torque is written as

$$dQ = r\ dN\sin(\alpha+\phi) + r\ dA\cos(\alpha+\phi) \tag{98}$$

where the elemental normal force and axial force are defined in Eq. (92). Also it may be seen from Figure 12 that

$$V_R = \frac{\Omega r}{\cos\phi} = \frac{2\pi rn}{\cos\phi} \tag{99}$$

and

$$\phi = \tan^{-1}\frac{V}{\Omega r} = \tan^{-1}\frac{JD}{2\pi r} \tag{100}$$

where $D = 2R$ = blade diameter

By definition,

$$\text{elemental thrust coefficient} = dC_T = \frac{dT}{\rho n^2 D^4} \qquad (101)$$

$$\text{elemental thrque coefficient} = dC_Q = \frac{dQ}{\rho n^2 D^5} \qquad (102)$$

where ρ is density and n is the frequency.

The section thrust and torque coefficients are obtained by dividing both sides of Eqs. (96) and (98) by an incremental radius, dr,

$$\frac{dT}{dr} = \frac{dN}{dr}\cos(\alpha+\phi) - \frac{dA}{dr}\sin(\alpha+\phi) \qquad (103)$$

and

$$\frac{dQ}{dr} = r\frac{dN}{dr}\sin(\alpha+\phi) + r\frac{dA}{dr}\sin(\alpha+\phi) \qquad (104)$$

Values of the overall thrust and torque coefficients C_T and C_Q are determined by a trapezoidal integration with respect to r of Eqs. (101) and (102) with the help of Eqs. (103) and (104).

The efficiency of the propeller, η, is defined as

$$\eta = \frac{\text{Power Output}}{\text{Power Input}} = \frac{(\text{Thrust})(\text{Velocity})}{(2\pi n)\ (\text{Torque})} = \frac{TV}{2\pi nQ}$$

From Eq. (101) and (102)

$$\begin{aligned} T &= C_T \rho n^2 D^4 \\ Q &= C_Q \rho n^2 D^5 \end{aligned} \qquad (105)$$

where

$$C_T = \text{thrust coefficient} = \int_0^{D/2} \frac{dC_T}{dr}\, dr$$

$$C_Q = \text{torque coefficient} = \int_0^{D/2} \frac{dC_Q}{dr}\, dr$$

such that

$$\eta = \frac{C_T}{2\pi C_Q} J \tag{106}$$

where $J = \frac{V}{nD}$

If we define a power coefficient, C_p, as

$$C_p = \text{power coefficient} = \frac{\text{Power}}{\rho n^3 D^5} = \frac{p}{\rho n^3 D^5} \tag{107}$$

then

$$\eta = \frac{TV}{p} = \frac{C_T}{C_p} J \tag{108}$$

where from Eqs. (106) and (108)

$$C_p = 2\pi C_Q \tag{109}$$

A typical plot of $\frac{dC_T}{dr}$ and $\frac{dC_p}{dr}$ against r/D is shown in Figure 13 and is compared with the theory of Rohrback. These curves are integrated in r to give total thrust and torque coefficients. Figure 14 presented the calculated performance coefficients of the blades.

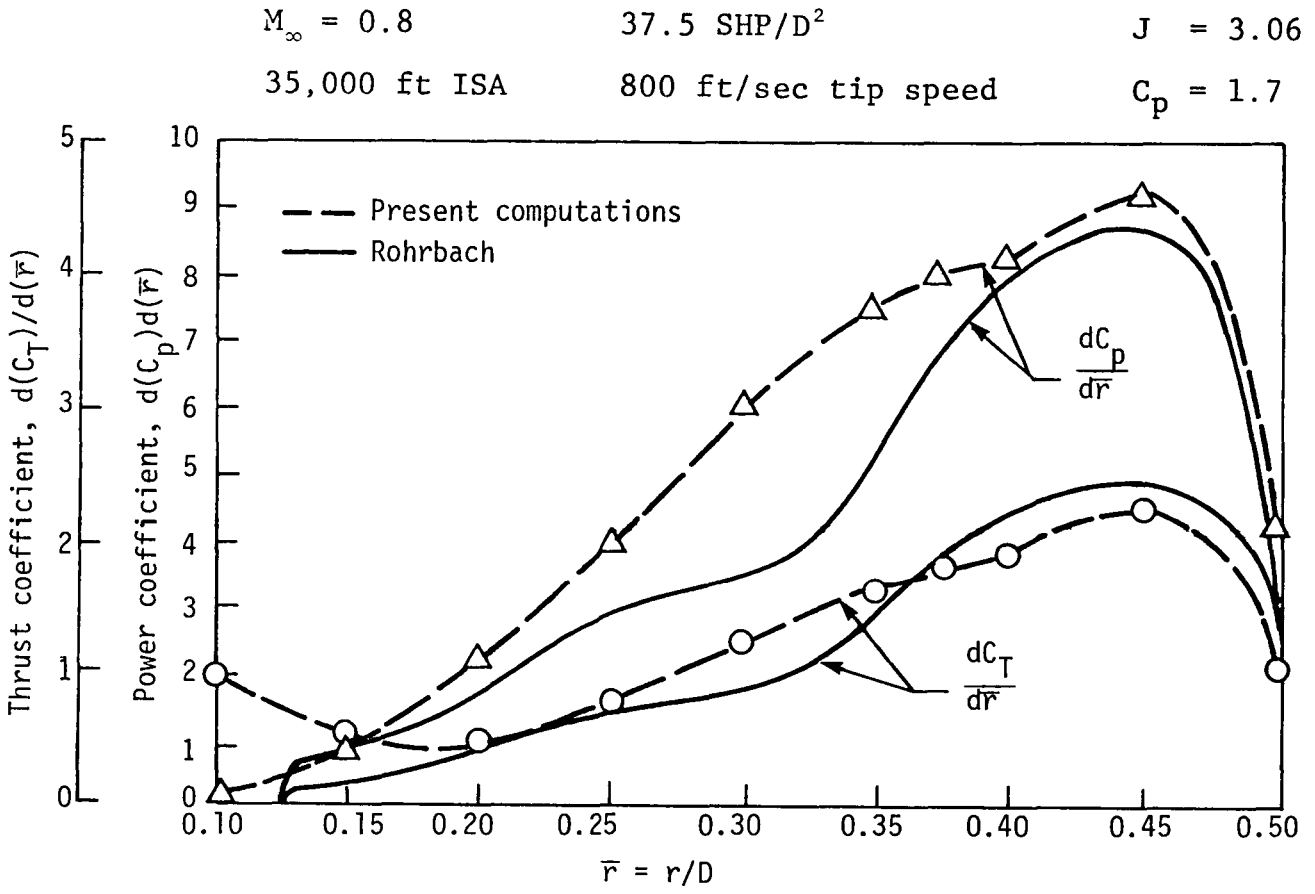

Figure 13. Thrust and Power Coefficient Loading as a Function of Blade Radius

```
**************************************
*                                    *
* PROPERTIES OF THE GIVEN BLADING    *
*                                    *
**************************************
```

```
**********************
*                    *
* GEOMETRIC PROPERTIES *
*                    *
**********************

NO. OF BLADES      =    8
BLADE DIAMETER     =  1.0000
```

```
*************************
*                       *
* FLOWFIELD PROPERTIES  *
*                       *
*************************

MACH NUMBER        =    .8000000
PRESSURE           =   1.0000000
DENSITY            =   1.0000000
VELOCITY           =    .9465728

ADVANCE RATIO      =   3.0600000
THRUST COEFFICIENT =    .7986009
TORQUE COEFFICIENT =    .5537881
POWER COEFFICIENT  =  3.4795530
BLADE EFFICIENCY   =    .7023082
```

Figure 14. Computer Output of Performance Coefficients

4.5.2. Nacelle Properties

The independent variables, pressure, density, velocity components, energy, and the force and moment coefficients are the properties of interest in this section. Again, as in the blade properties, the independent variables are a standard output and will not be discussed here. The forces and moments are presented in terms of the cylindrical coordinates, Eq. (90). The incremental forces and moments in cylindrical coordinates for the nacelle are

$$dF_{AXIAL} = - \frac{pR}{J_{cyl}} \eta_z \, d\xi d\zeta$$

$$dF_{NORMAL} = - \frac{pR}{J_{cyl}} (\cos \phi \, \eta_R - \frac{\sin \phi}{R} \eta_\phi) d\xi d\zeta$$

$$dF_{SIDE} = - \frac{pR}{J_{cyl}} (\sin \phi \, \eta_R + \frac{\cos \phi}{R} \eta_\phi) d\xi d\zeta$$

$$dM_{ROLL} = - \frac{pR}{J_{cyl}} \eta_\phi \, d\xi d\zeta$$

$$dM_{PITCH} = - \frac{pR}{J_{cyl}} (z\{\cos\phi \, \eta_R - \frac{\sin\phi}{R} \eta_\phi\} - R\cos\phi \, \eta_z) d\xi d\zeta$$

and

$$dM_{YAW} = - \frac{pR}{J_{cyl}} (-z\{\sin\phi \, \eta_R + \frac{\cos\phi}{R} \eta_\phi\} + R\sin\phi \, \eta_z) d\xi d\zeta \quad (110)$$

To obtain the total force and moments that are contributed by the nacelle equation Eqs. (110) are integrated using the trapezoidal rule.

5. MESH GENERATION PROGRAM

Before beginning the user's instructions, a few significant characteristics of the program should be described. In its present form, the program may be executed on a stand-alone basis. It has four OVERLAY links, the blade, nacelle, and grid boundary geometry link, geometry generation link, data card generation link, and the grid generation link with the last link requiring the most storage. At present, input for link I and for link II are stored on disc and tape and only changed when deemed necessary, i.e. completely new geometry definitions. In the following sections, a more detailed description of different facets of the program complex will be presented.

5.1. Program Organization and Interaction

This program is OVERLAYed with the four links being governed by a main driving program. This program calls each OVERLAY as needed and these occur in successive order of OVERLAY 01 through OVERLAY 04. The organization is such that the first link reads the blade and nacelle geometry data along with the definition of the outer boundary of the grid system. Thus in effect the complete outer and inner boundaries are defined here. These data are assumed to be fairly constant for a given problem and are stored on disc or tape (TAPE5),

to avoid the problem of reading in large amounts of data from cards. The first link then creates a series of patches which link the outer boundary and the inner boundary. This information is stored on TAPE10 and is used in the second link.

From TAPE4, the governing parameters of link two are read which are used to create patch coefficients from the data which was furnished by link one. These parameters are assumed to be the same for most geometries which this program will be associated with. Thus, it has been stored permanetly to keep from reading an unnecessary number of cards. This link in turn stores the data for use in link three.

Link three creates data cards on disc (TAPE3) which are read by link four. These data cards determine the number of points in the grid, the clustering of the grid lines, and other pertinent information in a grid generation process.

Link four reads the data cards from link three which determine the size and location of grid points and reads the parametric cubic coefficient data from link two which describe the general three-dimensional domain and finally combines the two to determine the finite difference mesh which is used by the 3-D flow field code. The final system is written to TAPE11.

5.2. Flow Chart

The overall logic of the OVERLAY system is presented with a further breakdown of each OVERLAY.

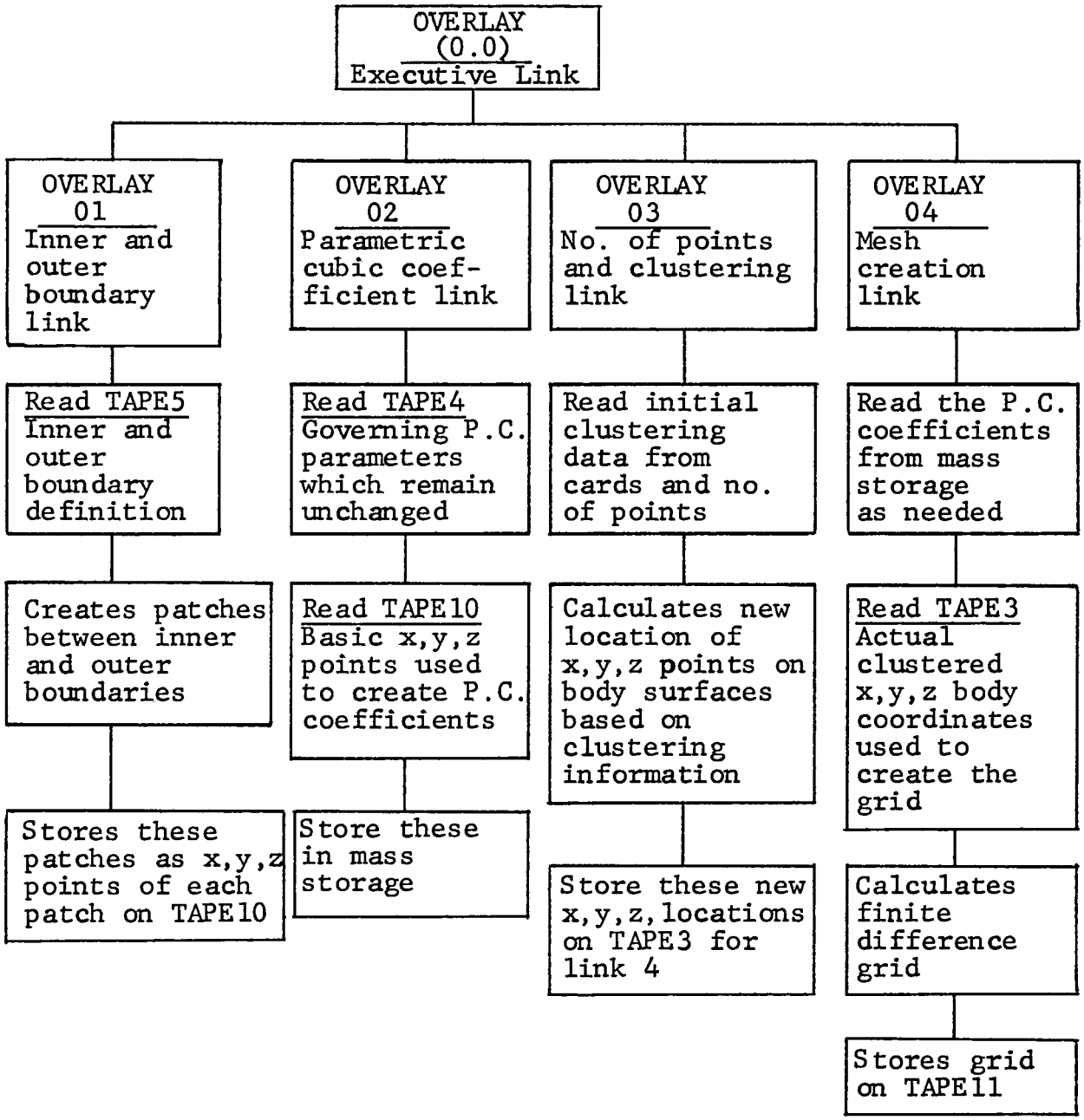

5.3. Program Input

The program input is described here. A dictionary of the input variables is provided followed by a description of the different input data formats. The user should only have to be familiar with the input variables of TAPE2 and TAPE5 with the input variables of TAPE4 furnished once.

5.3.1. Dictionary of Input Variables

For a general description of the variables read from TAPE4, the user is referred to Reference 15 which was produced for NASA/Ames Research Center, Moffett Field, CA with the cognizant person being Reese Sorenson. The following list describes all input variables to the program using TAPE2 or TAPE5. Those for TAPE5 will be discussed first.

VARIABLE	DESCRIPTION
AOD	the axial location of the nacelle stagnation point with respect to the coordinate system origin, < 0; normalized by the blade diameter.
BB(I)	chord of the blade at each radial station.
BETA34	twist of the blade at 75% span.
BOD	the axial location of the boundary between patches 9 and 10 at some station downstream of the blades, > 0; normalized by the blade diameter.

CCP	the radial location of the outer boundary; normalized by the blade diameter.
COD	the radial location where Patch 3 (Figure 2) becomes normal to the axial coordinate; normalized by the blade diameter.
D	physical blade diameter.
DBET(I)	twist of the blade at each radial station.
DDDP	the axial location of the far upstream boundary < 0; normalized by the blade diameter.
DOD	the axial location of the immediate upstream boundary < 0; normalized by the blade diameter.
EOD	the axial location of the far downstream boundary; normalized by the blade diameter.
LEA(I)	blade axial leading edge location with respect to the coordinate orgin.
NB	number of planes in the radial direction defining the blade geometry.
NBU	additional number of points between the blade tip (NB) and the outer boundary.
NN	number of points in the axial direction defining the nacelle geometry.
NP	number of points in the chordwise direction defining the blade geometry.
NT	total number of points in radial direction; NT = NB+NBU
RB(I)	radial location of the BB(I) and DBET(I).
RN(N)	cylindrical radius of the nacelle at each axial station.
XOB(N,K)	axial location of the YCOB(N,K) and YFOB(N,K) coordinates; normalized by the chord BB(N).
YCOB(N,K)	radial coordinate of the blade camber side at XOB(N,K); normalized by the chord BB(N).
YFOB(N,K)	radial coordinate of the blade face side at XOB(N,K); normalized by the chord BB(N).
ZN(N)	axial stations for which RN(N) is defined.

TAPE2 input variables are discussed next.

VARIABLES	DESCRIPTION
CFSL	fraction of the chord at which "midchord" clustering occurs.
DETNAC	actual physical spacing desired radially at the nacelle surface.
DETTIP	actual physical spacing desired radially at the blade tip.
DXILE	actual physical spacing desired axially at the blade leading edge.
DXISL	actual physical spacing desired axially at the blade "mid-chord".
DXITE	actual physical spacing desired axially at the blade trailing edge.
DZERAT	actual physical spacing desired meridionally at blade surfaces.
JCONE	number of cones (including z-axis) at nose of nacelle.
JLE	integer location of blade leading edge; usually 11.
JMAX	number of mesh points in ξ-direction; $\leq$ 45.
JSL	= 0, no clustering at mid-chord; = 1, clustering at mid-chord.
JTE	integer location of blade trailing edge; usually 27.
KMAX	number of mesh points in η-direction; $\leq$ 21
KTIP	integer location of blade tip; usually 11
LMAX	number of mesh points in ζ-direction; $\leq$ 11.
NBLADE	number of blades.

PRT10	logical variable for OVERLAY 1 print option; .TRUE. print; .FALSE. no print.
PRT20	logical variable for OVERLAY 2 print option; same as PRT10.
PRT30	logical variable for OVERLAY 3 print option, same as PRT10.
PRT40	logical variable for OVERLAY 4 print option; same as PRT10.

5.3.2. Input Data Format

The data could all be input from cards but due to the bulk of this data it was deemed best to store that data which does not change much on TAPE4 and TAPE5. The data on TAPE4 governs the parametric cubic patch program and would only change if a user had extensive experience with that part of the program. The data on TAPE5 is the blade and nacelle geometry definitions along with the axial and radial boundary information. This data usually remains constant for a given nacelle blade configuration. Consequently, only the clustering information is read from cards (TAPE2). The format for the cards to be stored on TAPE5 are:

CARD NO. 1

Column no.	1
	D

CARD NO. (16I5)

Column no.	1 → 5

CARD NO. 3 (2F10.5) There are NN of this type card.

Column no.	1	11
	ZN(N)	RN(N)

CARD NO. 4 (16I5)

Column no.	1 → 5	6 - 10	11 - 15	16 - 20
	NB	NP	NBU	NT

CARD NO. 5 8F10.5 There are NB of this type card.

Column no.	1	11	21	31	41
	RB(I)	DBET(I)	LEA(I)	BB(I)	

CARD NO. 6 (10X, 2(F10.4, 2F10.6)) There are (NP/2)X(K) of this type card.

Column no.	1	11	21	31	41	51	61
		XOB(N,K)	YCOB(N,K)	YFOB(N,K)	XOB(N+1,K)	YCOB(N+1,K)	YFOB(N+1,K)

CARD NO. 7 8F10.5

Column no.	1	11	21	31	41	51	61	71
	BETA34	AOD	BOD	COD	DOD	EOD	CCP	DDDP

This concludes the card types which are to be stored on TAPE5.

Next the cards read from TAPE2 are presented

CARD NO. 1 (4L5)

Column no.	1 → 5	6 - 10	11 - 15	16 - 20
	PRT10	PRT20	PRT30	PRT40

CARD NO. 2 (16I5)

Column no.	1 → 5	6-10	11-15	16-20	21-25	26-30	31-35	36-40	41-45 ---80
	JCONE	JLE	JSL	JTE	JMAX	KTIP	KMAX	LMAX	NBLADE

CARD NO. 3

Column no.	1	11	21	31	41	51	61	80
	DXILE	DXISL	DXITE	CFSL	DETNAC	DETTIP	DZERAT	

5.4. Program Output

Due to the nature and complexity of grid generating programs there are a large number of write statements in all four OVERLAYs. There are far too many to discuss in this manual. However, it is suggested that the user trigger the print options in all four links to get a feeling and understanding of what output data is available. A shortened version of a print from OVERLAY 4 can be found in Appendix A.3.

5.5. Operating Procedures and Trouble Shooting Hints

It would enhance the user's understanding of the validity of the grid system by displaying the grid using the local system plot packages. A detailed picture of the grid system can either ensure the grid or allow the user to quickly trace down possible problems.

Typical things to check in case of problems are:

- the coordinates of the blade and nacelle.
- location of the boundaries with respect to the origin of the coordinate system.
- the values of the clustering parameters read from cards.

Any or all these could cause problems in the grid generation phase which is probably the most important part of the calculation procedure.

6. THREE-DIMENSIONAL PROP-FAN FLOW FIELD PROGRAM

This program numerically calculates the flow field solution surrounding the Prop-Fan configuration much as a wind tunnel test calculates the experimental results. The benefit here is in the fact that a lot more detailed data is available for analysis from the present numerical results. These results consist of the density, velocity components, and energy which can be manipulated to determine any other necessary flow variable of interest. The following sections will present a more detailed description of the program.

6.1. Program Organization and Interaction

The organization is very logical and done in a straight forward matter. Usually, the mesh from the mesh generation program and a previously stored solution are attached in the starting process. The set of equations are then iterated in time to a steady-state thus yielding a wealth of information about the flow field. This solution is stored on disc (or tape) and can later be attached by either the flow field program or by the data reduction program. This allows the user at any given time to view the performance of the blade-nacelle configuration by using the flow field variables which were calculated from the 3-D flow field code.

6.2. Flow Chart

This section provides a brief flow chart describing the overall logical flow of the program.

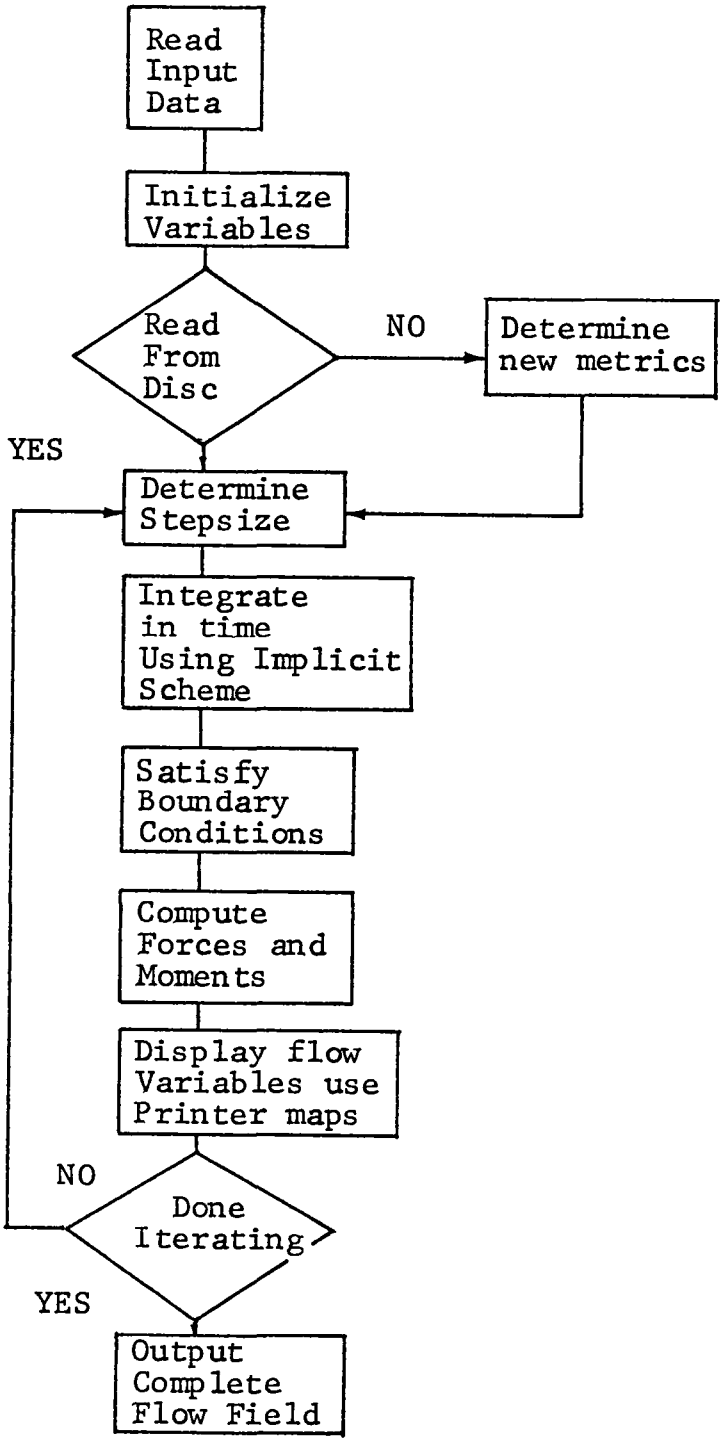

6.3. Program Input

The input required by the 3-D flow field program is described in this section. A dictionary of the input variables is provided followed by a description of the input data format.

6.3.1. Dictionary of Input Variables

The following list includes all of the variables which are input to the program.

VARIABLE	DESCRIPTION
ADVR	negative of the advance ratio of the blading, J, where positive is considered to being clockwise direction.
BETA34	geometric angle, Beta, at the 3/4 span of the blade $\beta_{3/4}$.
BLDIAM	physical blade diameter, D_b.
CN	Courant Number, used to determine marching step size.
FSMACH	free stream Mach number, M_∞
GAMMA	ratio of specific heats, γ
IBC	= 0, applies blade boundary condition; = 1, nacelle only.
IGRID	= 0, rescale by new Jacobian; = 1, old grid system.
IMETHD	has no effect in current version.
IMETOT	= 0, do nothing; = 1, print out metrics and exit.
IPTCH	= 0 } grid is read from Tape 11 = 1 } by user in GRID.

IREAD	= 0, start from scratch; = 1, read starting solution from Tape 1.
IWRIT	= 0, nothing; = 1, store solution on Tape 2.
JLE	integer location of blade leading edge; usually 11.
JMAX	number of mesh points in ξ-direction; ≤ 45.
JTE	integer location of blade trailing edge; usually 27.
KMAX	number of mesh points in η-direction; ≤ 21.
KTIP	integer location of blade tip; usually 11.
LMAX	number of mesh points in ζ-direction; ≤ 11.
METH	not used.
NBLADE	number of blades.
NC	parameter read from Tape 1.
NCHNGE	not used.
NMAX	number of iterations to be performed.
PER	angle between blades in degrees.
PINF	free stream pressure normalized by γP_∞; = $1/\gamma$
Q	3-D storage array of independent conservative variables read from Tape 1.
RINF	free stream density normalized by ρ_∞; = 1.
SMU	explicit smoothing coefficient; $0(\Delta t)$.
SMUIMP	implicit smoothing coefficient; 0(2*SMU).
TAU	current value of time.

6.3.2. Input Data Format

The data is either input from cards (Tape 5) or from disc (Tape 1 and/or Tape 11). In Appendix A.2 an example of a typical input is provided. In general, the input cards are as follows:

CARD NO. 1 (5F10.5)

Column no.	1	11	21	31	41	80
	FSMACH	GAMMA	PINF	RINF	ADVR	

CARD NO. 2 (6I5, 3F10.5)

Column no.	1 → 5	6 - 10	11 - 15	16 - 20	21 - 25
	IREAD	IWRIT	IPTCH	NMAX	METH

Column no.	26 - 30	313	41	51	80
	IMETHD	CN	SMU	SMUIMP	

CARD NO. 3 (6I5, 3F10.5)

Column no.	1 → 5	6 - 10	11 - 15	16 - 20	80
	IBC	IMETOT	NCHNGE	IGRID	

If IPTCH $\leq$ 0, the following card is read.

CARD NO. 4 (7I5, 3F10.5)

Column no.	1 → 5	6 - 10	11 - 15	16 - 20	21 - 25
	JMAX	KMAX	LMAX	JLE	JTE

Column no.	26 - 30	31 - 35	36	46	56	80
	KTIP	NBLADE	PER	BETA34	BLDIAM	

On the above cards, remember that all integers are right adjusted.

The possibility of reading the input data from discs is a real and distinct option within the 3-D flow field code.

If IPTCH > 0, the following data is read from TAPE11. From INPUT

TAPE11; JMAX, KMAX, LMAX, JLE, JTE, KTIP, NBLADE, PER, BETA34, BLDIAM

and from GRID

TAPE11; X(KL,J), Y(KL,J), Z(KL,J)

are read. This data is used in employing and determining the computational grid.

If the solution is continued from a previous solution the starting flow field is read from TAPE1 in INPUT as,

TAPE1; Q, TAU, NC.

6.4. Program Output

In the following section, a brief description of the 3-D flow field program output is presented. Typically the output can be broken up into various sections. The first section consists of printing the input data. This defines all of the options and the pertinant variables which are to be used during execution. Also, identifiers from the GRID subroutine and from the EIGEN subroutine acknowledge the reading of the grid and the determining of the stepsize respectively.

During execution (or marching), there is a different set of data printed. This can be considered the second section. It consists of the L2 and maximum residual with its location, the step number and the normalized density at the body one point away from the stagnation point, the forces and moments on the blade and the nacelle, and finally printer plots of the various independent variables. The forces and moments and the printer plots occur every IFREQ iterations where IFREQ is set in the main program.

The third section occurs at the end of the iteration and consists of a quite detailed print out of variables which are used to determine the boundary conditions on the blades and nacelle. This allows a user to observe these variables and to get a better understanding of the flow condition on the body surfaces. This is also useful in the process of debugging.

Finally, the flow field is printed in the fourth section in two parts. The first part prints the entire flow field at the periodic planes and it prints the body data only at the interior planes. The output consists of the normalized independent variables p, ρ, u, v, w, e, M, the total enthalpy ratio $H_T/H_{T\infty}$ and the geometric descriptions Z, R, and ϕ.

The second part prints these same variables on the camber and face side blade surface.

6.5. Operating Procedures and Trouble Shooting Hints

The only comment that should be made here on operating procedures is that if problems occur when starting the solution from a free-stream guess, the nacelle only should be calculated initially then allow the blades to enter into the solution at a later time. This makes for an easier transition of the flow field.

Usually problems associated with the code stopping are well documented by an appropriate output. In the past, the major cause of a stoppage has been too high a Courant Number or not enough grid resolution at the tip of the blade. The Courant Number problem is easy to correct but the grid resolution is not unless one has an increased storage capability. If increased storage is available, then adding more radial points at the surfaces would also enhance the chances for a better solution.

7. DATA REDUCTION PROGRAM

This program is designed to take the flow field data produced by the Three-Dimensional Prop-Fan Flow Field Program and generate printer plots, store data for computer generated plots, and to calculate the various propeller performance coefficients. The following sections will describe these tasks in more detail.

7.1. Program Organization and Interaction

As is the case in most computer programs, the input data is read from cards, disc, and/or tapes before any calculations begin. This input data is that which has been furnished by both the flow field program (Section 6) and the mesh generation program (Section 5). Once this interaction is complete, the data reduction program proceeds to manipulate the input data for the user. This results in:

- printer plots of the C_p distribution on the face and camber side of the blades at various specified radial locations;
- printer plots of the axial C_p distribution on the nacelle surface at various meridional angles;
- section properties on the face and camber side of the blades;
- geometric parameters for each section;
- integrated section properties to provide section left, drag, thrusts, and torques;
- integrated section thrusts and torques to calculate the power coefficient and efficiency;

- the output of the above calculated pertinent quantities;
- the three-dimensional data base being converted into various two-dimensional data bases which can be used by a plot routine to display the distribution of the various properties.

7.2. Flow Chart

This section provides a brief flow chart describing the overall logical flow of the program.

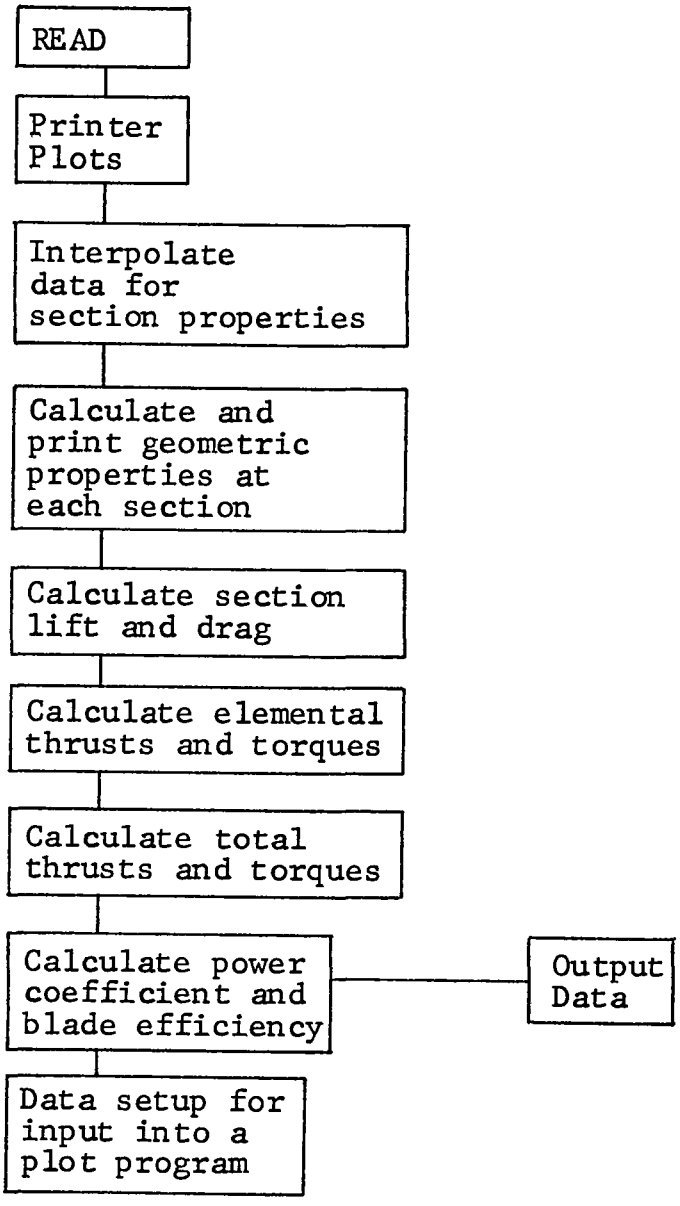

7.3. Program Input

In this section, the input required by the program is described. First a dictionary of the input variables is provided followed by a description of the input data format including an example.

7.3.1. Dictionary of Input Variables.

The variables which are input to this program are described in the following list.

VARIABLE	DESCRIPTION
ADVR	negative of the advance ratio of the blading, J. See Section 6.3.1.
BETA34	geometric angle, Beta, at the 3/4 span of the blade, $\beta_{3/4}$. See Section 6.3.1.
BLDIAM	physical blade diameter, D_b.
FSMACH	free stream Mach number, M_∞.
GAMMA	ratio of specific heats, γ
IPLOT	control option for storing RSEC(N) on tape 9; equal to 0 or 1.
JLE	integer location of blade leading edge.
JMAX	number of mesh points in ξ direction; ≤ 45
JTE	integer location of blade trailing edge.
KLMAX	number of KMAX*LMAX points; ≤ 240.
KMAX	number of mesh points in η direction; ≤ 21.

KTIP	integer location of blade tip.
LMAX	number of mesh points in ζ direction; ≤ 11.
NBLADE	number of blades.
NC	parameter read from tape 1; redefined within program.
NMAX	number of radial blade sections.
PERD	angle between blades in degrees.
PINF	free stream pressure normalized by γP_∞; $= 1/\gamma$.
Q	three dimensional storage array of independent conservative variables read from tape 1.
RINF	free stream density normalized by ρ_∞; $= 1$.
RSEC(N)	radial locations on blade for which flow properties will be printed; ≤ 20.
TAU	time the blade has traveled; not used.
X(KL,J)	vector array of length KLMAX by JMAX of user supplied X-mesh points; read from tape 11.
Y(KL,J)	vector array of length KLMAX by JMAX of user supplied Y-mesh points; read from tape 11.
Z(KL,J)	vector array of length KLMAX by JMAX of user supplied Z-mesh points; read from tape 11.

7.3.2. Input Data Format

The data are input from cards (TAPE5) and from disc (TAPE1 and TAPE11). An example of the input is provided in Appendix A.3. The input data cards would read:

CARD NO. 1 (8F10.6)

Column no.	1	11	21	31	41	80
	FSMACH	GAMMA	PINF	RINF	ADVR	

CARD NO. 2 (16I5)

Column no.	1 - 5	6 - 10	80
	NMAX	IPLOT	

CARD NO. 3 (8F10.6) There are (NMAX-1)/8 + 1 cards, i.e., NMAX = 10, 2 cards.

Column no.	1	11	21	- - - - 71	80
	RSEC(1)	RSEC(2)	RSEC(3)	- - - - RSEC(NMAX)	

The remainder of the data is furnished by the flow field program from TAPE1 and by the mesh generation program from TAPE11. These consist of:

READ 1

TAPE1; Q array, TAU, NC

READ 2

TAPE11; JMAX, KMAX, LMAX, KLMAX, JLE, JTE, KTIP, NBLADE, PERD, BETA34, BLDIAM

READ 3

TAPE11; X(KL,J), Y(KL,J), Z(KL,J), KL = 1, KLMAX, and J = 1, JMAX.

7.4. Program Output

The generated output is described in this section. A description of the output format is provided in the next subsection with an example furnished in Appendix B.3.

7.4.1. Output Format

To give the user a cursory look at the solution, printer plots of the pressure coefficient, C_p, are presented. These consist of the chordwise C_p variation on both the face and camber side of the blades at varying constant radii from the centerline of the nacelle and of the axial C_p variation for different meridional angles ϕ on the nacelle surface.

Next the local geometric and flow field properties of the face and camber side of the blade at a constant radius are printed. These consist of the z, ϕ, and y coordinates at a given point and of the pressure, density, axial velocity, radial velocity, rotational velocity, and energy at the same point.

The final major printouts consist of

- the index of each station
- the radius measured from the centerline of the nacelle
- the chord at each section (constant radius)
- the geometric angle at each section
- the effective pitch angle at each section
- the effective angle of attack at each section
- the lift coefficient per section
- the drag coefficient per section
- the relative velocity per section

- the dynamic pressure per section
- the thrust per blade per section
- the torque per blade per section
- the total thrust per section
- the total torque per section
- the total thrust coefficient
- the total torque coefficient

and of the geometric and flow field properties of the given blading. These consist of the number of blades, Mach numbers, blade diameter, free stream pressure, free stream density, free stream velocity, advance ratio, thrust coefficient, torque coefficient, power coefficient, and blade efficiency.

7.5. Operating Procedure and Trouble Shooting Hints

This particular program is extremely simple and straight forward to use. The only problems that could arise are possible bad data on the input cards or files.

8. PROGRAM SUMMARIES

It is intended here to discuss the compatibility of the complex of computer codes to various computer systems. Also, the typical run times on a CDC 7600 machine are presented for time comparisons.

8.1. Machine Compatibility

This particular complex of codes was developed on the CDC 7600 machine at NASA-Ames. It was intended to create the codes such that they are all machine independent. A version of these codes are running on the IBM 370/3033 system at Lewis Research Center. This shows the ability of the codes to be run on various systems.

Typical storage requirements on a CDC 7600 are presented next. For the mesh generation program, which is overlayed, the first overlay determines the shape of grid domain and needs 54401 octal words of small core storage. The second overlay which determines the patch coefficients uses 22612 octal words of small core storage and 360750 octal words of large core storage. The clustering of the grid points is done in the third overlay and uses 13407 octal words of small core storage. Finally, the fourth overlay creates the grid and uses 47422 octal words of small core storage and 1017260 octal words of large core storage.

The 3-D flow field code uses 105737 octal words of small core storage and 1044340 octal words of large core storage.

SCM 36650 octal words of small core storage and LCM 546460 octal words of large core storage are used in the data reduction program.

The 3-D flow field code used all available storage space on the NASA-Ames 7600, but if a virtual memory machine was available, the user could increase the useable core such that a far better grid resolution could be obtained. This should have a significant impact on the solution process. Even though it would take more computational time the obtained solution could be refined enough to give significant results since we believe that at present the solution procedure is correct, but there are not enough grid points available to obtain a well behaved solution.

8.2. Runtime Estimates

The mesh generation code and the data reduction code have insignificant running times as compared to the 3-D flow field code. Typically, these codes consume less than 30 seconds on a CDC 7600 machine for a 45 (axial direction) x 21 (radial direction) x 11 (meridional direction) grid.

There are three times given for the 3-D flow field code on a 45 x 21 x 11 grid system. The first time is for the

inviscid flow past the nacelle only, followed by the inviscid flow past the nacelle-blade combination and finally these same conditions calculated by the diagonal algorithm.

Table 1 shows that the diagonal algorithm is 26% faster than the regular algorithm, where the comparisons are based on solutions which were iterated from a uniform flow initial condition. Since only the timing ratio is of interest in Table 1, there was no need to run the solution to convergence.

TABLE 1

CONDITION (Inviscid)	ALGORITHM	ITERATIONS	TIME (CDC 7600)	RATIO
Nacelle	Reg.	201	1364 seconds	6.79
Nacelle-Blade	Reg.	100	700 seconds	7.0
Nacelle-Blade	Diag.	300	1545 seconds	5.15

REFERENCES

1. Lindemuth, I., and Killeen, I., "Alternating Direction Implicit Techniques for Two-Dimensional Magnetohydrodynamics Calculations," J. of Comp. Physics, Vol. 13, 1973, pp. 181-208.

2. Briley, W. F. and McDonald, H., "An Implicit Numerical Method for the Multi-Dimensional Compressible Navier-Stokes Equations," Report No. 911363-6, United Aircraft Research Laboratories, 1973.

3. Briley, W. R. and McDonald, H., "Solution of the Three-Dimensional Compressible Navier-Stokes Equations by an Implicit Technique," Lecture Notes in Physics, No. 35, Proceedings of the Fourth International Conference on Numerical Methods in Fluid Dynamics, ed. R. D. Richtmyer, Boulder, Colo., June 1974, pp. 105-110.

4. Beam, Richard M. and Warming, R. F., "An Implicit Finite-Difference Algorithm for Hyperbolic Systems in Conservation-Law Form," J. of Comp. Physics, Vol. 22, 1976, pp. 87-109.

5. Beam, R. and Warming, R. F., "An Implicit Factored Scheme for the Compressible Navier-Stokes Equations," AIAA Paper 77-645, Albuquerque, N. Mex., June 1977.

6. Steger, J. L. and Kutler, P., "Implicit Finite-Difference Procedures for the Computation of Vortex Wakes," AIAA J., Vol. 15, No. 4, April 1977, pp. 581-590.

7. Kutler, P., Chaussee, D., and Pulliam, T., "Supersonic Flow over Ablated Nosetips Using an Implicit Unsteady Euler Equation Solver," Paper presented at the Open Forum Session of the AIAA 10th Fluid and Plasma Dynamics Conference, Albuquerque, N. Mex., June 1977.

8. Steger, J. L., "Implicit Finite-Difference Simulation of Flow About Arbitrary Geometries with Application to Airfoils," AIAA Paper 77-665, Albuquerque, N. Mex., June 1977.

9. Pulliam, T. H. and Steger, J. L., "On Implicit Finite-Difference Simulations of Three-Dimensional Flow," AIAA J., Vol. 18, No. 2, Feb. 1980, pp. 159.

10. Warming, R. F. and Beam, R. M., "On the Construction and Application of Implicit Factored Schemes for Conservation Laws," to appear in the SIAM-AMS Proceedings of the Symposium on Computational Fluid Dynamics, New York, April 16-17, 1977.

11. Rohrbach, C., "A Report on the Aerodynamic Design and Wind Tunnel Test of a Prop-Fan Model," AIAA Paper 76-667, July 1976.

12. Isaacson, E. and Keller, H. B., "Analysis of Numerical Methods," John Wiley and Sons, Inc., New York/London/ Sidney, 1969, p. 58.

13. Pulliam, T. H., and Chaussee, D. S., "A Diagonal Form of an Implicit Approximate-Factorization Algorithm," To appear in the Journal of Computational Physics, 1980.

14. Warming, R. F., Beam, R. M., and Hyett, B. J., "Diagonalization and Simulaneous Symmetrization of the Gas Dynamic Matrices," Math. Comp., Vol. 29, No. 132, Oct. 1975, pp. 1037-1045.

Appendix A

Sample Input Data

Sample input decks have been reproduced and are presented in this appendix for the mesh generation program, the three-dimensional flow field program, and the data reduction program.

A.1. Mesh Generation Program

Input data for the mesh generation program is obtained from the INPUT file (TAPE2) and from an archives file (TAPE5) containing node clustering information along with the geometric representation of the prop-fan configuration. Sample data read from INPUT is given in Figure A-1, while sample data read from the archives file is given in Figures A-2 and A-3.

A.2. Three-Dimensional Flow Field Program

Sample input data for the three-dimensional flow field program is presented in Figure A-4 along with a set of control cards applicable to the CDC 7600.

A.3. Data Reduction Program

Sample input data for the data reduction program is given in Figure A-5.

```
T     F     F     T
3    11     0    27   45    11   21    11    8
.0041      0.0        .0041      0.5        .02025    .02025    0.5
1.05       -10.0      10.0       0.0
1.05       -1.00      1.0        0.0

0.0        -1.0       0.6        0.3
0.1        -0.5       1.0        0.0
1.05       0.00       1.0        0.0
0.2        -0.1       0.6        0.4
0.2        -0.1       1.0        0.0
```

Figure A-1. Sample Input for the Mesh Generation Program--Read from Input

```
        1.0
   45
-.2654      0.0
-.2690      .003
-.267713    .005084
-.266025    .007676
-.254635    .0141218
-.2512439   .019433
-.243853    .025154
-.23646     .029833
-.229072    .0340155
-.221681    .0377465
-.21429     .041075
-.2069      .044047
-.196483    .0485133
-.186066    .0526777
-.17565     .0566150
-.165233    .0603984
-.154817    .0640987
-.1444      .067792
-.0209413   .1110041
0.10144     .15542
.112688     .159335
.1356       .166063
.162692     .171092
.1941352    .1762713
.225393     .170157
.250636     .18048
.27214      .181044
.291709     .18117
.311155     .180732
.3306       .180373
.350145     .179534
.36949      .178444
.388935     .177144
.427625     .174069
.466715     .170002
.505605     .167009
.52545      .165576
.56354      .162088
.6345       .158244
.70509      .157126
.77568      .1579040
.84628      .16006
.91673      .162718
.987327     .165374
1.058       .16753
```

Figure A-2. Input to Mesh Generation Program from Archives File--Nodal Clustering Data

```
   13    53    15    25
0.0          24.6          -.0548      .1395
     1     1      0.0      -0.000000  -0.000000   0.0100   0.013744  -0.014524   0.2392
     1     2      0.0200   0.018608   -0.020138   0.0300   0.022219  -0.025161   0.2392
     1     3      0.0400   0.025593   -0.029569   0.0500   0.028758  -0.033534   0.2392
     1     4      0.0600   0.031684   -0.037256   0.0700   0.034393  -0.040793   0.2392
     1     5      0.0800   0.036917   -0.044163   0.0900   0.039287  -0.047382   0.2392
     1     6      0.1000   0.041542   -0.050466   0.1250   0.046815  -0.057695   0.2392
     1     7      0.1500   0.051660   -0.064393   0.1750   0.056146  -0.070742   0.2392
     1     8      0.2000   0.060344   -0.076830   0.2250   0.064311  -0.082708   0.2392
     1     9      0.2500   0.068051   -0.088370   0.2750   0.071557  -0.093803   0.2392
     1    10      0.3000   0.074812   -0.098985   0.3250   0.077806  -0.103898   0.2392
     1    11      0.3500   0.080503   -0.108452   0.3750   0.082862  -0.112542   0.2392
     1    12      0.4000   0.084843   -0.116059   0.4250   0.086394  -0.118902   0.2392
     1    13      0.4500   0.087413   -0.120983   0.4750   0.087763  -0.122236   0.2392
     1    14      0.5000   0.087313   -0.122586   0.5250   0.085945  -0.121979   0.2392
     1    15      0.5500   0.083782   -0.120418   0.5750   0.081074  -0.117972   0.2392
     1    16      0.6000   0.078086   -0.114697   0.6250   0.075060  -0.110655   0.2392
     1    17      0.6500   0.072137   -0.105873   0.6750   0.069382  -0.100359   0.2392
     1    18      0.7000   0.066864   -0.094117   0.7250   0.064621  -0.087165   0.2392
     1    19      0.7500   0.062472   -0.079592   0.7750   0.060073  -0.071544   0.2392
     1    20      0.8000   0.057089   -0.063165   0.8250   0.053207  -0.054611   0.2392
     1    21      0.8500   0.048408   -0.046145   0.8750   0.042818  -0.038080   0.2392
     1    22      0.9000   0.036447   -0.030681   0.9100   0.033672  -0.027961   0.2392
     1    23      0.9200   0.030768   -0.025361   0.9300   0.027755  -0.022838   0.2392
     1    24      0.9400   0.024642   -0.020337   0.9500   0.021442  -0.017813   0.2392
     1    25      0.9600   0.018107   -0.015220   0.9700   0.014813  -0.012567   0.2392
     1    26      0.9800   0.011369   -0.009885   0.9900   0.007834  -0.007179   0.2392
     1    27      1.0000   0.0        0.0                                       0.2392
.1196          19.8          -.0636      .1438
     1     1      0.0      -0.000000  -0.000000   0.0100   0.013744  -0.014524   0.2392
     1     2      0.0200   0.018608   -0.020138   0.0300   0.022219  -0.025161   0.2392
     1     3      0.0400   0.025593   -0.029569   0.0500   0.028758  -0.033534   0.2392
     1     4      0.0600   0.031684   -0.037256   0.0700   0.034393  -0.040793   0.2392
     1     5      0.0800   0.036917   -0.044163   0.0900   0.039287  -0.047382   0.2392
     1     6      0.1000   0.041542   -0.050466   0.1250   0.046815  -0.057695   0.2392
     1     7      0.1500   0.051660   -0.064393   0.1750   0.056146  -0.070742   0.2392
     1     8      0.2000   0.060344   -0.076830   0.2250   0.064311  -0.082708   0.2392
     1     9      0.2500   0.068051   -0.088370   0.2750   0.071557  -0.093803   0.2392
     1    10      0.3000   0.074812   -0.098985   0.3250   0.077806  -0.103898   0.2392
     1    11      0.3500   0.080503   -0.108452   0.3750   0.082862  -0.112542   0.2392
     1    12      0.4000   0.084843   -0.116059   0.4250   0.086394  -0.118902   0.2392
     1    13      0.4500   0.087413   -0.120983   0.4750   0.087763  -0.122236   0.2392
     1    14      0.5000   0.087313   -0.122586   0.5250   0.085945  -0.121979   0.2392
     1    15      0.5500   0.083782   -0.120418   0.5750   0.081074  -0.117972   0.2392
     1    16      0.6000   0.078086   -0.114697   0.6250   0.075060  -0.110655   0.2392
     1    17      0.6500   0.072137   -0.105873   0.6750   0.069382  -0.100359   0.2392
     1    18      0.7000   0.066864   -0.094117   0.7250   0.064621  -0.087165   0.2392
     1    19      0.7500   0.062472   -0.079592   0.7750   0.060073  -0.071544   0.2392
     1    20      0.8000   0.057089   -0.063165   0.8250   0.053207  -0.054611   0.2392
     1    21      0.8500   0.048408   -0.046145   0.8750   0.042818  -0.038080   0.2392
     1    22      0.9000   0.036447   -0.030681   0.9100   0.033672  -0.027961   0.2392
     1    23      0.9200   0.030768   -0.025361   0.9300   0.027755  -0.022838   0.2392
     1    24      0.9400   0.024642   -0.020337   0.9500   0.021442  -0.017813   0.2392
     1    25      0.9600   0.018107   -0.015220   0.9700   0.014813  -0.012567   0.2392
     1    26      0.9800   0.011369   -0.009885   0.9900   0.007834  -0.007179   0.2392
```

Figure A-3. Input to Mesh Generation Program from Archives File--Geometric Representation of Prop-Fan

```
    1   27    1.0000   0.0          0.0                                          0.2392
.1429       18.2        -.06502     .14456
    2    1    0.0      -0.000000   -0.000000    0.0100   0.009476  -0.010010    0.2857
    2    2    0.0200    0.012832   -0.013639    0.0300   0.015298  -0.016670    0.2857
    2    3    0.0400    0.017579   -0.019274    0.0500   0.019692  -0.021563    0.2857
    2    4    0.0600    0.021608   -0.023676    0.0700   0.023351  -0.025649    0.2857
    2    5    0.0800    0.024948   -0.027502    0.0900   0.026429  -0.029247    0.2857
    2    6    0.1000    0.027823   -0.030903    0.1250   0.031051  -0.034723    0.2857
    2    7    0.1500    0.033942   -0.038159    0.1750   0.036510  -0.041272    0.2857
    2    8    0.2000    0.038792   -0.044134    0.2250   0.040824  -0.046792    0.2857
    2    9    0.2500    0.042629   -0.049265    0.2750   0.044219  -0.051574    0.2857
    2   10    0.3000    0.045615   -0.053731    0.3250   0.046821  -0.055752    0.2857
    2   11    0.3500    0.047823   -0.057603    0.3750   0.048597  -0.059247    0.2857
    2   12    0.4000    0.049115   -0.060643    0.4250   0.049352  -0.061757    0.2857
    2   13    0.4500    0.049294   -0.062570    0.4750   0.048926  -0.063073    0.2857
    2   14    0.5000    0.048235   -0.063256    0.5250   0.047215  -0.063110    0.2857
    2   15    0.5500    0.045909   -0.062614    0.5750   0.044376  -0.061754    0.2857
    2   16    0.6000    0.042676   -0.060513    0.6250   0.040870  -0.058875    0.2857
    2   17    0.6500    0.039033   -0.056831    0.6750   0.037245  -0.054378    0.2857
    2   18    0.7000    0.035580   -0.051512    0.7250   0.034100  -0.048285    0.2857
    2   19    0.7500    0.032724   -0.044591    0.7750   0.031324  -0.040639    0.2857
    2   20    0.8000    0.029769   -0.036440    0.8250   0.027933  -0.032063    0.2857
    2   21    0.8500    0.025761   -0.027610    0.8750   0.023213  -0.023217    0.2857
    2   22    0.9000    0.020231   -0.019077    0.9100   0.018905  -0.017536    0.2857
    2   23    0.9200    0.017504   -0.016051    0.9300   0.016032  -0.014599    0.2857
    2   24    0.9400    0.014493   -0.013154    0.9500   0.012803  -0.011691    0.2857
    2   25    0.9600    0.011237   -0.010188    0.9700   0.009520  -0.008652    0.2857
    2   26    0.9800    0.007736   -0.007101    0.9900   0.006485  -0.005535    0.2857
    2   27    1.0000    0.000000    0.000000                                     0.2857
.1837       15.5        -.06682     .1461
    3    1    0.0       0.000000    0.000000    0.0100   0.007114  -0.007066    0.3673
    3    2    0.0200    0.009917   -0.009309    0.0300   0.012129  -0.011102    0.3673
    3    3    0.0400    0.014114   -0.012613    0.0500   0.015921  -0.013920    0.3673
    3    4    0.0600    0.017582   -0.015102    0.0700   0.019117  -0.016163    0.3673
    3    5    0.0800    0.020538   -0.017177    0.0900   0.021865  -0.018093    0.3673
    3    6    0.1000    0.023113   -0.018944    0.1250   0.025955  -0.020854    0.3673
    3    7    0.1500    0.028446   -0.022494    0.1750   0.030628  -0.024928    0.3673
    3    8    0.2000    0.032537   -0.025182    0.2250   0.034201  -0.028282    0.3673
    3    9    0.2500    0.035634   -0.027241    0.2750   0.036847  -0.030867    0.3673
    3   10    0.3000    0.037853   -0.028769    0.3250   0.038656  -0.032956    0.3673
    3   11    0.3500    0.039247   -0.029814    0.3750   0.039613  -0.034122    0.3673
    3   12    0.4000    0.039734   -0.030266    0.4250   0.039600  -0.034231    0.3673
    3   13    0.4500    0.039215   -0.030026    0.4750   0.038598  -0.033669    0.3673
    3   14    0.5000    0.037738   -0.029180    0.5250   0.036669  -0.032573    0.3673
    3   15    0.5500    0.035402   -0.027844    0.5750   0.033959  -0.030998    0.3673
    3   16    0.6000    0.032364   -0.026016    0.6250   0.030643  -0.028863    0.3673
    3   17    0.6500    0.028839   -0.023622    0.6750   0.027007  -0.026239    0.3673
    3   18    0.7000    0.025200   -0.020734    0.7250   0.023464  -0.023130    0.3673
    3   19    0.7500    0.021792   -0.017450    0.7750   0.020158  -0.019728    0.3673
    3   20    0.8000    0.018537   -0.013994    0.8250   0.016902  -0.016281    0.3673
    3   21    0.8500    0.015229   -0.010604    0.8750   0.013483  -0.012996    0.3673
    3   22    0.9000    0.011616   -0.007586    0.9100   0.010824  -0.009710    0.3673
    3   23    0.9200    0.010009   -0.006279    0.9300   0.009179  -0.008279    0.3673
    3   24    0.9400    0.008341   -0.005093    0.9500   0.007502  -0.006906    0.3673
    3   25    0.9600    0.006669   -0.003905    0.9700   0.005837  -0.005697    0.3673
    3   26    0.9800    0.005003   -0.004291    0.9900   0.004166  -0.003886    0.3673
    3   27    1.0000   -0.000000   -0.000000                                     0.3673
.2245       12.2        -.06862     .14737
    4    1    0.0       0.000000    0.000000    0.0099   0.005288  -0.005288    0.4490
    4    2    0.0199    0.007757   -0.006278    0.0299   0.009817  -0.007217    0.4490
```

Figure A-3. (Continued)

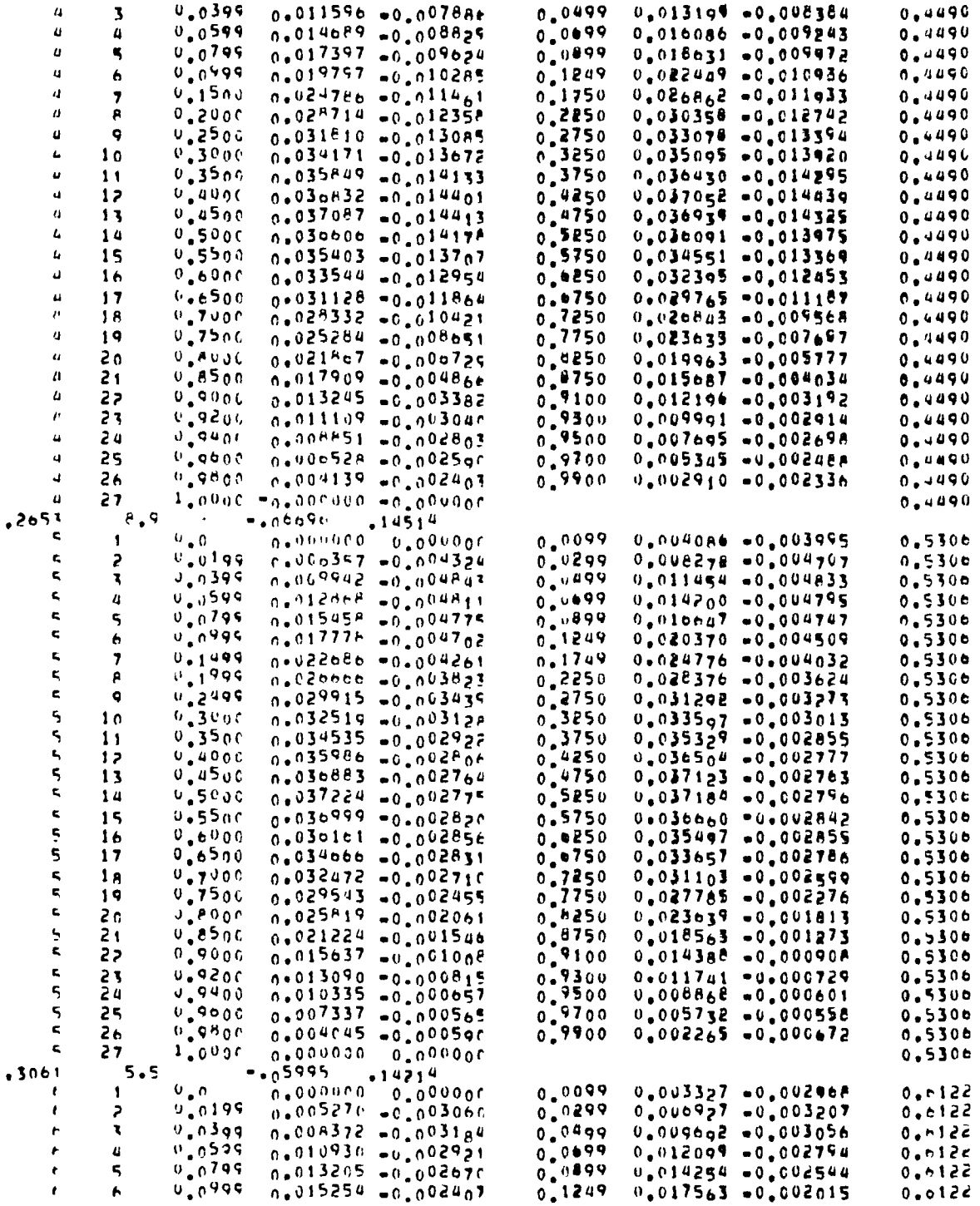

Figure A-3. (Continued)

	7	0.1499	0.019037	-0.001598	0.1750	0.021520	-0.001208	0.0122
	8	0.1999	0.025231	-0.000848	0.2250	0.024749	-0.000510	0.0122
	9	0.2499	0.026205	-0.000197	0.2750	0.027483	0.000104	0.0122
	10	0.3000	0.026030	0.000369	0.3250	0.029652	0.000603	0.0122
	11	0.3500	0.025550	0.000806	0.3750	0.031325	0.000977	0.0122
	12	0.4000	0.031980	0.001122	0.4250	0.032516	0.001240	0.0122
	13	0.4500	0.032929	0.001330	0.4750	0.033222	0.001394	0.0122
	14	0.5000	0.033393	0.001431	0.5250	0.033444	0.001445	0.0122
	15	0.5500	0.033368	0.001436	0.5750	0.033159	0.001409	0.0122
	16	0.6000	0.032814	0.001370	0.6250	0.032327	0.001324	0.0122
	17	0.6500	0.031689	0.001271	0.6750	0.030894	0.001215	0.0122
	18	0.7000	0.029933	0.001160	0.7250	0.028799	0.001107	0.0122
	19	0.7500	0.027483	0.001061	0.7750	0.025971	0.001020	0.0122
	20	0.8000	0.024256	0.000991	0.8250	0.022330	0.000974	0.0122
	21	0.8500	0.020166	0.000954	0.8750	0.017740	0.000918	0.0122
	22	0.9000	0.015049	0.000880	0.9100	0.013897	0.000867	0.0122
	23	0.9200	0.012692	0.000846	0.9300	0.011428	0.000814	0.0122
	24	0.9400	0.010096	0.000761	0.9500	0.008688	0.000681	0.0122
	25	0.9600	0.007194	0.000565	0.9700	0.005606	0.000405	0.0122
	26	0.9800	0.003914	0.000192	0.9900	0.002106	-0.000086	0.0122
	27	1.0000	0.000000	0.000000				0.0122
.3469	2.1		-.04816	.13957				
	1	0.0	0.000000	0.000000	0.0100	0.002869	-0.002286	0.0939
	2	0.0200	0.004463	-0.002376	0.0300	0.005847	-0.002470	0.0939
	3	0.0400	0.007045	-0.002446	0.0500	0.008128	-0.002335	0.0939
	4	0.0600	0.009145	-0.002223	0.0700	0.010110	-0.002114	0.0939
	5	0.0800	0.011025	-0.002008	0.0900	0.011896	-0.001896	0.0939
	6	0.1000	0.012725	-0.001778	0.1250	0.014637	-0.001446	0.0939
	7	0.1500	0.016352	-0.001099	0.1750	0.017912	-0.000772	0.0939
	8	0.2000	0.019336	-0.000476	0.2250	0.020634	-0.000185	0.0939
	9	0.2500	0.021914	0.000083	0.2750	0.022880	0.000328	0.0939
	10	0.3000	0.023840	0.000556	0.3250	0.024605	0.000743	0.0939
	11	0.3500	0.025452	0.000913	0.3750	0.026107	0.001055	0.0939
	12	0.4000	0.026661	0.001173	0.4250	0.027117	0.001270	0.0939
	13	0.4500	0.027474	0.001345	0.4750	0.027729	0.001397	0.0939
	14	0.5000	0.027884	0.001427	0.5250	0.027938	0.001438	0.0939
	15	0.5500	0.027885	0.001430	0.5750	0.027722	0.001409	0.0939
	16	0.6000	0.027443	0.001377	0.6250	0.027043	0.001338	0.0939
	17	0.6500	0.026518	0.001296	0.6750	0.025859	0.001251	0.0939
	18	0.7000	0.025061	0.001204	0.7250	0.024119	0.001162	0.0939
	19	0.7500	0.023022	0.001121	0.7750	0.021765	0.001087	0.0939
	20	0.8000	0.020338	0.001061	0.8250	0.018731	0.001040	0.0939
	21	0.8500	0.016923	0.001011	0.8750	0.014895	0.000964	0.0939
	22	0.9000	0.012645	0.000907	0.9100	0.011680	0.000883	0.0939
	23	0.9200	0.010672	0.000852	0.9300	0.009613	0.000808	0.0939
	24	0.9400	0.008496	0.000744	0.9500	0.007311	0.000652	0.0939
	25	0.9600	0.006052	0.000527	0.9700	0.004714	0.000364	0.0939
	26	0.9800	0.003294	0.000158	0.9900	0.001784	-0.000096	0.0939
	27	1.0000	0.000000	0.000000				0.0939
.3878	-1.0		-.0317A	.13614				
	1	0.0	-0.000000	-0.000000	0.0100	0.002530	-0.001863	0.7755
	2	0.0200	0.003809	-0.002029	0.0300	0.004937	-0.002169	0.7755
	3	0.0400	0.005904	-0.002203	0.0500	0.006778	-0.002175	0.7755
	4	0.0600	0.007589	-0.002137	0.0700	0.008366	-0.002098	0.7755
	5	0.0800	0.009106	-0.002055	0.0900	0.009810	-0.002006	0.7755
	6	0.1000	0.010480	-0.001950	0.1250	0.012025	-0.001771	0.7755
	7	0.1500	0.013413	-0.001571	0.1750	0.014677	-0.001381	0.7755
	8	0.2000	0.015833	-0.001202	0.2250	0.016890	-0.001032	0.7755
	9	0.2500	0.017851	-0.000871	0.2750	0.018724	-0.000720	0.7755
	10	0.3000	0.019509	-0.000587	0.3250	0.020214	-0.000468	0.7755

Figure A-3. (Continued)

	11	0.3500	0.020836	-0.000360	0.3750	0.021378	-0.000284	0.7755
	12	0.4000	0.021838	-0.000215	0.4250	0.022219	-0.000160	0.7755
	13	0.4500	0.022518	-0.000120	0.4750	0.022734	-0.000092	0.7755
	14	0.5000	0.022869	-0.000080	0.5250	0.022919	-0.000061	0.7755
	15	0.5500	0.022884	-0.000068	0.5750	0.022756	-0.000108	0.7755
	16	0.6000	0.022534	-0.000128	0.6250	0.022210	-0.000151	0.7755
	17	0.6500	0.021782	-0.000172	0.6750	0.021248	-0.000189	0.7755
	18	0.7000	0.020587	-0.000202	0.7250	0.019609	-0.000207	0.7755
	19	0.7500	0.018904	-0.000201	0.7750	0.017864	-0.000185	0.7755
	20	0.8000	0.016682	-0.000152	0.8250	0.015351	-0.000105	0.7755
	21	0.8500	0.013854	-0.000053	0.8750	0.012177	-0.000003	0.7755
	22	0.9000	0.010320	0.000056	0.9100	0.009526	0.000084	0.7755
	23	0.9200	0.008697	0.000110	0.9300	0.007828	0.000129	0.7755
	24	0.9400	0.006911	0.000139	0.9500	0.005940	0.000122	0.7755
	25	0.9600	0.004910	0.000088	0.9700	0.003821	0.000025	0.7755
	26	0.9800	0.002671	-0.000067	0.9900	0.001458	-0.000171	0.7755
	27	1.0000	0.000000	0.000000				0.7755
.428	-4.0		-.01012	.12956				
	1	0.0	-0.000000	-0.000000	0.0100	0.002210	-0.001660	0.8571
	2	0.0200	0.003197	-0.001956	0.0300	0.004070	-0.002208	0.8571
	3	0.0400	0.004806	-0.002350	0.0500	0.005459	-0.002437	0.8571
	4	0.0600	0.006074	-0.002510	0.0700	0.006661	-0.002575	0.8571
	5	0.0800	0.007218	-0.002631	0.0900	0.007747	-0.002677	0.8571
	6	0.1000	0.008250	-0.002712	0.1250	0.009402	-0.002754	0.8571
	7	0.1500	0.010432	-0.002760	0.1750	0.011371	-0.002757	0.8571
	8	0.2000	0.012229	-0.002745	0.2250	0.013011	-0.002733	0.8571
	9	0.2500	0.013722	-0.002714	0.2750	0.014364	-0.002694	0.8571
	10	0.3000	0.014903	-0.002675	0.3250	0.015461	-0.002660	0.8571
	11	0.3500	0.015917	-0.002645	0.3750	0.016313	-0.002641	0.8571
	12	0.4000	0.016648	-0.002636	0.4250	0.016924	-0.002633	0.8571
	13	0.4500	0.017139	-0.002631	0.4750	0.017291	-0.002633	0.8571
	14	0.5000	0.017391	-0.002637	0.5250	0.017409	-0.002641	0.8571
	15	0.5500	0.017371	-0.002644	0.5750	0.017263	-0.002642	0.8571
	16	0.6000	0.017082	-0.002632	0.6250	0.016824	-0.002613	0.8571
	17	0.6500	0.016486	-0.002582	0.6750	0.016063	-0.002536	0.8571
	18	0.7000	0.015551	-0.002474	0.7250	0.014946	-0.002393	0.8571
	19	0.7500	0.014244	-0.002290	0.7750	0.013440	-0.002164	0.8571
	20	0.8000	0.012528	-0.002012	0.8250	0.011503	-0.001833	0.8571
	21	0.8500	0.010356	-0.001637	0.8750	0.009078	-0.001411	0.8571
	22	0.9000	0.007670	-0.001161	0.9100	0.007069	-0.001052	0.8571
	23	0.9200	0.006443	-0.000940	0.9300	0.005789	-0.000836	0.8571
	24	0.9400	0.005101	-0.000723	0.9500	0.004377	-0.000623	0.8571
	25	0.9600	0.003615	-0.000532	0.9700	0.002815	-0.000449	0.8571
	26	0.9800	0.001978	-0.000374	0.9900	0.001103	-0.000307	0.8571
	27	1.0000	-0.000000	-0.000000				0.8571
.469	-7.0		.01744	.11292				
	1	0.0	0.000000	0.000000	0.0100	0.002168	-0.001826	0.9388
	2	0.0200	0.003025	-0.002298	0.0300	0.003783	-0.002690	0.9388
	3	0.0400	0.004408	-0.002966	0.0500	0.004955	-0.003176	0.9388
	4	0.0600	0.005470	-0.003365	0.0700	0.005960	-0.003540	0.9388
	5	0.0800	0.006426	-0.003695	0.0900	0.006867	-0.003843	0.9388
	6	0.1000	0.007284	-0.003971	0.1250	0.008233	-0.004228	0.9388
	7	0.1500	0.009076	-0.004426	0.1750	0.009844	-0.004594	0.9388
	8	0.2000	0.010544	-0.004737	0.2250	0.011181	-0.004856	0.9388
	9	0.2500	0.011757	-0.004956	0.2750	0.012276	-0.005040	0.9388
	10	0.3000	0.012743	-0.005111	0.3250	0.013159	-0.005172	0.9388
	11	0.3500	0.013526	-0.005224	0.3750	0.013842	-0.005268	0.9388
	12	0.4000	0.014108	-0.005299	0.4250	0.014323	-0.005322	0.9388
	13	0.4500	0.014488	-0.005336	0.4750	0.014601	-0.005341	0.9388
	14	0.5000	0.014664	-0.005336	0.5250	0.014674	-0.005322	0.9388

Figure A-3. (Continued)

```
    10    15     0.5500    0.014628 -0.005296     0.5750    0.014524 -0.005255    0.9388
    10    16     0.6000    0.014357 -0.005196     0.6250    0.014126 -0.005117    0.9388
    10    17     0.6500    0.013827 -0.005017     0.6750    0.013456 -0.004892    0.9388
    10    18     0.7000    0.013010 -0.004739     0.7250    0.012485 -0.004559    0.9388
    10    19     0.7500    0.011878 -0.004346     0.7750    0.011185 -0.004099    0.9388
    10    20     0.8000    0.010402 -0.003815     0.8250    0.009524 -0.003493    0.9388
    10    21     0.8500    0.008546 -0.003133     0.8750    0.007465 -0.002736    0.9388
    10    22     0.9000    0.006277 -0.002295     0.9100    0.005772 -0.002106    0.9388
    10    23     0.9200    0.005247 -0.001910     0.9300    0.004700 -0.001709    0.9388
    10    24     0.9400    0.004132 -0.001504     0.9500    0.003538 -0.001296    0.9388
    10    25     0.9600    0.002919 -0.001066     0.9700    0.002275 -0.000874    0.9388
    10    26     0.9800    0.001606 -0.000660     0.9900    0.000913 -0.000442    0.9388
    10    27     1.0000    0.000000  0.000000                                      0.9388
.4898      -8.4          .04184      .09179
    11     1     0.0       0.000000  0.000000     0.0100    0.002055 -0.001867    0.9796
    11     2     0.0200    0.002858 -0.002481     0.0300    0.003516 -0.002960    0.9796
    11     3     0.0400    0.004044 -0.003316     0.0500    0.004522 -0.003628    0.9796
    11     4     0.0600    0.004972 -0.003917     0.0700    0.005394 -0.004184    0.9796
    11     5     0.0800    0.005789 -0.004429     0.0900    0.006157 -0.004650    0.9796
    11     6     0.1000    0.006500 -0.004851     0.1250    0.007274 -0.005288    0.9796
    11     7     0.1500    0.007966 -0.005666     0.1750    0.008591 -0.006000    0.9796
    11     8     0.2000    0.009152 -0.006293     0.2250    0.009656 -0.006550    0.9796
    11     9     0.2500    0.010108 -0.006776     0.2750    0.010514 -0.006977    0.9796
    11    10     0.3000    0.010875 -0.007154     0.3250    0.011193 -0.007309    0.9796
    11    11     0.3500    0.011467 -0.007440     0.3750    0.011699 -0.007549    0.9796
    11    12     0.4000    0.011889 -0.007637     0.4250    0.012038 -0.007702    0.9796
    11    13     0.4500    0.012144 -0.007746     0.4750    0.012209 -0.007769    0.9796
    11    14     0.5000    0.012231 -0.007769     0.5250    0.012207 -0.007748    0.9796
    11    15     0.5500    0.012134 -0.007691     0.5750    0.012018 -0.007608    0.9796
    11    16     0.6000    0.011837 -0.007493     0.6250    0.011607 -0.007345    0.9796
    11    17     0.6500    0.011321 -0.007162     0.6750    0.010977 -0.006942    0.9796
    11    18     0.7000    0.010572 -0.006684     0.7250    0.010104 -0.006385    0.9796
    11    19     0.7500    0.009572 -0.006045     0.7750    0.008974 -0.005662    0.9796
    11    20     0.8000    0.008307 -0.005235     0.8250    0.007570 -0.004765    0.9796
    11    21     0.8500    0.006761 -0.004251     0.8750    0.005878 -0.003691    0.9796
    11    22     0.9000    0.004920 -0.003082     0.9100    0.004515 -0.002826    0.9796
    11    23     0.9200    0.004096 -0.002562     0.9300    0.003662 -0.002292    0.9796
    11    24     0.9400    0.003214 -0.002016     0.9500    0.002751 -0.001734    0.9796
    11    25     0.9600    0.002273 -0.001446     0.9700    0.001780 -0.001152    0.9796
    11    26     0.9800    0.001274 -0.000851     0.9900    0.000792 -0.000544    0.9796
    11    27     1.0000    0.0       0.0                                           0.9796
.5         -9.0          .05000      .08653
    12     1     0.0       0.000000  0.000000     0.0100    0.001998 -0.001867    1.0000
    12     2     0.0200    0.002800 -0.002537     0.0300    0.003418 -0.003027    1.0000
    12     3     0.0400    0.003924 -0.003409     0.0500    0.004393 -0.003757    1.0000
    12     4     0.0600    0.004831 -0.004078     0.0700    0.005238 -0.004371    1.0000
    12     5     0.0800    0.005614 -0.004638     0.0900    0.005961 -0.004875    1.0000
    12     6     0.1000    0.006286 -0.005094     0.1250    0.007026 -0.005584    1.0000
    12     7     0.1500    0.007687 -0.006016     0.1750    0.008279 -0.006395    1.0000
    12     8     0.2000    0.008807 -0.006730     0.2250    0.009281 -0.007025    1.0000
    12     9     0.2500    0.009704 -0.007289     0.2750    0.010082 -0.007524    1.0000
    12    10     0.3000    0.010415 -0.007731     0.3250    0.010705 -0.007911    1.0000
    12    11     0.3500    0.010952 -0.008064     0.3750    0.011156 -0.008191    1.0000
    12    12     0.4000    0.011320 -0.008293     0.4250    0.011444 -0.008369    1.0000
    12    13     0.4500    0.011527 -0.008419     0.4750    0.011568 -0.008442    1.0000
    12    14     0.5000    0.011564 -0.008435     0.5250    0.011515 -0.008397    1.0000
    12    15     0.5500    0.011417 -0.008324     0.5750    0.011270 -0.008217    1.0000
    12    16     0.6000    0.011073 -0.008074     0.6250    0.010824 -0.007893    1.0000
    12    17     0.6500    0.010522 -0.007673     0.6750    0.010166 -0.007414    1.0000
    12    18     0.7000    0.009756 -0.007114     0.7250    0.009290 -0.006773    1.0000
```

Figure A-3. (Continued)

```
    12    19    0.7500   0.008767 -0.006389    0.7250   0.008185 -0.005963    1.0000
    12    20    0.8000   0.007546 -0.005494    0.8250   0.006847 -0.004985    1.0000
    12    21    0.8500   0.006090 -0.004434    0.8750   0.005274 -0.003838    1.0000
    12    22    0.9000   0.004397 -0.003199    0.9100   0.004029 -0.002932    1.0000
    12    23    0.9200   0.003649 -0.002659    0.9300   0.003259 -0.002379    1.0000
    12    24    0.9400   0.002857 -0.002093    0.9500   0.002445 -0.001801    1.0000
    12    25    0.9600   0.002024 -0.001502    0.9700   0.001593 -0.001196    1.0000
    12    26    0.9800   0.001151 -0.000885    0.9900   0.000699 -0.000568    1.0000
    12    27    1.0000   0.0       0.0                                       1.0000
61.0       .2694       .3500      1.00        4.0       1.05       10.        10.
```

Figure A-3. (Concluded)

```
CYLNDR,T1500.                                    PROP FAN CYCLINDRICAL GRID
ACCOUNT,STTPK,15101.
PURGE,A,NACELLELEWISSPIN,CY=3,ID=STTPK,PR=0.
EXIT,U.
ATTACH,OLDPL,IMPL3D,ID=STTPK,MR=1.
UPDATE.
RETURN,OLDPL.
FTN,I,R=3,OPT=2,LCM=I,L=0.
RETURN,COMPILE.
ATTACH,XYZ,IMPL3D6,ID=STTPK,MR=1.
COPY,XYZ,LGO.
RETURN,XYZ.
ATTACH,TAPE1,NACELLELEWISSPIN,ID=STTPK.
REQUEST,TAPE2,*PF.
LOAD,LGO/R.
NOGO,DUM.
RETURN,CFDLIB,PLOTS,LGO.
DUM,FL=15000.
CATALOG,TAPE2,NACELLELEWISSPIN,ID=STTPK.
EXIT,U.
AUDIT,ID=STTDSC.

*IDENT DEC77
*D GRID.12
      NOSE=22

0.80        0.0          1.4          1.0          1.0          3.06         61.0         2.0          8
   45    25     5  501     2           5.0         0.030        0.1
    1     1
```

Figure A-4. Sample Input for Three-Dimensional Flow Field Code Including Control Cards for CDC 7600

```
0.8       1.4       1.0       1.0       -3.0600
   1      0
0.1       0.15      0.2       0.25      0.3       0.35      0.375     0.4
0.45      0.5
```

Figure A-5. Sample Input for the Data Reduction Program

Appendix B

Sample Output Data

Sample output has been generated and is presented in this appendix for the mesh generation program, the three-dimensional flow field program, and the data reduction program. Typical outputs from the first two programs are very lengthy and are presented here in a very abbreviated form.

B.1. Mesh Generation Program

Sample outputs are presented in Figures B-1, B-2, and B-3 showing the Nacelle coordinates, the definition of one of the patches, and the coordinate locations in both Cartesian and cylindrical coordinates.

B.2. Three-Dimensional Flow Field Program

Sample outputs are presented in Figures B-4, B-5, and B-6 showing functions of time, surface variables, and general flow field variables.

B.3. Data Reduction Program

Sample outputs are presented in Figures B-7, B-8, and B-9 showing the printer plots obtained for C_p, a summary of the local properties, and a summary of the force data.

```
NACEL= 45     NPATMX=180     NLRG= 11     LMAX= 11     NGFSB= 8     NFO= 2     NFI= 7     NBLADF= 8

JLE= 11     JTE= 27     KTIP= 11

RTIP=  .501687   ZNOSE= -.269400   ZVERT= -.247924   ZLEAD=-10.000000     RMAX= 10.000000

DBLADE= 1.000000     BETA34= 61.00

NACELLE COORDINATES:
N=  1     ZNAC(N)= -.269400     RNAC(N)= 0.000000
N=  2     ZNAC(N)= -.269000     RNAC(N)=  .003000
N=  3     ZNAC(N)= -.267713     RNAC(N)=  .005684
N=  4     ZNAC(N)= -.266025     RNAC(N)=  .007676
N=  5     ZNAC(N)= -.258635     RNAC(N)=  .014122
N=  6     ZNAC(N)= -.251244     RNAC(N)=  .019933
N=  7     ZNAC(N)= -.243853     RNAC(N)=  .025154
N=  8     ZNAC(N)= -.236460     RNAC(N)=  .029833
N=  9     ZNAC(N)= -.229072     RNAC(N)=  .034016
N= 10     ZNAC(N)= -.221681     RNAC(N)=  .037747
N= 11     ZNAC(N)= -.214290     RNAC(N)=  .041075
N= 12     ZNAC(N)= -.206900     RNAC(N)=  .044047
N= 13     ZNAC(N)= -.196483     RNAC(N)=  .048513
N= 14     ZNAC(N)= -.186066     RNAC(N)=  .052678
N= 15     ZNAC(N)= -.175650     RNAC(N)=  .056616
N= 16     ZNAC(N)= -.165233     RNAC(N)=  .060398
N= 17     ZNAC(N)= -.154817     RNAC(N)=  .064099
N= 18     ZNAC(N)= -.144400     RNAC(N)=  .067792
N= 19     ZNAC(N)= -.020941     RNAC(N)=  .111604
N= 20     ZNAC(N)=  .101440     RNAC(N)=  .155420
N= 21     ZNAC(N)=  .112888     RNAC(N)=  .159335
N= 22     ZNAC(N)=  .135800     RNAC(N)=  .166003
N= 23     ZNAC(N)=  .162892     RNAC(N)=  .171692
N= 24     ZNAC(N)=  .194135     RNAC(N)=  .176271
N= 25     ZNAC(N)=  .225393     RNAC(N)=  .179157
N= 26     ZNAC(N)=  .256636     RNAC(N)=  .180680
N= 27     ZNAC(N)=  .272640     RNAC(N)=  .181044
N= 28     ZNAC(N)=  .291709     RNAC(N)=  .181170
N= 29     ZNAC(N)=  .311155     RNAC(N)=  .180932
N= 30     ZNAC(N)=  .330600     RNAC(N)=  .180373
N= 31     ZNAC(N)=  .350045     RNAC(N)=  .179534
N= 32     ZNAC(N)=  .369490     RNAC(N)=  .178444
N= 33     ZNAC(N)=  .388935     RNAC(N)=  .177144
N= 34     ZNAC(N)=  .427825     RNAC(N)=  .174069
N= 35     ZNAC(N)=  .466715     RNAC(N)=  .170602
N= 36     ZNAC(N)=  .505605     RNAC(N)=  .167009
N= 37     ZNAC(N)=  .525050     RNAC(N)=  .165276
```

Figure B-1. Sample Mesh Generation Output--Nacelle Coordinates (z,R)

```
USING PATCH GROUP NO.  2     POINTS WILL BE GENERATED FOR K BETWEEN 12 AND 21 INCLUSIVE
AND FOR J BETWEEN  4 AND 11 INCLUSIVE.     NTO= 1

ETA DISTRIBUTION FOR THIS PATCH GROUP:
    .00105    .00316    .00790    .01811    .03684    .06842    .11790    .21053    .40526   1.00000

XI DISTRIBUTION FOR THIS PATCH GROUP:
   .131416   .194248   .308178   .491344   .694302   .867607   .961818  1.000000

J= 4     XIJC=   .394248     NCOL= 0     NPAT= 10   W=   .394248
 K   KL     ETAC    NPAT     U,UB        WB     IT NER       X          Y          Z          R        PHI
12   12   .001053    10    .001239              4   0   -.089556    .503791   -.225267    .511689   -10.08
13   13   .003158    10    .007941              3   0   -.088323    .524295   -.224527    .531683    -9.56
14   14   .007895    10    .022952              4   0   -.085595    .570288   -.222927    .576676    -8.54
15   15   .018105    10    .055049              4   0   -.079918    .668897   -.219766    .673654    -6.81
16   16   .036842    10    .113294              4   0   -.070154    .848729   -.214886    .851624    -4.73
17   17   .068421    10    .210202              4   0   -.055421   1.150237   -.208985   1.151571    -2.76
18   18   .117895    10    .360033              4   0   -.036269   1.621085   -.204392   1.621491    -1.28
19   19   .210526    10    .637061              4   0   -.011947   2.501300   -.205344   2.501329    -.27
20   20   .405263    11    .218674              5   0    .000001   4.351002   -.210159   4.351002     .00
21   21  1.000000    12   1.000000              4   0    .000000  10.000000   -.210159  10.000000     .00

J= 5     XIJC=   .582744     NCOL= 0     NPAT= 10   W=   .582744
 K   KL     ETAC    NPAT     U,UB        WB     IT NER       X          Y          Z          R        PHI
12   12   .001053    10    .001394              4   0   -.086859    .504263   -.204204    .511689    -9.77
13   13   .003158    10    .008100              3   0   -.085378    .524783   -.203111    .531683    -9.24
14   14   .007895    10    .023119              4   0   -.082120    .570799   -.200749    .576676    -8.19
15   15   .018105    10    .055218              4   0   -.075434    .669417   -.196082    .673654    -6.43
16   16   .036842    10    .113445              4   0   -.064236    .849198   -.188880    .851624    -4.33
17   17   .068421    10    .210307              4   0   -.048125   1.150565   -.180172   1.151571    -2.40
18   18   .117895    10    .360080              4   0   -.028826   1.621234   -.173393   1.621491    -1.02
19   19   .210526    10    .637066              4   0   -.007939   2.501316   -.174798   2.501329     -.18
20   20   .405263    11    .218674              5   0    .000001   4.351002   -.181908   4.351002     .00
21   21  1.000000    12   1.000000              4   0    .000000  10.000000   -.181909  10.000000     .00
```

Figure B-2. Sample Mesh Generation Program Output--Patch Group Definition

```
J= 2   K=10   TAD=  45.00
    L= 2   KL= 31  X=  -.040548   Y=   .265098   Z=  -.617056   R=   .268181   PHI=  -8.70   ROT=   4.09
    L= 3   KL= 52  X=  -.020713   Y=   .267380   Z=  -.617056   R=   .268181   PHI=  -4.43   ROT=   8.36
    L= 4   KL= 73  X=   .000584   Y=   .268181   Z=  -.617056   R=   .268181   PHI=    .12   ROT=  12.91
    L= 5   KL= 94  X=   .022772   Y=   .267213   Z=  -.617056   R=   .268181   PHI=   4.87   ROT=  17.66
    L= 6   KL=115  X=   .045245   Y=   .264337   Z=  -.617056   R=   .268181   PHI=   9.71   ROT=  22.50
    L= 7   KL=136  X=   .067396   Y=   .259575   Z=  -.617056   R=   .268181   PHI=  14.55   ROT=  27.34
    L= 8   KL=157  X=   .088642   Y=   .253108   Z=  -.617056   R=   .268181   PHI=  19.30   ROT=  32.09
    L= 9   KL=178  X=   .108460   Y=   .245271   Z=  -.617056   R=   .268181   PHI=  23.86   ROT=  36.64
    L=10   KL=199  X=   .126407   Y=   .236521   Z=  -.617056   R=   .268181   PHI=  28.12   ROT=  40.91
    L=11   KL=220  X=   .142958   Y=   .226901   Z=  -.617056   R=   .268181   PHI=  32.21   ROT=  45.00

J= 2   K=11   TAD=  45.00
    L= 2   KL= 32  X=  -.045220   Y=   .291122   Z=  -.653437   R=   .294613   PHI=  -8.83   ROT=   4.09
    L= 3   KL= 53  X=  -.023435   Y=   .293680   Z=  -.653437   R=   .294613   PHI=  -4.56   ROT=   8.36
    L= 4   KL= 74  X=  -.000041   Y=   .294613   Z=  -.653437   R=   .294613   PHI=   -.01   ROT=  12.91
    L= 5   KL= 95  X=   .024335   Y=   .293606   Z=  -.653437   R=   .294613   PHI=   4.74   ROT=  17.66
    L= 6   KL=116  X=   .049031   Y=   .290505   Z=  -.653437   R=   .294613   PHI=   9.58   ROT=  22.50
    L= 7   KL=137  X=   .073377   Y=   .285329   Z=  -.653437   R=   .294613   PHI=  14.42   ROT=  27.34
    L= 8   KL=158  X=   .096733   Y=   .278280   Z=  -.653437   R=   .294613   PHI=  19.17   ROT=  32.09
    L= 9   KL=179  X=   .118525   Y=   .269720   Z=  -.653437   R=   .294613   PHI=  23.72   ROT=  36.64
    L=10   KL=200  X=   .138263   Y=   .260154   Z=  -.653437   R=   .294613   PHI=  27.99   ROT=  40.91
    L=11   KL=221  X=   .156470   Y=   .249628   Z=  -.653437   R=   .294613   PHI=  32.08   ROT=  45.00

J= 2   K=12   TAD=  45.00
    L= 2   KL= 33  X=  -.054537   Y=   .354086   Z=  -.741045   R=   .358262   PHI=  -8.76   ROT=   4.09
    L= 3   KL= 54  X=  -.028043   Y=   .357162   Z=  -.741045   R=   .358262   PHI=  -4.49   ROT=   8.36
    L= 4   KL= 75  X=   .000406   Y=   .358261   Z=  -.741045   R=   .358262   PHI=    .06   ROT=  12.91
    L= 5   KL= 96  X=   .030048   Y=   .356999   Z=  -.741045   R=   .358262   PHI=   4.81   ROT=  17.66
    L= 6   KL=117  X=   .060074   Y=   .353189   Z=  -.741045   R=   .358262   PHI=   9.65   ROT=  22.50
    L= 7   KL=138  X=   .089671   Y=   .346858   Z=  -.741045   R=   .358262   PHI=  14.50   ROT=  27.34
    L= 8   KL=159  X=   .118063   Y=   .338249   Z=  -.741045   R=   .358262   PHI=  19.24   ROT=  32.09
    L= 9   KL=180  X=   .144549   Y=   .327806   Z=  -.741045   R=   .358262   PHI=  23.80   ROT=  36.64
    L=10   KL=201  X=   .168537   Y=   .316144   Z=  -.741045   R=   .358262   PHI=  28.06   ROT=  40.91
    L=11   KL=222  X=   .190661   Y=   .303315   Z=  -.741045   R=   .358262   PHI=  32.15   ROT=  45.00

J= 2   K=13   TAD=  45.00
    L= 2   KL= 34  X=  -.055760   Y=   .508130   Z=  -.951525   R=   .511180   PHI=  -6.26   ROT=   4.09
    L= 3   KL= 55  X=  -.017802   Y=   .510870   Z=  -.951525   R=   .511180   PHI=  -2.00   ROT=   8.36
    L= 4   KL= 76  X=   .022820   Y=   .510670   Z=  -.951525   R=   .511180   PHI=   2.56   ROT=  12.91
    L= 5   KL= 97  X=   .064995   Y=   .507031   Z=  -.951525   R=   .511180   PHI=   7.30   ROT=  17.66
    L= 6   KL=118  X=   .107560   Y=   .499736   Z=  -.951525   R=   .511180   PHI=  12.15   ROT=  22.50
    L= 7   KL=139  X=   .149358   Y=   .488873   Z=  -.951525   R=   .511180   PHI=  16.99   ROT=  27.34
    L= 8   KL=160  X=   .189295   Y=   .474839   Z=  -.951525   R=   .511180   PHI=  21.73   ROT=  32.09
    L= 9   KL=181  X=   .226402   Y=   .458309   Z=  -.951525   R=   .511180   PHI=  26.29   ROT=  36.64
    L=10   KL=202  X=   .259872   Y=   .440195   Z=  -.951525   R=   .511180   PHI=  30.56   ROT=  40.91
    L=11   KL=223  X=   .290613   Y=   .420534   Z=  -.951525   R=   .511180   PHI=  34.65   ROT=  45.00
```

Figure B-3. Sample Mesh Generation Program Output--Cartesian and Cylindrical Definition of Each Coordinate Point

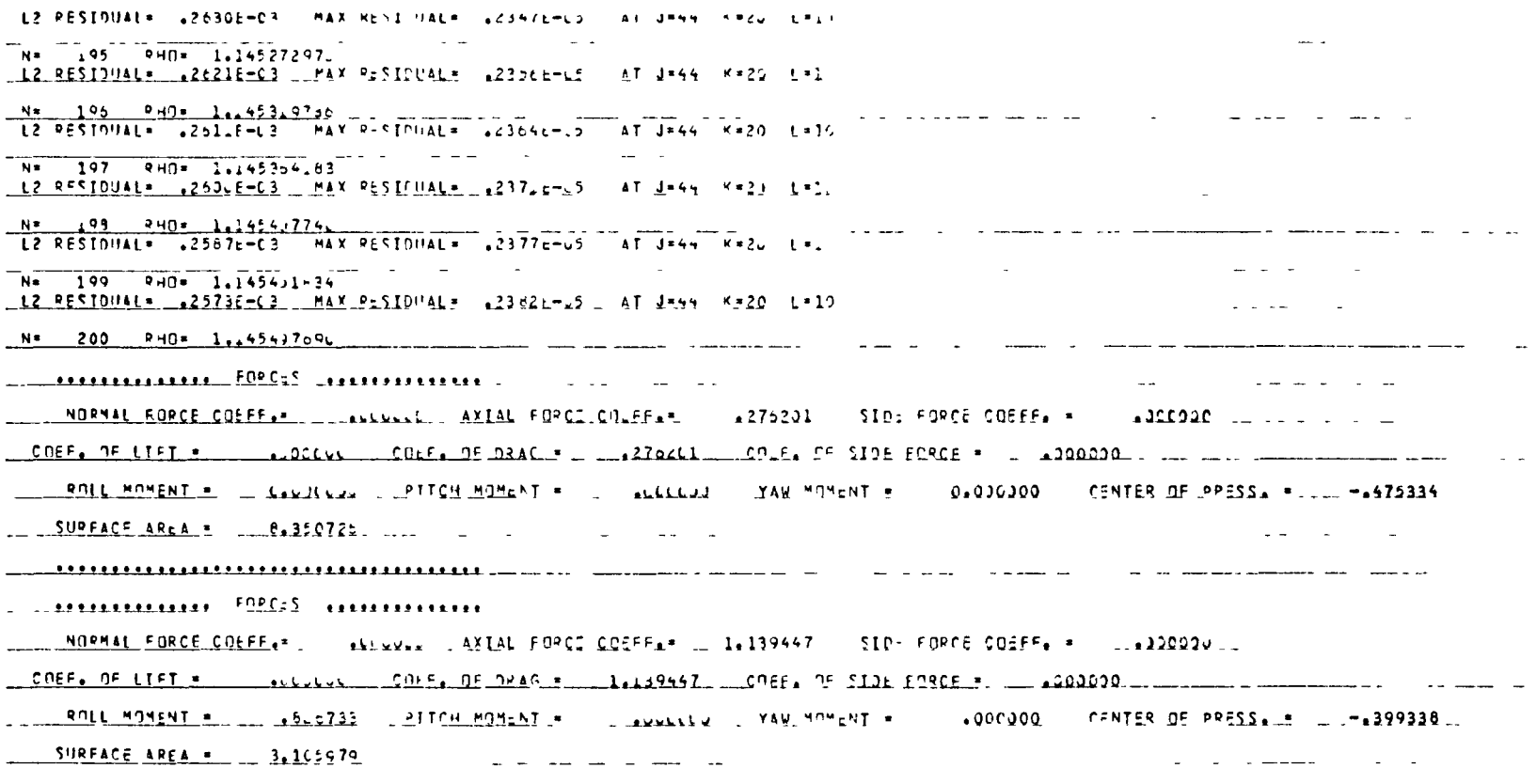

Figure B-4. Sample Flow Field Output--Function of Time

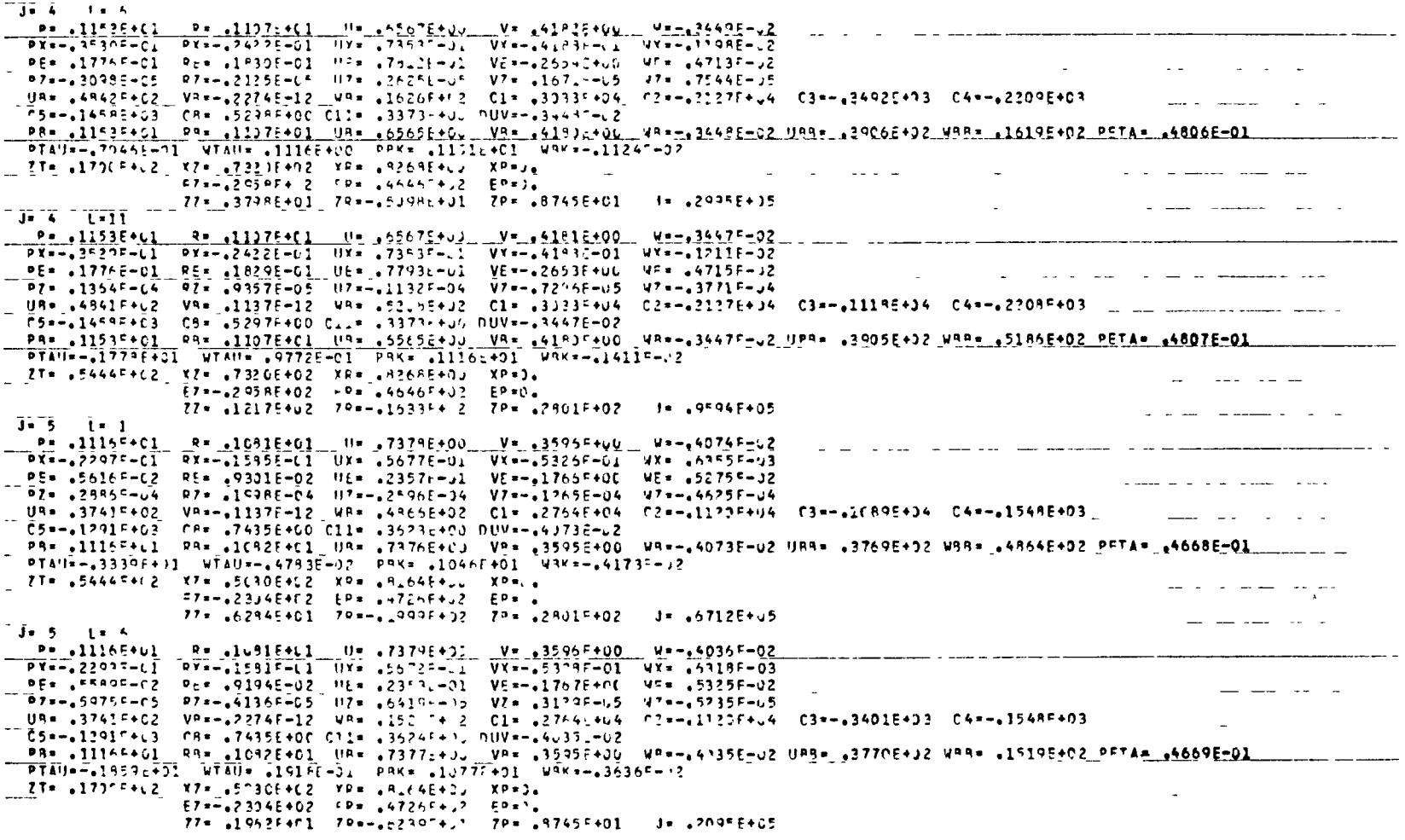

Figure B-5. Sample Flow Field Output--Surface Variables

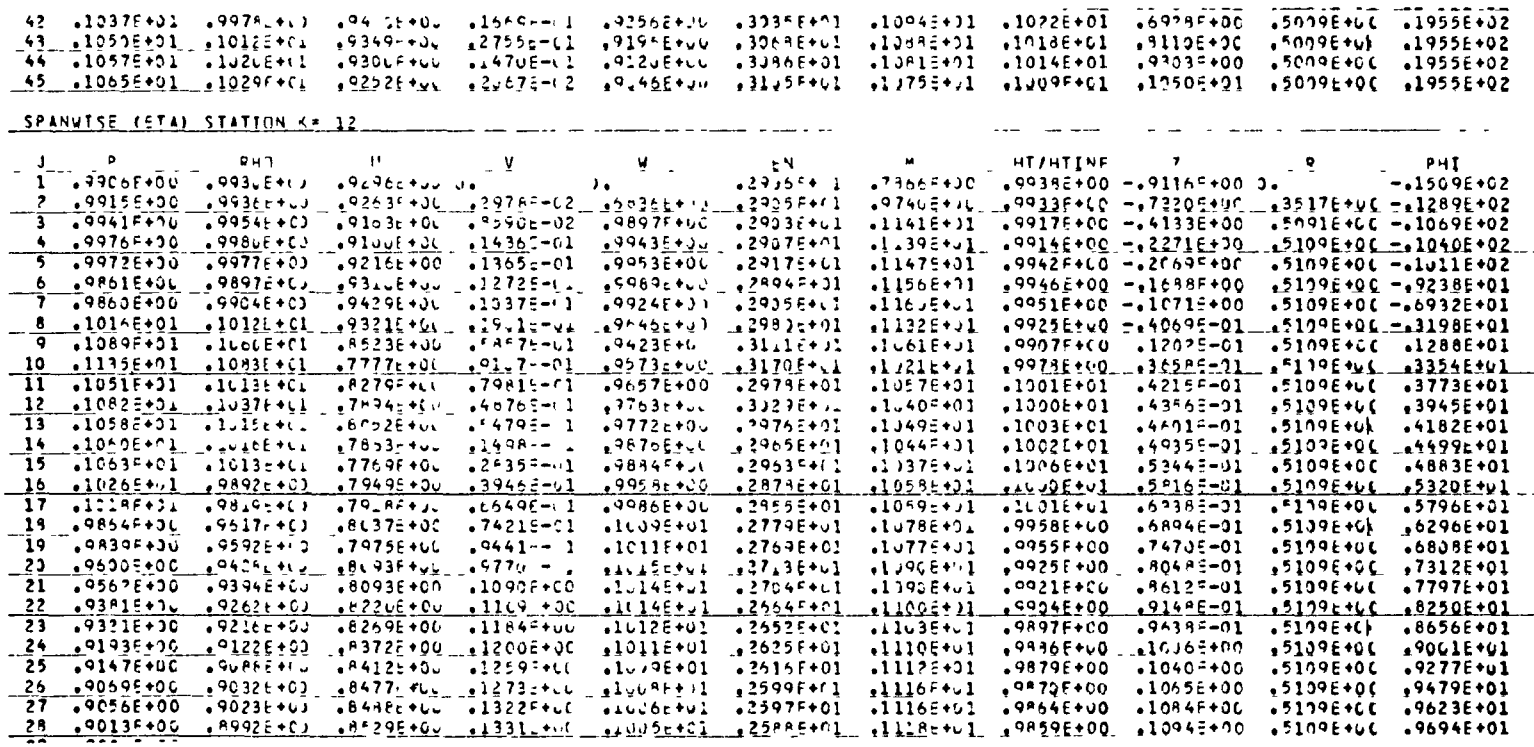

42	.1037E+01	.9978E+00	.9[illegible]E+00	.1[illegible]E-01	.9256E+00	.3335E+01	.1094E+01	.1022E+01	.6978E+00	.5009E+00	.1955E+02
43	.1050E+01	.1012E+01	.9349E+00	.2755E-01	.9195E+00	.3068E+01	.1088E+01	.1018E+01	.9110E+00	.5009E+00	.1955E+02
44	.1057E+01	.1026E+01	.9306E+00	.3147E-01	.9126E+00	.3086E+01	.1081E+01	.1014E+01	.9303E+00	.5009E+00	.1955E+02
45	.1065E+01	.1029E+01	.9252E+00	.2967E-02	.9046E+00	.3145E+01	.1075E+01	.1009E+01	.1050E+01	.5009E+00	.1955E+02

SPANWISE (ETA) STATION K= 12

J	P	RHO	U	V	W	EN	M	HT/HTINF	T	R	PHI
1	.9906E+00	.9936E+00	.9[illegible]E+00	0.	0.	.2935E+01	.7866E+00	.9938E+00	-.9116E+00	0.	-.1509E+02
2	.9915E+00	.9938E+00	.9263E+00	.2978E-02	.6[illegible]3E+00	.2935E+01	.9740E+00	.9933E+00	-.7320E+00	.3517E+00	-.1289E+02
3	.9941E+00	.9954E+00	.9103E+00	.9590E-02	.9897E+00	.2903E+01	.1141E+01	.9917E+00	-.4133E+00	.5091E+00	-.1069E+02
4	.9976E+00	.9986E+00	.9100E+00	.1436E-01	.9943E+00	.2907E+01	.1139E+01	.9914E+00	-.2271E+00	.5109E+00	-.1040E+02
5	.9972E+00	.9977E+00	.9216E+00	.1365E-01	.9953E+00	.2917E+01	.1147E+01	.9942E+00	-.2669E+00	.5109E+00	-.1011E+02
6	.9861E+00	.9897E+00	.9316E+00	.1272E-01	.9969E+00	.2894E+01	.1156E+01	.9946E+00	-.1688E+00	.5109E+00	-.9238E+01
7	.9860E+00	.9904E+00	.9429E+00	.1037E-01	.9924E+00	.2905E+01	.1165E+01	.9951E+00	-.1071E+00	.5109E+00	-.6932E+01
8	.1014E+01	.1012E+01	.9321E+00	.2[illegible]E-02	.9945E+00	.2982E+01	.1132E+01	.9925E+00	-.4069E-01	.5109E+00	-.3198E+01
9	.1089E+01	.1066E+01	.8523E+00	.[illegible]E-01	.9423E+00	.3121E+01	.1061E+01	.9907E+00	.1209E-01	.5109E+00	.1288E+01
10	.1135E+01	.1083E+01	.7777E+00	.9[illegible]E-01	.9573E+00	.3170E+01	.1021E+01	.9978E+00	.3658E-01	.5109E+00	.3354E+01
11	.1051E+01	.1013E+01	.8279E+00	.7981E-01	.9657E+00	.2979E+01	.1057E+01	.1001E+01	.4215E-01	.5109E+00	.3773E+01
12	.1082E+01	.1037E+01	.7894E+00	.4076E-01	.9763E+00	.3023E+01	.1040E+01	.1000E+01	.4356E-01	.5109E+00	.3945E+01
13	.1058E+01	.1015E+01	.8092E+00	.[illegible]479E-01	.9772E+00	.2976E+01	.1049E+01	.1003E+01	.4401E-01	.5109E+00	.4182E+01
14	.1050E+01	.[illegible]E+01	.7883E+00	.1498E-01	.9870E+00	.2965E+01	.1044E+01	.1002E+01	.4935E-01	.5109E+00	.4499E+01
15	.1063E+01	.1013E+01	.7769E+00	.2835E-01	.9884E+00	.2963E+01	.1037E+01	.1006E+01	.5344E-01	.5109E+00	.4883E+01
16	.1026E+01	.9892E+00	.7949E+00	.3946E-01	.9958E+00	.2879E+01	.1058E+01	.1009E+01	.5916E-01	.5109E+00	.5320E+01
17	.1019E+01	.9819E+00	.7982E+00	.4649E-01	.9986E+00	.2955E+01	.1059E+01	.1001E+01	.6938E-01	.5109E+00	.5796E+01
18	.9854E+00	.9617E+00	.8037E+00	.7421E-01	.1009E+01	.2779E+01	.1078E+01	.9958E+00	.6894E-01	.5109E+00	.6296E+01
19	.9839E+00	.9592E+00	.7975E+00	.9441E-01	.1011E+01	.2769E+01	.1077E+01	.9955E+00	.7470E-01	.5109E+00	.6808E+01
20	.9690E+00	.9405E+00	.8093E+00	.9770E-01	.1015E+01	.2743E+01	.1096E+01	.9925E+00	.8048E-01	.5109E+00	.7312E+01
21	.9567E+00	.9394E+00	.8093E+00	.1090E+00	.1014E+01	.2704E+01	.1098E+01	.9921E+00	.8612E-01	.5109E+00	.7797E+01
22	.9381E+00	.9262E+00	.8220E+00	.1169E+00	.1014E+01	.2664E+01	.1100E+01	.9904E+00	.9149E-01	.5109E+00	.8250E+01
23	.9321E+00	.9216E+00	.8269E+00	.1184E+00	.1012E+01	.2652E+01	.1103E+01	.9897E+00	.9638E-01	.5109E+00	.8656E+01
24	.9193E+00	.9122E+00	.8372E+00	.1200E+00	.1011E+01	.2625E+01	.1110E+01	.9886E+00	.1006E+00	.5109E+00	.9001E+01
25	.9147E+00	.9088E+00	.8412E+00	.1259E+00	.1009E+01	.2616E+01	.1112E+01	.9879E+00	.1040E+00	.5109E+00	.9277E+01
26	.9059E+00	.9032E+00	.8477E+00	.1273E+00	.1008E+01	.2599E+01	.1116E+01	.9870E+00	.1065E+00	.5109E+00	.9479E+01
27	.9056E+00	.9023E+00	.8448E+00	.1322E+00	.1006E+01	.2597E+01	.1116E+01	.9864E+00	.1084E+00	.5109E+00	.9623E+01
28	.9013E+00	.8992E+00	.8529E+00	.1331E+00	.1005E+01	.2588E+01	.1118E+01	.9859E+00	.1094E+00	.5109E+00	.9694E+01

Figure B-6. Sample Output--Variables Across the Flow Field

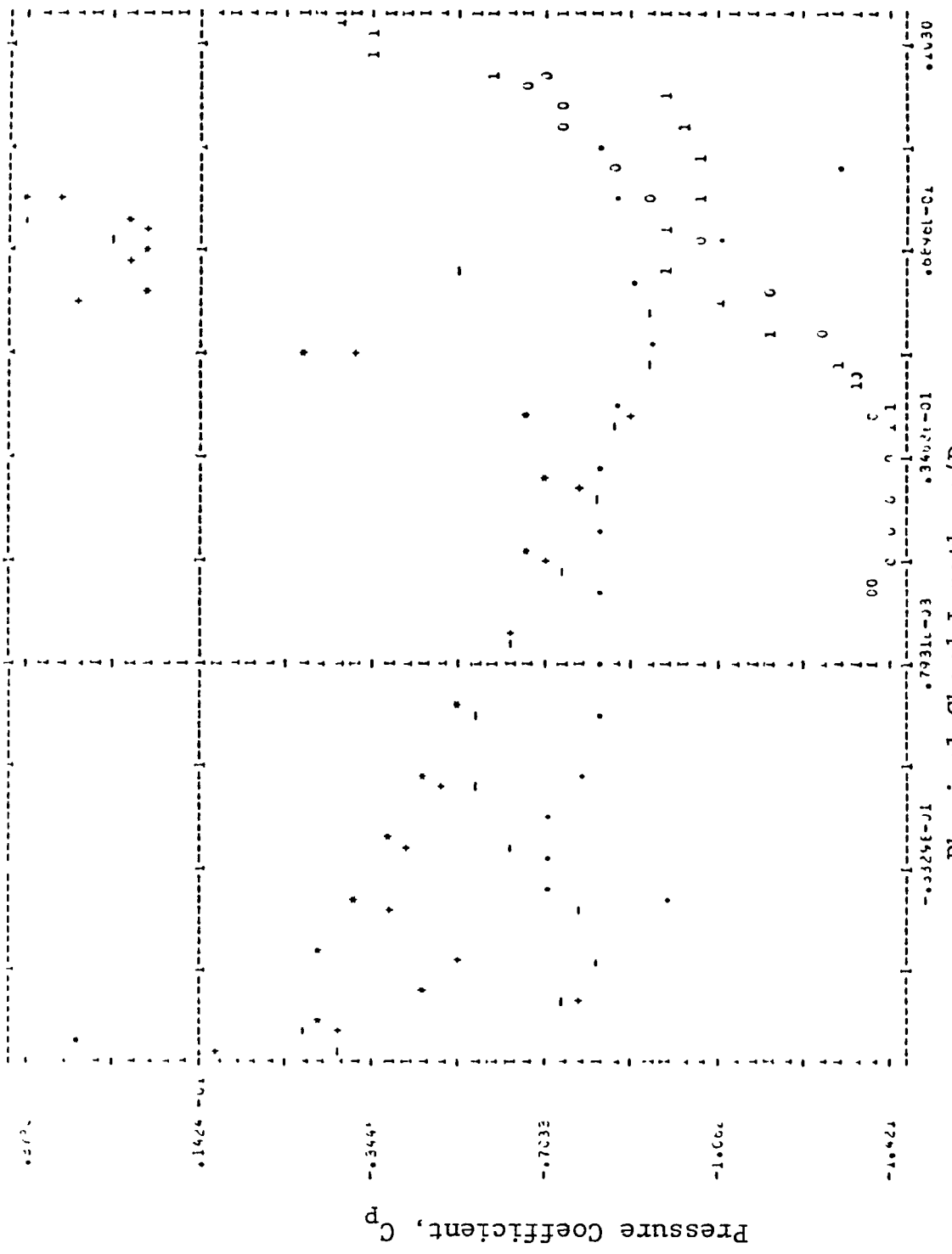

Figure B-7. Printer Plot of C_p from Data Reduction Program

LOCAL GEOMETRIC AND AERODYNAMIC PROPERTIES OF THE CAMBER SIDE OF THE BLADE.

RADIAL LOCATION= .375000

Z(AXIAL)	PHI(DEG)	Y(ROTATE)	CP	PRESSURE	DENSITY	U-VEL(AXIAL)	V-VEL(RADIL)	W-VEL(ROTAT)	ENERGY
-.03146047	-2.63520032	-.01724127	-1.05921125	.52547336	.63137634	1.35464065	.04065090	.14723445	1.99984465
-.02288846	-2.29607967	-.01503686	-.88623044	.60296876	.69721506	1.23779910	.06646163	.18495471	2.05509696
-.02459092	-1.85510441	-.01213451	-.81339739	.63559797	.72343096	1.25896079	.04700987	.10123797	2.16661420
-.01672428	-1.27175258	-.00832292	-.79599037	.64339273	.72977017	1.26459950	.04088828	.07984577	2.19494670
-.01153916	-.57710658	-.00377710	-.60391517	.63984600	.72691206	1.27752837	.03602146	.06590774	2.19465426
-.00322341	.20474510	.00134005	-.61306046	.63536154	.72329823	1.29039396	.03141306	.05317462	2.19202123
.00593223	1.04374164	.00683090	-.62431466	.63070702	.71950543	1.30291155	.02670639	.04093100	2.18833533
.01569995	1.91502702	.01203672	-.62150286	.63196672	.72054403	1.31074033	.02130795	.02540624	2.19927600
.02502544	2.79497249	.01825500	-.62932022	.62040454	.71770158	1.32266562	.01542880	.01080901	2.19926723
.03599043	3.65064533	.02387725	-.83922529	.62402707	.71406792	1.33670900	.00668229	-.00572547	2.19805134
.04593544	4.45743509	.02914442	-.85723531	.61595850	.70744210	1.35492484	.00145356	-.02413436	2.18947167
.05543186	5.19538634	.03395714	-.91363125	.59769320	.68656734	1.38636571	-.00582516	-.03614156	2.13896276
.06414229	5.84093863	.03816287	-.67264737	.60905398	.70173534	1.36506915	-.01250317	-.07239464	2.19841666
.07170507	6.37331653	.04162730	-1.07368023	.51890166	.62586694	1.47713486	-.01943008	-.06458507	1.98147571
.07789235	6.76047515	.04431354	-.85201390	.61802695	.70908535	1.40278062	-.02311738	-.13067427	2.24696269
.08246477	7.07463266	.04610709	-1.30039777	.41742180	.53583277	1.60464647	-.03060280	-.09623711	1.73624625
.08592174	7.26986900	.04745361	-.80495594	.63937974	.72650325	1.39481623	-.02895378	-.16291604	2.31510567

Figure B-8. Summary of Local Properties from the Data Reduction Program

INDEX OF EACH SECTION	1	2	3	4	5	6	7	8	9	10
RADIUS FROM C/L OF NACELLE	.1000000	.1500000	.2000000	.2500000	.3000000	.3500000	.3750000	.4000000	.4500000	.5000000
CHORD AT THE SECTION	.0624400	.1447522	.1461890	.1451421	.1424779	.1388115	.1340299	.1259698	.1043640	.0847907
GEOMETRIC ANGLE, BETA	81.87828	78.81311	75.40541	71.45121	67.17188	63.00279	61.13878	59.34651	55.78198	52.56040
EFFECTIVE PITCH ANGLE	78.39657	72.98121	67.67373	62.82711	58.36699	54.29652	52.40379	50.60266	47.26213	44.24622
EFFECTIVE ANGLE OF ATTACK	3.48170	5.93190	7.73169	8.62409	8.80488	8.70627	8.73498	8.74385	8.51984	8.31418
LIFT COEFFICIENT PER SECTION	.42566	.13829	.29499	.44463	.57719	.67111	.71763	.77636	.86160	.67239
DRAG COEFFICIENT PER SECTION	-.42703	-.07653	-.02114	.00055	-.00296	-.00469	-.00211	.00051	.00639	.00622
RELATIVE VELOCITY PER SECTION	.96632	.99045	1.02328	1.06400	1.11175	1.16566	1.19467	1.22492	1.28879	1.35662
DYNAMIC PRESSURE PER SECTION	.46689	.49050	.52355	.56605	.61800	.67938	.71362	.75021	.83049	.92021
THRUST PER BLADE PER SECTION	.0140781	.0072356	.0072551	.0115776	.0199574	.0291242	.0333077	.0373654	.0415364	.0315085
TORQUE PER BLADE PER SECTION	.0010532	.0012867	.0042882	.0086616	.0140220	.0196672	.0225058	.0252568	.0279284	.0209755
TOTAL THRUST PER SECTION	.1126250	.0578851	.0580407	.0926208	.1596592	.2329935	.2664614	.2989236	.3322915	.2520683
TOTAL TORQUE PER SECTION	.0084254	.0102934	.0343059	.0692929	.1121756	.1573372	.1800467	.2020548	.2234274	.1678042
TOTAL THRUST COEFFICIENT	1.17698	.60493	.60655	.96793	1.66851	2.43489	2.78464	3.12388	3.47259	2.63423
TOTAL TORQUE COEFFICIENT	.08805	.10757	.35851	.72414	1.17229	1.64424	1.88157	2.11156	2.33492	1.75363

Figure B-9. Summary of Forces from the Data Reduction Program

1 Report No	2 Government Accession No	3 Recipient's Catalog No
NASA CR-167959		

4 Title and Subtitle	5 Report Date
USER'S MANUAL FOR THREE-DIMENSIONAL ANALYSIS OF PROPELIER FLOW FIELDS	January 1983
	6 Performing Organization Code
7 Author(s)	8 Performing Organization Report No
Denny S. Chaussee and Paul Kutler	FSI-80-04
	10 Work Unit No
9 Performing Organization Name and Address	11 Contract or Grant No
Flow Simulations, Inc. 298 S. Sunnyvale Ave., Suite 204 Sunnyvale, California 94086	NAS 3-22375
	13 Type of Report and Period Covered
12 Sponsoring Agency Name and Address	Contractor Report
National Aeronautics and Space Administration Washington, D. C. 20546	14 Sponsoring Agency Code 505-32-12

15 Supplementary Notes

Final report. Project Manager, Lawrence J. Bober, Propulsion Aerodynamics Division, NASA Lewis Research Center, Cleveland, Ohio 44135.

16 Abstract

A detailed operating manual is presented for the prop-fan computer code (in addition to supporting programs) recently developed by Kutler, Chaussee, Sorenson, and Pulliam while at the NASA's Ames Research Center. This code solves the inviscid Euler equations using an implicit numerical procedure developed by Beam and Warming of Ames. A description of the underlying theory, numerical techniques, and boundary conditions with equations, formulas, and methods for the mesh generation program (MGP), three-dimensional prop-fan flow field program (3DPFP), and data reduction program (DRP) is provided, together with complete operating instructions. In addition, a programmer's manual is also provided to assist the user interested in modifying the codes. Included in the programmer's manual for each program is a description of the input and output variables, flow charts, program listings, sample input and output data, and operating hints.

17 Key Words (Suggested by Author(s))	18 Distribution Statement
Propellers Computer program Transonic flow Euler equations Finite difference method	Unclassified - unlimited STAR Category 02

19 Security Classif (of this report)	20 Security Classif (of this page)	21 No of Pages	22 Price*
Unclassified	Unclassified	128	A07

* For sale by the National Technical Information Service, Springfield, Virginia 22161

End of Document